Wave damping potential of woody riparian vegetation

Comparing terrestrial laser scanning with manual measuring techniques

S. A. Kalloe

Delft University of Technology

Wave damping potential of woody riparian vegetation

Comparing terrestrial laser scanning with manual measuring techniques

by

S. A. Kalloe

in partial fulfillment of the requirements for the degree of

Master of Science

in Civil Engineering

at the Delft University of Technology,

to be defended on Monday May 13, 2019 at 12:00 PM.

Student number:	4295269	
Project duration:	July, 2018 – May, 2019	
Thesis committee:	Dr. ir. B. Hofland	TU Delft , Supervisor
	Prof. dr. ir. S. G. J. Aarninkhof	TU Delft , Chairman
	Dr. B. K. van Wesenbeeck	Deltares
	Dr. ir V. Vuik	TU Delft
	Dr. ir J. A. A. Antolinez	Deltares

This thesis is confidential and cannot be made public until May, 2020.
Cover: Willow trees in the Delta flume at Deltares.

Abstract

Including vegetation in flood defense systems has the potential to be a more cost-effective solution than conventional dike reinforcement measures, as vegetation contains wave damping properties. However, more insight is required on the complex physical processes due to wave-vegetation interaction in order to predict the amount of wave damping. Past research found that these processes are dependent on both flow conditions and vegetation characteristics. Therefore, reliable quantification of these vegetation characteristics is of importance to understand these processes and thus to improve predictions for wave dissipation due to vegetation. This study aims to gain insight on practical methods for quantifying relevant vegetation characteristics for wave damping.

Data is used from full scale physical experiments conducted in the Delta Flume at Deltares, with 40 meters of willow forest. The vegetation characteristics are quantified in this study both by manual measurements on the willow trees and by executing Terrestrial 3D laser scans (TLS) of the whole forest. The frontal area of vegetation is found in literature to be a relevant parameter for determining the wave attenuation, therefore the focus in this study lies on schematizing this parameter over the vertical, which is seen as representations of the average willow tree. This schematization is referred to in this report as "tree model".

In this study, four tree models are obtained. The four tree models include: tree model 1a (manual measurements on the primary branches, excluding side branches), tree model 1b (branching method based on Strahlers ordering scheme, including side branches), tree model 1c (adjusted branching method) and tree model 2 (from terrestrial laser scanner). The reconstructed area from the TLS point cloud is determined by using Matlab built-in alpha shape function. The tree models are compared in terms of frontal area distribution over the vertical and of their effect on the corresponding wave attenuation. The latter comparison is achieved by using the numerical wave model SWAN and confronting the results with the measured wave attenuation from the physical experiments.

With regards to the manual measuring methods, the frontal area of the average tree from tree model 1a serves as a lower limit, while tree model 1b gives the upper limit. The TLS outcome (tree model 2) underestimates the frontal area as computed by the other tree models. In particular, the underestimation is 70% when compared with tree model 1b, and 30 % when compared to tree model 1a. Adjustments on tree model 1b leads to tree model 1c. This tree model accounts for the tapering form of the branches and results in a total frontal area in between tree model 1a and tree model 1b. In this study, the representative area for the willow trees can be best captured with tree model 1c. This tree model results in a drag coefficient (C_D) of 1.15 averaged over the tests with leafless willows and showed a negative correlation with the Keulegan-Carpenter number (KC).

However, the capabilities of the TLS should be analyzed further and this study encourages to use a larger data set of trees in order to find a relation between the laser penetration and corresponding mismatch. Gathering of vegetation parameters by hand is in fact not economically attractive for woody riparian vegetation, as these trees are characterized by complex canopy structures and high elevations. The TLS can serve as a practical tool for obtaining these relevant vegetation parameters for applying willows in hybrid solutions.

Preface

This thesis has been produced as final work to fulfill my Master in Science program in Hydraulic Engineering at the Delft University of Technology.
This work was mainly carried out at Deltares as part of the WOODY project. I am grateful to have worked in the Delta flume, one of the most unique test facilities in the world, and in such an energetic and motivated team.

I first want to thank my thesis committee: Stefan Aarninkhof, Bas Hofland, Bregje van Wesenbeeck, Vincent Vuik and Jose Antolines. I am grateful for your feedback, discussions and support during our meetings. Thank you Bregje, for the guidance during the thesis and also for providing a working space at Deltares. I am grateful for having experienced both the flume test as the working experience at Deltares. I am also grateful for the support from Vincent and Jose, thank you for the guidance and especially the helpful advice in working with SWAN. Special thanks goes to my daily supervisor, Bas Hofland, for introducing me to this topic. Also thank you for always showing enthusiasm in this work and supporting me during these challenging months of my thesis.

I definitely cannot forget thanking my family and friends, Ceylan, Samantha, Davini, Boedjie, Avinash, D'tasha and Rais, for being there for me. Finally my parents and my boyfriend, for the unconditional love and support during these months.

S. A. Kalloe
Delft, May 2019

Contents

List of Tables

List of Figures

Nomenclature

Abbreviations

JONSWAP	Joint North Sea Wave Project
RMSE	Root-mean-square-error
SWAN	Simulating WAves Nearshore
TLS	Terrestrial laser scanner
WHM	Wave height meter or wave gauge

Symbols

	Frequency number or Sarpkaya	[-]
ϵ_v	averaged vegetation dissipation	[N/m/s]
ν	Kinematic viscosity	[m^2/s]
$\frac{\partial u}{\partial t}$	Acceleration in oscillatory motion	$[m/s^2]$
$\tilde{C_D}$	Bulk drag coefficient	[-]
b_v	plant area per unit height of each vegetation stand normal to the horizontal orbital velocity	[m^2/m]
d_{high}	Diameter of the highest order branch	[m]
d_{min}	Diameter of the branch tips	[m]
H_{rms}	Root mean square wave height	[m]
L_{high}	Length of the highest order branch	[m]
B	Buoyancy parameter	[-]
b	Vogel exponent	[-]
C$_t$	Transmission coefficient	[-]
C$_a$	Cauchy number	[-]
C$_D$	Drag coefficient	[-]
C$_M$	Inertia coefficient	[-]
D	Pile diameter	[m]
D$_b$	Diameter at breast height	[m]
h	water depth	[m]
KC	Keulegan- Carpenter number	[-]
KC$_m$	Keulegan- Carpenter number with Mazda length scale	[-]
L	Blade length to wave orbital excursion	[-]
LAI	Leaf area index	[-]
LF	Leaf factor	[-]
N	plant density	[units/m^2]
R	Wave reduction	[-]

R_B	Branching ratio	[-]
R_D	Diameter ratio	[-]
R_L	Length ratio	[-]
Re	Reynolds number	[-]
u	Velocity	[m/s]

1

Introduction

This chapter starts with the problem description in section 1.1, which gives a general description of vegetation as part of flood defence systems and the corresponding complications. This section is closed with the motive behind this study. Subsequently the chapter proceeds with the research questions and scope in section 1.2. Finally, the research approach and outline of this report are described in section 1.3.

1.1. Problem description

The use of vegetation in flood protection systems around the world has gained a lot of interest over the years, for example mangroves along tropical coasts and rivers, kelps in front of the coast and salt marshes in front of dikes (Suzuki and Arikawa, 2010). It is expected that dikes in the Netherlands will need to be made higher and stronger to keep up with heavier rainfall and sea level rise, in order to prevent the hinterlands from flooding (Aerts, 2009). This will lead to increasing costs regarding dike-maintenance. Because of this, the interest broadened over the past years to more cost-effective solutions for river dikes. As vegetation adapts to the rising sea level, promotes sedimentation and has the property of damping the incoming waves, the use of the naturally occurring vegetation in front of dikes (riparian vegetation) has a lot of potential to contribute to the safety against flooding. In this way the dike dimensions can be reduced, thus leading to a decrease of the cost.
Besides the flood-safety contribution, riparian vegetation also provides benefits for the aquatic ecosystem (Tabacchi et al., 1998), such as thermal control and provision of organic matter (Van Looy et al., 2013).

In Europe, and especially in the Netherlands a widely distributed type of riparian vegetation is the willow tree also known as Sallows (broader leafed) or Osiers (narrow leaved) (Houston Durrant et al., 2016). These are deciduous trees and have a large number of species. The most common is the Salix Alba (white willow) and can be found in its two forms; the rising white willow and the pollard willow (knotwilg) which are depicted in figure 1.1. The former shows a natural form of the tree, while the latter is a consequence of active management, in which the tree is periodically pruned. This leads to faster growing young sprouts relative to an old trunk (Ferrini, 2006). Other common types are the Salix Viminalis (katwilg), the Salix Caprea (boswilg) and the Salix Aurita (geoorde wilg).

Figure 1.1: Left: Rising white willow in the Netherlands (Source: GerardM, 2004), Right: Pollarded willow in the Netherlands (Source: Bj.schoenmakers, 2012).

The wave damping property of vegetation has been described in several papers as result of the work done by the waves on the vegetation (Suzuki et al., 2011a; Dalrymple et al., 1984). The relevant processes that lead to wave energy dissipation through a forest are wave breaking and wave-vegetation interaction (Vo-Luong and Massel, 2008). Both vegetation characteristics and hydrodynamic conditions influence these processes. The vegetation characteristics of influence include the vegetation density, geometry, buoyancy, stiffness, foliage abundance, relative vegetation height and the degrees of freedom of motion of the plant (Västilä et al., 2013a; Västilä and Järvelä, 2014; Luhar and Nepf, 2011; Mendez and Losada, 2004). The amount of wave dissipation depends on whether the vegetation is subject to the combination of wave and current or solely to waves as well as on wave parameters such as horizontal orbital velocity, wave amplitude, direction and wave period (Hu et al., 2014).

Besides the knowledge on benefits of vegetation and physics behind wave- vegetation interaction, "building with nature" solutions come with large uncertainties. The vegetation strength and stability during extreme wave conditions are not fully known yet (Vuik et al., 2018), which is crucial information in order to know whether riparian vegetation can withstand future storms. Also, the effect of vegetation characteristics on the amount of wave damping is not sufficiently known yet, as experiments in the past were done on small scales leading to scaling errors (Heller, 2011).

In order to gain more insight on the effect of vegetation on wave dissipation, the quantification of relevant vegetation parameters is necessary.
The collection of these data is generally done by manual measurements, which can be destructive or non-destructive (Lin et al., 2017). The destructive methods are mostly done for biomass estimations (Nordh and Verwijst, 2004). Non-destructive methods include allometric relations, where an easily measured parameter is used, for example diameter at breast height, to derive indirectly other parameters which are more difficult to measure, such as tree height or biomass (Nordh and Verwijst, 2004).
A relatively new method applies remote sensing techniques and is already widely used for evaluating forest information, such as deforestation and carbon storage. Techniques such as airborne LiDAR, aerial photography, terrestrial laser scanning (TLS) can make field survey data gathering more efficient and economical than the tree scale manual measurements. The Airborne LiDAR can be used for large areas, but underestimates some parameters, such as tree height and fails to capture the complex structures of the trees. The TLS gathers more detailed and reliable data in the form of a 3D point cloud which has the potential to be translated into actual vegetation parameters. This technique is thus a good non-destructive way to gather structural tree parameters (Srinivasan et al., 2015).
Difficulties in gaining insight on vegetation parameters can lie in the dimensions of the tree, seasonal and spatial variety of vegetation states. Practical measuring tools which are reliable and time-efficient, are therefore needed to make these hybrid solutions applicable especially regarding design and maintenance. The present thesis aims to analyse methods in order to obtain structural tree parameters relevant for quantifying wave attenuation and thereby to contribute to the use of vegetation in hybrid engineering.

1.2. Scope and research questions

The main focus of this report lies on the quantification of relevant vegetation parameters for wave damping. Both manual measuring techniques and TLS are applied during physical experiments and the corresponding wave attenuation by the vegetation input is modelled in SWAN wave model 1D stationary mode.
The used data from physical flume experiments result from the WOODY physical modelling project, which were conducted in the Delta Flume at Deltares using real scale woody vegetation, namely white willow trees (Salix Alba). The primary aim of the WOODY project is to gain knowledge about wave attenuation by vegetation under storm conditions in order to improve wave damping predictions by vegetation and to eventually include them in design methods (Lenssinck, 2018). The present thesis uses data collected from these physical experiments. The remote sensing data is solely taken from a terrestrial laser scanner and the focus mainly lies on the scans of the leaf-less conditions of the trees. This vegetation state coincides with extreme conditions (storm conditions), which are characterized by high-water levels, high wave height and leaf-less condition of the trees (winter season).

1.2.1. Research questions

The main research question is formulated as follows:
How to determine relevant vegetation parameters for wave damping?

To be able to answer this question, the following sub-questions are formulated:

1. What are the relevant vegetation parameters for wave attenuation?
2. Which link can be found between the vegetation characteristics and the amount of wave damping out of the woody experimental data?
3. Which effective measure can be obtained out of TLS data to characterize the trees regarding the wave attenuation?
4. How does the TLS input effect the SWAN output values?

1.3. Research approach and outline

In order to answer main research question, this research is carried out by analyzing the physical experiments and by vegetation modelling. The results of the experiments are assumed to be the 'real' values for the amount of wave attenuation due to the specific vegetation, while vegetation modelling aims to reproduce these measured values. A schematic overview of the approach is given in figure 1.2. This schematic consists of two main boxes namely "Plant characteristics" and "Wave attenuation", where the experimental results define the line that connects them.
The first indirect link between these boxes is the conventional method for reproducing the amount of wave attenuation shown in figure 1.2 as the light grey boxes. This method is via numerical models that generally use the Dalrymple formula or Mendez and Losada formula to account for vegetation. The input for these formulas is extracted from a tree model (tree model 1, seen in the figure) based on manually gathered vegetation data.

Another measuring method is schematized as the second indirect link between the "Plant characteristics" and the "Wave attenuation" as the dark grey boxes. The TLS data is used to obtain an alternative tree model (tree model 2), which is illustrated as the arrow between the "Plant characteristics" and "Tree model 2". This tree model (tree model 2) is compared with the conventional tree model (tree model 1), shown with the green colored arrow between "Tree model 1" and "Tree model 2".

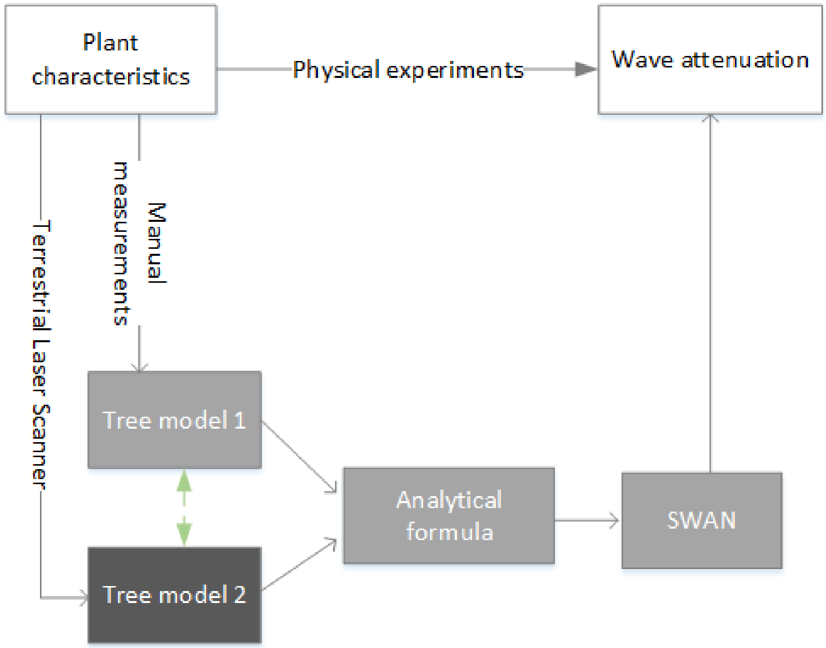

Figure 1.2: Schematic overview of the research approach

The sub-questions described in the previous section 1.2 are answered in the upcoming chapters of this report. First, past research, theoretical background information, and numerical modelling efforts are presented in chapter 2. This chapter contributes to the description of the relevant parameters for wave attenuation (sub-question 1). Its content includes theoretical background on wave dissipation due to vegetation, where first the simple rigid cylinder approach is introduced, followed by more complex approximations for example by formulas which consider the flexibility of the plants. Also, theoretical background and past research on measurements of vegetation characteristics are given, where past research mostly focuses on tree allometry and the use of TLS to define tree parameters relevant for flow-resistance formulas. In the next chapter, chapter 3, the focus lies on analyzing the experimental measurements regarding the vegetation and obtaining tree models based on hand measurements on willow trees. This chapter also contributes to finding an effective measure to characterize the trees regarding the amount of wave attenuation, and obtaining a tree model out of the TLS data (sub-objective 3). Chapter 4 presents the outcome of the physical model regarding the wave attenuation (sub-question 2) and the wave model SWAN with the implementation of the obtained tree models (sub-question 4). Hereafter discussions and recommendations are found in chapter 5. Lastly, the conclusions are presented in chapter 6.

2

Literature review

This chapter gives an overview of relevant research done on topics regarding wave energy dissipation due to vegetation. First, the theories on wave vegetation interaction are summed up in section 2.1, starting from the simple models (rigid cylinders) to more complex models (flexible cylinders). Past flume experiments and field measurements are listed in section 2.2 for woody vegetation. Furthermore, current methods for extracting structural tree information are given in section 2.3, including research done on using terrestrial laser scanning for the latter purpose. Hereafter, numerical modellings efforts are presented in section 2.4. In the final section 2.5, the identified knowledge gaps and conclusion on the literature review are stated.

2.1. Wave energy dissipation due to vegetation

2.1.1. Rigid vegetation

The presence of vegetation induces turbulence development which dissipates part of the energy of the incoming waves. The dissipation of the waves through a forest is foremost due to the wave-vegetation interaction and due to the wave breaking (Vo-Luong and Massel, 2008). The remaining part of the energy is redistributed into reflected waves and transmitted waves. The wave field can also diffract around this vegetation area if there is high energy dissipation in the water column (Dalrymple et al., 1984).

One of the first analytic approaches to determine the wave dissipation by vegetation is the bottom friction or bed roughness approach. This adjusts the bottom friction parameters such that it includes for the resistance by vegetation and the bottom itself, which makes measuring data a necessity in order to calibrate and validate for each different case. This approach is useful to determine the wave dissipation without considering the underlying physical processes. Several studies (Tolman, 1992; Padilla-Hernandez and Monbaliu, 2001) analysed the wave dissipation due to pure wave conditions and wave-current conditions and the effect of using different bottom friction formulation (Luo and Monbaliu, 1994). Eventually, this method is also used on vegetation, e.g. (Mazda, 1997; Quartel et al., 2007) used the bottom friction approach on mangrove vegetation.

A second approach is the structural-element approach or the cylinder approach which directly determines the forces on the vegetation, by schematizing the vegetation as structural elements. (Morison et al., 1950) Morison did experiments on single smooth piles without wake interaction and calculated the forces in oscillatory flow. He found that the total force on a pile can be determined by superposition of inertia and drag with the equation:

$$F(t) = F_m + F_d = \left(\frac{\pi}{4}\right)\rho C_M D^2 \frac{\partial u}{\partial t} + \frac{1}{2}\rho C_D D u(t)|u(t)|^1 \tag{2.1}$$

Where C_M is the inertia coefficient $[-]$, C_D is the drag coefficient $[-]$, D is the pile diameter $[m]$, $\frac{\partial u}{\partial t}$ is the acceleration in oscillatory motion $[m/s^2]$ and $u(t)$ is the time dependent velocity $[m/s]$. Two important

[1]Note: For pure wave and wave-current conditions, the work done by Fm equals zero over a wave period (Hu et al., 2014).

findings by Morison are the relative importance of the inertia force with the ratio pile diameter to wave height and the dependency of the drag coefficient on the Reynold number ($Re = \rho u L_c/\mu = u L_c/\nu$) (Morison et al., 1950). This is a dimensionless parameter which gives the relative importance of inertial and viscous effects . Several author described the drag coefficient Cd as function of the Reynolds number (Losada et al., 2016; Hu et al., 2014).

Other researchers found a dependency of the drag coefficient on other hydraulic dimensionless parameters, for instance the Iversen Modulus (Iversen and Balent, 1951) and later the Keulegan Carpenter ($KC = uT/L_c$)(Keulegan and Carpenter, 1958) number which is relatively easier to use in practice (Mendez and Losada, 2004; Bradley and Houser, 2009). Mendez and Losada found that the drag coefficient not only depends on the KC number, but also on the relative height of the plants, α, and made an empirical relation of C_D as function of the modified Keulegan-Carpenter number ($Q = KC/\alpha^{0.76}$) for artificial kelps (Mendez and Losada, 2004).
For mangroves, the KC number with Mazda length scale (KC_M) was determined to be the best relation with Cd for mangroves (Hendriks, 2014). The Mazda length scale includes vegetation information to the conventional characteristic length scale L_c (L_c= uT/π in oscillatory flow), which leads to $L_c = (V_c - V_m/A_p)$. Where V_m is the mangrove volume $[m^3]$, V_c is the control volume $[m^3]$ and A_p is the projected surface area of the vegetation withing this control volume $[m^2]$. It is also found that the drag coefficient is a function of the parameter 2a/S (2a is the stroke of motion and S is the spacing between the cylinders) and β frequency parameter (Re/KC or $D^2/\nu T$) (Suzuki, 2011). Another factor that influences the drag coefficient is the roughness of the object (Journée and Massie, 2001).

Dalrymple determined the dissipation of wave energy by applying the Morison equation and linear wave theory while looking at the forces on rigid cylinders for non-sloping bed with regular waves (Dalrymple et al., 1984). Mendez and Losada modified the Dalrymple formula to account also for sloping beds and irregular waves and is given by:

$$< \epsilon_v >= \frac{1}{2\sqrt{\pi}} \rho C_D b_v N (\frac{kg}{2\sigma})^3 (\frac{\sinh^3 k\alpha h_v + 3 \sinh k\alpha h_v}{3k \cosh^3 kh_v}) H_{rms}^3 \tag{2.2}$$

Where ϵ_v averaged vegetation dissipation [N/m/s], N is the plant density $[units/m^2]$, k is the wave number $[1/m]$, σ is wave frequency $[rad/s]$, h_v is vegetation height $[m]$, α is relative vegetation height [-], $\tilde{C_D}$ is bulk drag coefficient. [2] [-], b_v is plant area per unit height of each vegetation stand normal to u $[m^2/m]$ and H_{rms} is root mean square wave height $[m]$ to account for the irregular wave field. For a narrow banded spectrum (such as $JONSWAP$ spectrum), the energy is concentrated in the peak period. The dissipated energy is over the entire frequency domain of a narrow banded spectrum, leading to constant shape of the spectrum and no change in peak period.

2.1.2. Flexible vegetation

In reality vegetation has a certain degree of flexibility, especially aquatic vegetation. Dynamic blade models have already been used to capture the vegetation motion for this type of vegetation (Gijón Mancheño, 2016; Luhar and Nepf, 2011, 2015). The motion consists of swaying and reconfiguration of the plant. Plants tend to have a swaying motion when they are objected to waves, in order to decrease the relative velocity and acceleration. Plant reconfiguration is through plant bending which decreases the plant projected area to the waves and creates a more streamlined form which decreases the drag forces on the plant. Parameters that capture the reconfiguration of the vegetation are the Cauchy number (C_a) , blade length to wave orbital excursion (L) and buoyancy parameter (B). (Luhar and Nepf, 2015). The buoyancy parameter is the ratio between the restoring forces (buoyancy and stiffness) (Luhar and Nepf, 2015). Another way to include the effect of plant configuration is by adjusting the exponent of the velocity of the drag formula, this is adjusted by the Vogel exponent (b). As woody vegetation is generally rigid and emergent, the Vogel component is not expected to be really relevant (Västilä and Järvelä, 2014).

[2]Note: The bulk drag coefficient consists not only of the drag, but also covers other physical processes which are not considered like reconfiguration of the plant, swaying motion (which are influenced by the bio-mechanical properties of the plant and the hydrodynamics) and wake interaction in the formula. This makes site-specific calibration necessary to get reliable results.

2.2. Past laboratory experiments and field measurements

Most laboratory experiments used aquatic vegetation (kelp plants) and salt marshes, both artificial and natural. More recently, experiments on mangroves and woody vegetation were conducted, where mostly the rigid cylinder approach was applied. Most of this research was conducted with branches or small trees because of the flume dimensions which is one of the determinate factors for the maximum size of vegetation that can be tested. Several of these experiments on woody vegetation types are listed in table 2.2.

Past laboratory tests			
Vegetation type	setup	hydraulic conditions	Reference
Plant mimics (stiff wooden rods)	height= 0.36 m, diameter= 0.01 m	waves (Hmax= 0.2m)+ currents (umax= 0.3m/s)	(Hu et al., 2014)
4 species (Alnus glutinosa, Betula pendula, Betula pubescens, Salix caprea)	height 0.9-3.4 m	Currents (Umax= 2.5 m/s)	(Jalonen and Järvelä, 2014)
3 species (Salix sp, Alnus glutinosa, Polulus alba)	height 1.4-4 m	Currents (0.25-1.75 m/s)	(Wilson et al., 2010)
Black poplar (Polulus nigra)	Natural twigs (height= 0.23m)	Currents 0.1-0.61 m/s	(Västilä et al., 2013b)
4 species (Salix viminalis, Salix x rubens, Alnus Glutinosa and Betula pendula)	Natural twigs (height 0.23m)	Currents 0.2-0.8 m/s (waterdepth 15-30cm)	(Västilä and Järvelä, 2014)
Willows (Salix Alba)	Natural willow branches (height 1-2.5m)	Currents	(Armanini et al., 2005)

Table 2.1: Past flume experiments regarding woody vegetation

Also most field measurements were obtained for salt marshes, where view could capture extreme wave conditions. Winter storm in 2015, Hellegat polder, western Scheldt, the Netherlands by the BE SAFE study is one of the view field measurements with high waves (maximum wave height of 0.9 m and through salt marshes) (Vuik et al., 2016). The field measurements on woody vegetation also exhibit very low wave height. An example is the measurement campaign done on the foreshore of the river Noord by Deltares in 2015, where they used boxes (7x7m) containing old and young willow branches. A list of field studies on woody vegetation can be found in table 2.2.

Table 2.2: Past field measurements with woody vegetation

Past field measurements			
Vegetation type	Location, year	Hydraulic conditions	Reference
Mangroves (450 m mixed mangrove species forest)	Red river delta, Vietnam, 2000	H=0.25 m, d∼1.55 m, T=3.5-6.5 s	(Quartel et al., 2007)
Mangroves (80 m forest Avicenna and Rhizophora	Can Gio, Vietnam, 2006	H= 0.4m, d= 2.5m	(Phuoc and Massel, 2006)
Mangroves (100m mixed mangrove species forest)	5 sites in Vietnam, 2011	H ∼ 0.55m	(Bao, 2011)
Mangroves (98-246 m mangrove forest	Southern Andaman region, Thailand dec-2010-may 2011	H_s= 0.3 m, T= 2.9-6.4 s, d= 1.5-1.75 m	(Horstman et al., 2014)
Willows (7 m of 1-3 year old Salix Alba, height=1.2-4m)	Rivier Noord, Netherlands, 2015	H ∼ 0.2m, d= 0.8-1.4m	(Del, 2018 (accessed November 12, 2018)

2.3. Vegetation measuring methods

Wave dissipation and flow resistance are dependent on several parameters. The reference projected area is one of the parameters used for flow resistance, and is often determined by cameras (Wunder et al., 2011).

Another method for determining the projected area is the branching method (Järvelä, 2004), which requires manual tree data to apply the Strahler ordering scheme. This scheme is originated from river bifurcations, in which it was originally applied for identifying the branching of a river system. This method starts at the end of the rivers (lowest order, Order=1), where two small bifurcations of the same order meet, they sum up to a higher order stream and so on, until they reach the origin of the river (highest order, Order = n). The same method is used for branches. The branching method (Järvelä, 2004) had been compared with TLS method regarding the projected reference area for leafless woody vegetation (Antonarakis et al., 2009). The roughness coefficients obtained by these methods had been compared with values of literature and not with results from direct physical experiments on the measured trees, thus not with the "true" roughness values of the trees. Also the branching method provides the total frontal area and assumes a linear decay of this area over the height. Although these assumptions, the TLS and the branching method gave similar results for the total frontal area (Antonarakis et al., 2009). Furthermore, the leaf area index was determined with TLS by using directional gap fractions as input for the Beer-Lambert transmittance law (Antonarakis et al., 2010). This method was only necessary due to the lack of scans without leaves. Having both scans of the trees with leaves and without leaves makes it relatively easier to obtain the foliage abundance. The difference between these scans can already provide a good estimate for the area of the leaves.

2.4. Numerical modelling efforts

For moving vegetation under hydraulic loads, an maximum displacement of approximately 1/20 of the stem length can be safely simplified as rigid cylinders for the sake of wave attenuation. This was one of the outcomes of a study on flexible vegetation that used a one dimensional model that models plant motion (Gijón Mancheño, 2016). Most of the models are based on the cylinder approach by Dalrymple (rigid vegetation). Some examples of models that use the Dalrymple approach are the WAPROMAN (Wave propagation through Mangroves) model, which is specifically for mangrove forests (Vo-Luong and Massel, 2008). This model has been compared with SWAN-veg model (Mcivor et al., 2012). Both models succeeded in predicting the measured waves (Hs$\approx$ 0.4m), but more insight is needed for obtaining the drag coefficients required by both models for the mangrove species under storm conditions. (Mcivor et al., 2012).
The well-known SWAN-veg model (phase-averaged model/spectral-wave energy model) uses the spectral action balance equation for changes in wave spectrum (Booij et al., 1999). The effects of vegetation is included by the Mendez and Losada formulation implemented by Suzuki (Suzuki, 2011). The input for the vegetation characterization is the average projected area per layer. The layers in this model give a big advantage of assigning different vegetation properties over the height. Still the drag coefficient has no certain formula and needs to be calibrated for each case. This model is validated for physical tests with natural salt marshes and applied on practical cases (willows, mangroves) (Suzuki, 2011). A 3D model CADMAS-SURF (Immersed Boundary Method) has been used to gain more insight in the bulk drag coefficient (Suzuki, 2011). SWASH (phase-resolving) wave flow model is a non-hydrostatic model and is already used in the past for simulating the wave dissipation through willow patches along a river, but was not successful in reproducing the measured wave dissipation (Stam, 2018).
Also X-beach-veg, (process based model, uses the short wave action balance) varying the vegetation parameters along the height is also possible in this model (Songy, 2016). Just as in SWAN, for similar drag coefficient and hydraulic conditions, the vegetation input of $N = 1[units/m^2]$ and $b_v = 2[m]$ gives the same results as $N = 2[units/m^2]$ and $b_v = 1[m]$, which is physically not correct. X-beach also has a non-hydrostatic module, where non-linear waves can be simulated. Emerged vegetation which can lead to non-linear wave effects can potentially be incorporated in this model (van Rooijen et al., 2015).

2.5. Summary

Firstly, it can be seen that most research in the past has been done by linking the hydraulic properties to the drag coefficient, thus to the wave dissipation. Other physical processes regarding the vegetation were calibrated in the bulk drag coefficient. More complex methods take the plant reconfiguration into account by relations between the drag coefficient and effective length, where the effective length is a function of dimensionless parameters like Cauchy number. These models determined the flow resistance and few models accounted for wave dissipation, mostly based on flexible blades that mimic aquatic vegetation.
Secondly, research on TLS as input for flow resistance by live vegetation has been done in few research for

flow resistance through woody vegetation. Semi-automatic methods for obtaining the reference area and the Leaf Area Index were made and compared with outcome from other measuring methods and vegetation resistance from literature. But no physical model tests were done on those trees, so the direct results on the resistance by these trees could not be achieved. Also these comparisons with live vegetation were drawn for vegetation under steady flow (currents) and not yet under oscillatory flow conditions.
Lastly regarding numerical modelling, SWAN-VEG, is more practical in terms of computational demand and is thus preferred in engineering applications to other models (2DV, 3D models), although it has more limitations. SWASH gives the vertical structure of the velocity and oscillatory flow through canopies can be calculated. Although the SWASH model can give more insight on the physics, SWAN is used due to its more practical use (limited computational demand).

3 Physical model

From the literature review it emerged that the vegetation parameters can be schematized in tree models. In this thesis this expression is used with specific regard to area distribution, in particular:

Tree model means the frontal area distribution over the height of one tree determined from various measuring methods.

This chapter describes the applied methods and analysis that result in tree models 1a, 1b and 1c (based on manual measurements) and tree model 2 (based on the TLS data). The first section starts with a description of the experimental set-up as used during the WOODY project. It is important to note that this description does not cover the full overview of measuring equipment used during the measuring campaign, but only relevant measuring equipment for this work. This study mainly focuses on the quantification of the vegetation characteristics during this measuring campaign, which involves hand and TLS measurements. The analysis and results of these manual measurements are given in section 3.2, which consist of height distributions of tree parameters like branch diameter; number of branches and gathered damaged biomass after the test series. These parameters form the input for tree models 1a,1b and 1c, given at the end of this section. Tree model 2 follows after analysis of the TLS data, presented in section 3.3. An overview of the tree models is given in the last section 3.4.

3.1. Physical modelling campaign

3.1.1. Experimental set-up

Experiments were performed in the Delta flume of Deltares from 27 June till 19 July 2018 in Delft, the Netherlands. The flume is 291 m long, 9.5 m deep and 5 m wide. Approximately 200 meters of the total length of the flume was used to execute the tests with woody vegetation, namely willows trees, species Salix Alba. The experimental set-up was constructed in such a way to have a typical dike slope at the end of the flume and to mimic the state of a foreshore by placement of the willows on a plateau in front of the dike. The plateau had a length of 85 m, thickness of 2.33 m and a slope of 1:10 at the offshore end. The willow trees were placed in a staggered manner (16 rows) and occupied 40 m of the plateau (See figure A.1 of Appendix A.1). The 10 m high wave board can ensure significant wave heights up to 2.0 m (irregular waves) and consist of active re-reflection compensation, in order to reduce the occurrence of reflected waves in the flume. Several measuring tools were placed in the flume, where especially the Wave Height Meters (WHM) in front and behind the forest are relevant during this thesis to measure the wave damping. An overview of the experimental setup is shown in figure 3.1.

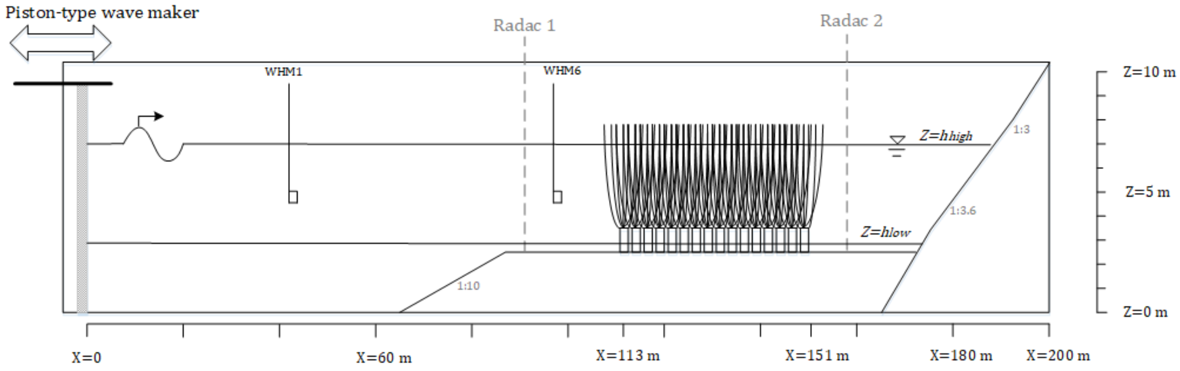

Figure 3.1: Flume set-up impression; The tested water depth range is given between $z = h_{max}$ and $z = h_{max}$, and the leafless state of the vegetation is shown. The positions of relevant wave height meters (WHM) are also given.

The wave board generated Joint North Sea Wave Project (JONSWAP) spectrum of incoming irregular waves with shape parameter γ= 3.3. The water levelsvaried between 2.93 and 6.83 m and the wave heights varied between 0.2 and 1.5 m. The variations in hydraulic conditions were tested for three vegetation configurations (vegetation with foliage, without foliage and 50 % vegetation density without foliage). Based on the height of the vegetation relative to the water level and the vegetation states, the program consisted of four test series and the calibration tests (without trees). An overview of the test series is given in table 3.1. The full program is given in table A.1 of Appendix A.2.

Table 3.1: Lists the wave parameters, vegetation state and measurements regarding the vegetation. TS=Test series, h= water depth, H_{m0}= Significant wave height and T= wave period.

Overview experimental test series						
Test series (TS)	Vegetation configuration	h (m)	$H_{m0}(m)$	T (s)	Biomass	FARO scans
TS 1 (T001-T004)	trunks	2.93- 3.03	0.2- 0.25	1.79- 2.83	-	T001B
TS 2 (T005-T012)	canopy with leaves	5.33- 6.83	0.5- 1.0	2.83- 5.66	floating biomass	T012A
TS 3 (T013-T022)	canopy without leaves	5.33- 6.83	0.5-1.61	2.83- 6.93	floating biomass	T013B, T022A
TS 4 (T023-T030)	thinned density	5.33- 6.83	0.5- 1.5	2.83- 6.93	floating biomass	T023B, T030A
Calibration(T031-T042)	no vegetation	2.93- 6.83	0.2- 1.61	1.79- 6.93	-	T031B

3.1.2. Physical modelling results

Due to wave dissipation in the forest, the wave amplitude decreases and thereby the oscillatory velocity also decreases along the length of the vegetation. This affects the drag coefficients of each tree along the flume, thus varying drag coefficient in horizontal space. However, the drag coefficient of the entire forest is determined, generally referred to the bulk drag coefficient ($C_{\tilde{D}}$). The drag due to the forest is obtained by measuring hydraulic parameters in front and behind the forest, such as velocity and wave height. These measurements are generally easier to obtain and more accurate than measurements inside the forest, above this it is well used in practice.

The physical model setup, as explained in section 3.1.1, figure 3.1 showed the measuring equipment relevant for this study. It must be noted that the generated waves are also affected by the set-up of the flume, in particular by the foreshore (plateau). This leads to additional processes such as wave shoaling and wave breaking, besides dissipation due to vegetation and bottom friction. These relative importance of these processes are dependent on the wave characteristics and varied varied between 2- 18 % of wave dissipation. Furthermore the dike behind the forest lead to reflected wave energy, which is removed from the measured spectra by the Maximum entropy method (MEM) (Massel and Brinkman, 1998) (In more detail in WOODY measuring report (Report)).

A general method for quantifying the amount of dissipation is with the transmission coefficient (Ct), where $C_t = H_{m0}/H_{m0\,behind forest}$. However, the transmission coefficient is not used to quantify the effect of vegetation on the wave dissipation, due to the uncertainty in WHM06. Instead the difference in wave height between the calibration tests and the test runs with vegetation for the same wave conditions, is seen as more reliable quantification of the wave damping due to vegetation. This quantified by the difference between the measured wave height behind the vegetation (with Radac2) for test with (Test series 1,2,3 and 4) and without vegetation (Test series 5 "calibration tests"). This method of quantifying the wave disspation limits the uncertainty in the measurements and the influences in front of the forest are also accounted for, namely the wave transformations due to the foreshore. Reflection during the real tests is removed from the spectra by the Maximum entropy method (MEM) (Massel and Brinkman, 1998) (In more detail in WOODY measuring report (Report)).

$$Dissipation = \frac{(H_{m0_{vegetation}} - H_{m0_{calibration}})}{H_{m0_{calibration}}} \tag{3.1}$$

Physical experimental results are taken from the measuring report (Report). The maximum measured wave attenuation is 22%, which was found for test series 2 (with leaves,full canopy density). The difference of the wave dissipation for the test runs with and without leaves was 1.5-4%. The largest amount for wave dissipation by the branches was approximately 20 % for full canopy configuration (Test series 3). The effect of the reduced canopy density is the difference in wave dissipation between test series 3 and test series 4, which resulted in 3-7 % difference in wave dissipation. Furthermore, the highest wave attenuation rates were found for water depth of 3 meters. These values are already excluding the wave dissipation due to the foreshore.

3.1.3. Collection of vegetation data

Vegetation data was gathered in a time span of one week before the start of the experiments. This data includes the dimensions of the trunk (height and diameter) of each tree, diameter and length of the branches at breast height and the number of branches for every tree at breast height. Trunk dimension and diameters of branches were measured with measuring tape and vernier caliper respectively.
The branches were at first categorized into three classes, based on their measured base diameter (D_b) and then counted per class for every tree. This branch classification is explained further in the following section, section 3.2.

Biomass loss during the test runs was monitored by capturing most of the amount of the damaged loose branches after each test series. Also, the state of the trees was captured by executing laser scans before and after test series (see table 3.1). These scans were done by using a FARO 3D scanner, which calculates the distances between the object and the laser scanner based on the phase shift of the emitted infra red wave. The scanner specifications are listed in table 3.2.

Table 3.2: Lists the specifications of the used TLS scanner and the settings used for the experiments.

TLS Specifications	
Model	FARO FOCUS 3D S 120
Type	Phase
Max range	0.6- 120 m
Max scan rate	976 000 pts/sec
Single scan duration	39 628 sec
Resolution	176.9 MPts
Quality	2 X
Field of view	360°horizontal, -60°- 90°vertical
Point distance	3mm/10m
Exposure metering mode	Zenith Weighted Metering
Scan size	20622 x 8534 Pt

In order to capture the 40 meter willow forest, single scans on three positions were taken. Positioning of these scans for scan registration is done by placing reference targets in the scanning area. These were placed on the side edges on top of the flume. An indication of the three scanning positions and rotation of the scanner (360 degrees around the z-axis and 300 degrees around the y-axis) during the multi-scans are given in figure 3.2. Along the length of the flume, the first position was just after the start of the forest, the second position was in the center of the forest and the third position was just before the end of the forest. Each position was approximately 10.5 m above the bottom of the flume (8.17 m above the plateau), and located in the center of the width of the flume.

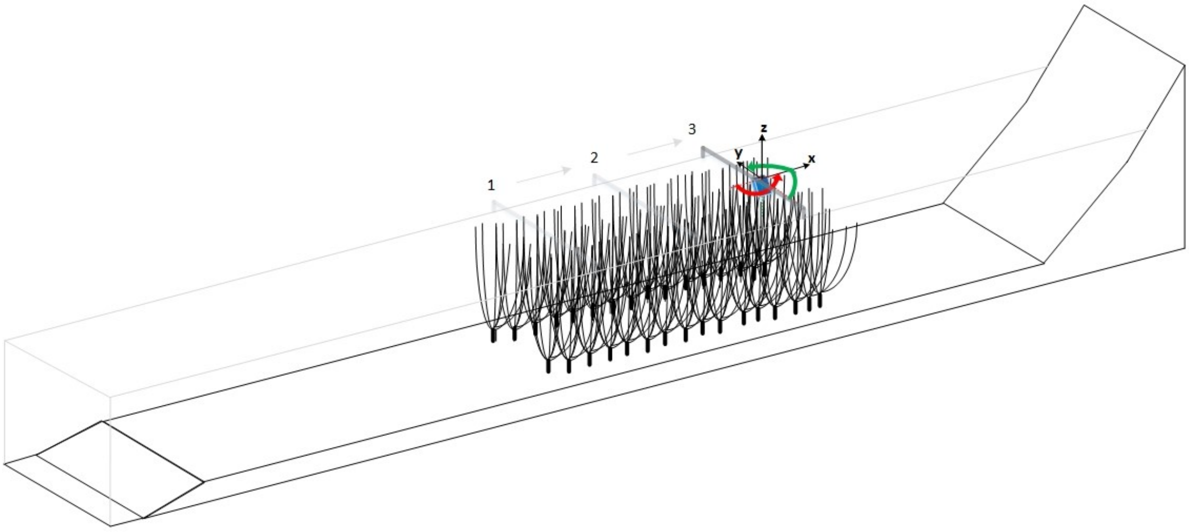

Figure 3.2: Gives the scanning position 1, 2 and 3 of the TLS, situated on a movable bridge above the flume. During the scanning procedure, the scan rotates around the z-axis and y-axis given respectively with the green and red arrow.

Next to the non-destructive method (TLS), also destructive methods (manual measurements) were performed. This includes biomass measurements, followed by detailed sketches of the removed branches. The biomass of the leaves was weighted after test series 1 and the one of the removed branches after test series 2. Also, mechanical properties (bending tests) were determined for different diameters of the branches and for different sections of the branches. Finally, for the preparation of the calibration test; the trees were removed from the flume and weighted. These trees were sparser and contained no foliage.

3.2. Manual measurements analysis

This section presents the analysis of measured vegetation data (manually measured) by means of investigating the distribution of relevant vegetation parameters in space. These include the average diameter and the number of branches (branch density), as seen from literature review, determine the frontal area and thus influence the wave dissipation. The distribution of these parameters in space is therefore analysed in subsection 3.2.1. This analysis is done solely on the primary branches, as measured during the experiments. The amount of foliage is found in literature to contribute to the drag force (Västilä and Järvelä, 2014) . Therefore this analysis also focuses on quantifying the amount of foliage. Finally, the manual measurements regarding the damaged biomass after each test series is presented in subsection 3.2.3 and appendix C.4, which leads to findings about the state of the willows after storm conditions. The analysis of subsection 3.2.1 done on the primary branches, excludes the side branches. In order to gain more information of the total frontal area (primary branches including the side branches), another method is applied. Measured diameters at breast height (D_b) together with detailed sketches of the branches are used to determine the total frontal area based on a branch structure method of Järvelä (2004), discussed in section 3.2.2. Lastly, these vegetation parameters result in tree models 1, described in section 3.2.3.

3.2.1. Manually gathered data

Primary branches

The branches were at first divided into three classes, based on their measured base diameter (D_b) and then counted per class for every tree. This branch classification is presented in table 3.3.

Counting of the number of branches has been done at breast height and not at higher elevations in the tree.

Table 3.3: List the classes of the primary branches based on their base diameter.

Branch classes	
Class 1	$D_b \geq 50$ mm
Class 2	20 mm $< D_b <$ 50 mm
Class 3	$D_b \leq 20$ mm

In order to gain more information about the evolution of the main branches in the height, relation graphs were made. These relation graphs include a D_b-length relation, a D_b-weight relation and diameter decay of the main branches over the height.

The relation between length and base diameter was determined by measuring the total length and corresponding base diameter of 324 randomly picked branches throughout the forest. For the same 324 branches, also the diameter evolution over the height of the tree is estimated by measuring the diameter at every meter from the breast height until the tip of the branch, this is done for 10 branches per class (30 branches). Additionally, weight measurements were done after the test series to obtain a weight-diameter relation for this type of vegetation. These relations are presented in graphs given in appendix B.1.

This data is mainly used for determining the distribution of relevant tree parameters such as the average frontal area over the height of the tree. The number of branches, the average diameter and the average frontal area distributions over the height are shown respectively in figure 3.3 and figure 3.4. It must be noted that the information relative to the first 2 meters of these graphs (z ≤ 2m) is directly measured, while higher in the tree (z ≥ 2m) is calculated for the primary branches (branches that sprout from the knot of the trunk) by using the diameter decay of the branches over the height and the diameter-length relation graph described in appendix B.1.

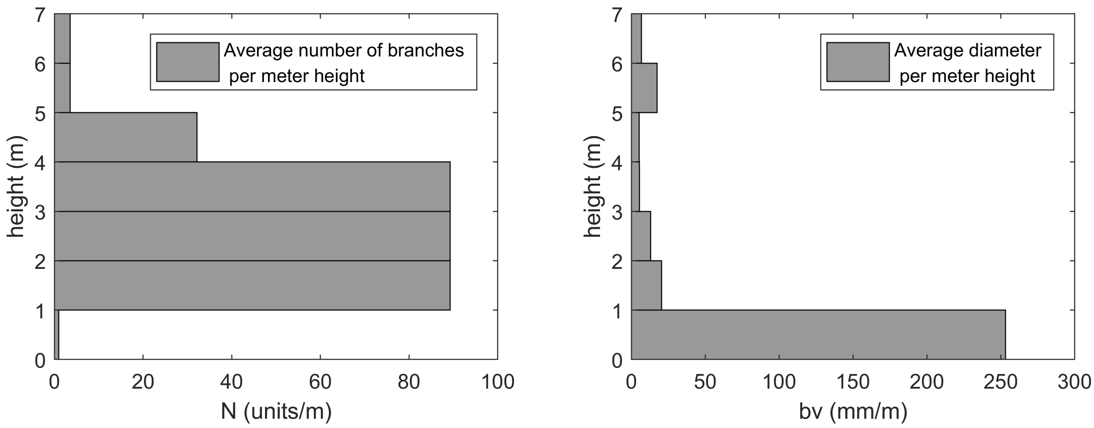

Figure 3.3: Left: The distribution of the number of branches (N) over the height of the average tree in the flume. Right: The average diameter (b_v) over the height of the average tree in the flume.

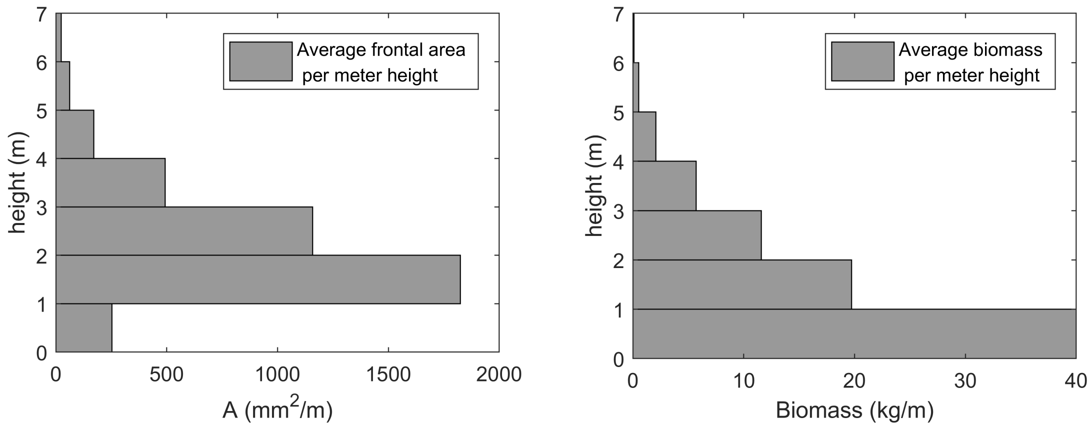

Figure 3.4: Left: Average frontal area (A) distribution over the height of the average tree in the flume. Right: The average biomass ($Biomass$) distribution over the height of the average tree in the flume.

Leaves

The total amount of the removed leaves was weighted after the experiments and resulted in total fresh weight of approximately 90 kg. The dry weight (biomass) of these leaves is determined by using the ratio between fresh and oven dry weight. Due to the large amount of biomass, this is done by taking 7 samples of the total amount of leaves. The fresh weight per sample is measured and afterwards dried in a oven at 60 for 48 hours. The average ratio was 0.45 and lead to a total dry weight of 38 kg. Using a specific leaf area of 145 cm^2/gram out of literature (Wuyts et al., 2009), the corresponding frontal area of the leaves is 551.1 m2. This corresponds to approximately 18 m^2 per tree. A well known parameter to account for the area contributed by the leaves is the leaf area index (LAI). Another parameter is the ratio leaf area to total plant area, this value was determined for white willows and resulted in a value between 3.5-3.6 (Armanini et al., 2005).

Damaged Biomass

It is crucial that the vegetation withstands future storm events to be able to function as part of the flood defense system. To be able to assure this, the vegetation needs to be tested under storm conditions. The damage is measured by documenting the completely damaged branches and leaves out of the willow forest. Completely damaged means that the branches are no longer attached to the tree and are floating on the water surface. The floating parts of the tree were captured after each test series and the fresh weight was measured on a scale (0.2 kg accurate). The fresh weight of the floating biomass can be seen in table 3.4. A more in depth documentation of the damage is given in appendix B.2.

Table 3.4: Presents the biomass measurements

Overview gathered biomass	
Test series 1	-
Test series 2	6.8 kg
Test series 3	6.6 kg
Test series 4	3.9 kg
Total	17.3 kg

The total amount of damage is approximately 17 kg for the whole forest, which is less than 1 % of the total amount of biomass (approximately 2600 kg). It can be said that the willows could withstand storms of 1.5 meter significant wave heights.

3.2.2. Branch structure method

The contribution of the side branches to the frontal area is assessed by using a branch structure method. The branch structure method has already been used on Salix Alba branches of 70 cm in the experiments performed by Järvelä (2004). This method assumes that the tree is self-similar, which means that the structure of part of the tree, for example the main branch, is the same as the structure of the whole tree model. It is expected that the the outcome of Järvelä, which is for a branch of a Salix Alba tree, should also hold for the average tree in this project.
The method contains 3 rules: The tip of the branches are assigned to be the lowest order, which is order 1, the convergence of two branches of the same order (m) result in a branch which is an order higher (m+1). In the case of convergence between two branches of not the same order, for example order (m) and order (m+1); the resulting branch takes the order of the highest order branch (m+1). In figure 3.5 the method is illustrated.

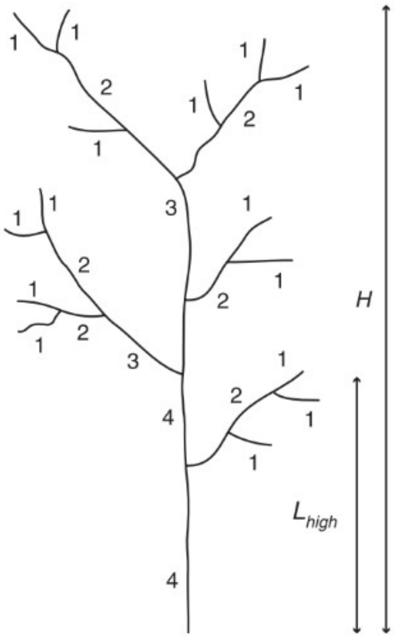

Figure 3.5: Strahlers ordering scheme (Source: (Järvelä, 2004)). The tips of the branches are the smallest order and evolve to higher order branches.

The three parameters needed for this method are:

$$R_B = N_m / N_{(m+1)}$$

$$R_D = d_{(m+1)} / d_m \ \approx (1/2) \mathrm{R}_B$$

$$R_L = L_{(m+1)} / L_m \approx R_D^{(2/3)}$$

Where N is the number of branches, d is the average diameter and L is the average length within an order. R_B (branching ratio) gives the number of branches that an branch can support, R_D (diameter ratio) is the ratio of the diameter difference between orders and R_L (length ratio) is the ratio of the length differences between subsequent orders. It is also stated that the length ratio is approximately equal to the diameter ratio to the power 2/3 and the diameter ratio is in the order of half the branching ratio for elastically similar branches (McMahon and Kronauer, 1976). To completely define the tree structure down to the smaller branches there are four additional parameters needed according to Jarvela, namely: smallest diameter at the tip of the branch (d_{min}), the height of the plant (H), the diameter of the highest order branch (d_{high}) and the length of the highest order branch (L_{high}).
Knowing these parameters and the respecting ratios, the total area of the tree can be computed by starting with the vegetation parameters of the highest order branch and iterating until the average diameter of the smallest order (tip of the branches) reaches the value of d_{min}. The highest order branch is generally the trunk.

However, in the case of pollard willows, these rules do not hold for the transition between trunk and primary branch, therefore the highest order branch is set to the primary branch. In this way, the frontal area out of this method is excluding the area of the trunk. The detailed sketches of nine primary branches are used to obtain the relevant parameters for this method. One example for a detailed sketch of a class 1 (D>50mm) and class 2 branch (20mm< $D \geq$ 50 mm) is given in Appendix B.3.

Table 3.5: Average parameter values for each order estimated out of the nine detailed sketches. The decimals for the number of branches (N) is due to averaging of this parameter over the nine branches (detailed sketches).

1^{st} order			2^{th} order			3^{th} order		
D (m)	L (m)	N (units)	D (m)	L (m)	N (units)	D (m)	L (m)	N (units)
0.005±0.001	0.53±0.106	44.2±24.8	0.009±0.003	0.76±0.30	10.5±5.87	0.054±0.01	3.41±0.94	1±0

Table 3.5 gives the average value for the diameter, number of branches and the length within an order. The sample branches contain three orders in the case of class 1 and class 2 branches, while smaller branches that sprout from the trunk have less. An impression of the three branch classes is given in figure 3.6.

Figure 3.6: Example of branches for each class. The relative small branch is class 3, the middle size is a class 2, and the largest branch type is a class 1 branch.

Table 3.6: The computed ratios between the orders

	1^{st} order to 2^{th} order	2^{th} order to 3^{th} order
R_B	4.19	10.56
R_D	1.71	6.26
R_L	1.44	4.50

The obtained ratios between the second and the third order are not similar to the ratio between the smaller orders. The ratios of smaller orders are well in order with the branching rules for elastically similar branches, namely R_D is approximately equal to Rd to the power (2/3) and R_B is approximately two times the Rd ratio. While the ratios between the second and third order deviate from these rules. It is therefore decided that the calculation for the total frontal area is based on two separate values for each ratio (R_B,R_D and R_L) and not on the averaged ratios for the whole canopy. The number of branches at the knot were counted for each class for each tree in the flume with the corresponding average diameter per class. Also the d_{min} is set in the order of 3-4 mm. An overview of the initial parameters of one tree (A1) is listed in table 3.7.

Table 3.7: The initial parameters for tree A1 in the flume

	$N_{m,high}$ (m)	d_{high} (m)	L_{high} (m)	d_{min}
class 1 ($D_b > 50$ mm)	10	0.061	3.85	0.003
class 2 ($20 < D_b \geq 50$mm)	19	0.037	2.52	0.003
class 3 ($D_b < 20$mm)	29	0.013	0.82	0.003

Table 3.8: Frontal area calculation for all the branches of class 1 (Db>50mm) out of tree A1. The highest order is order m, which is generally signed to the trunk. But in this work the primary branches are the highest order. The iteration steps can be seen, as the diameter for the lowest order branch is 0.003m. This value is equal to the d_{min}.

	N (units)	d (m)	L (m)	Frontal area (m^2)
$Branch-order$				
m, primary branch	10	0.061	3.85	2.35
m-1	105	0.009	0.86	0.88
m-2	442.2	0.005	0.6	1.55
m-3	1852.67	0.003	0.41	2.56
Frontal area, total				7.29

An example is given in table 3.8, where the total frontal area is calculated for class 1 branches in tree A1. This is done in the same way for class 2 and class 3 branches, but these branches have less orders.

To gain insight on the validity of this method, the obtained factors are applied on the nine branches to obtain their frontal area. The resulting frontal areas by this branching method is compared to calculated frontal areas under the assumption that the branches are cylinders. This lead to an average overestimation of the total frontal area per branch of approximately 27 %, which can strongly be the consequence of the heterogeneity of vegetation.
The assumption of having cylindrical shapes is also assessed. The tapering form of the branches is shown in figure 3.7. This suggests that the branches have the shape of a trunk of a cone is more appropriate to determine the diameter evolution over the vertical, therefore the calculation is adjusted to this shape.

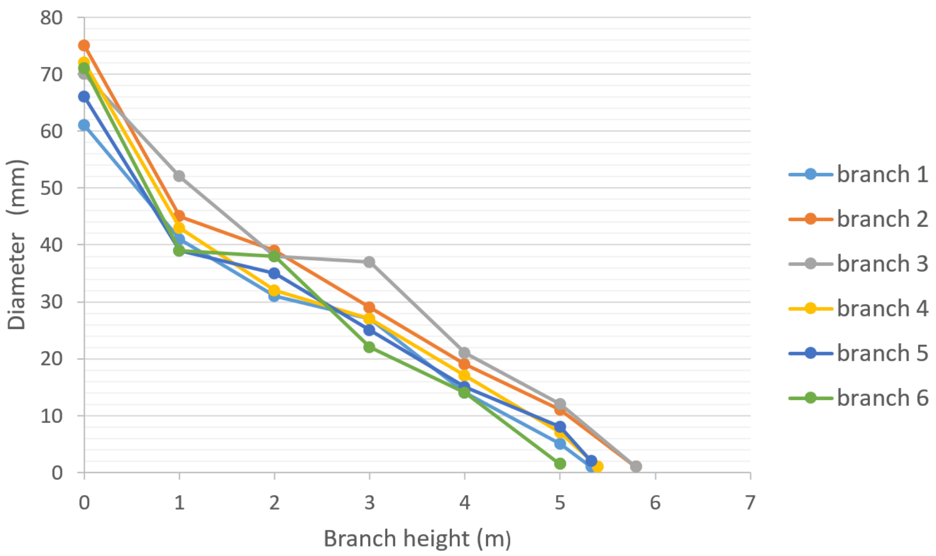

Figure 3.7: Presents the diameter decay of branches from class 1.

3.2.3. Tree models 1a, 1b and 1c

Tree model 1 follows from the manual measurements presented in the previous sections. The analysis presented in the previous sections of this chapter made clear that there are several ways to define the frontal area distribution of woody vegetation. The first method is based on the primary branches only, this is referred to as tree model 1a, which is called the primary tree model. Secondly, the addition of side branches by following the branching method leads to tree model 1b and is called the branching tree model. Lastly the branching tree model is adjusted slightly to account for trapezoidal shape branches, this adjustment results in tree model 1c.

Primary tree model

The tree model solely based on measurement data can be seen as a lower limit for obtaining frontal area and biomass. The tree measurements were done at breast height level for the primary branches (branches that sprout out from the trunk), and not at higher levels in the tree. The values for the higher layers (z > 2 m) are calculated by using the evolution of these primary branches over the height, which do not account for side branches (see appendix B.1). This tree model is presented in figure 3.8. The frontal area per tree range between 2.6 m^2 and 5.7 m^2 and the distribution over the height is given in figure 3.4. The average tree over the flume contains according to this tree model, a total frontal area of 3.95 m^2.

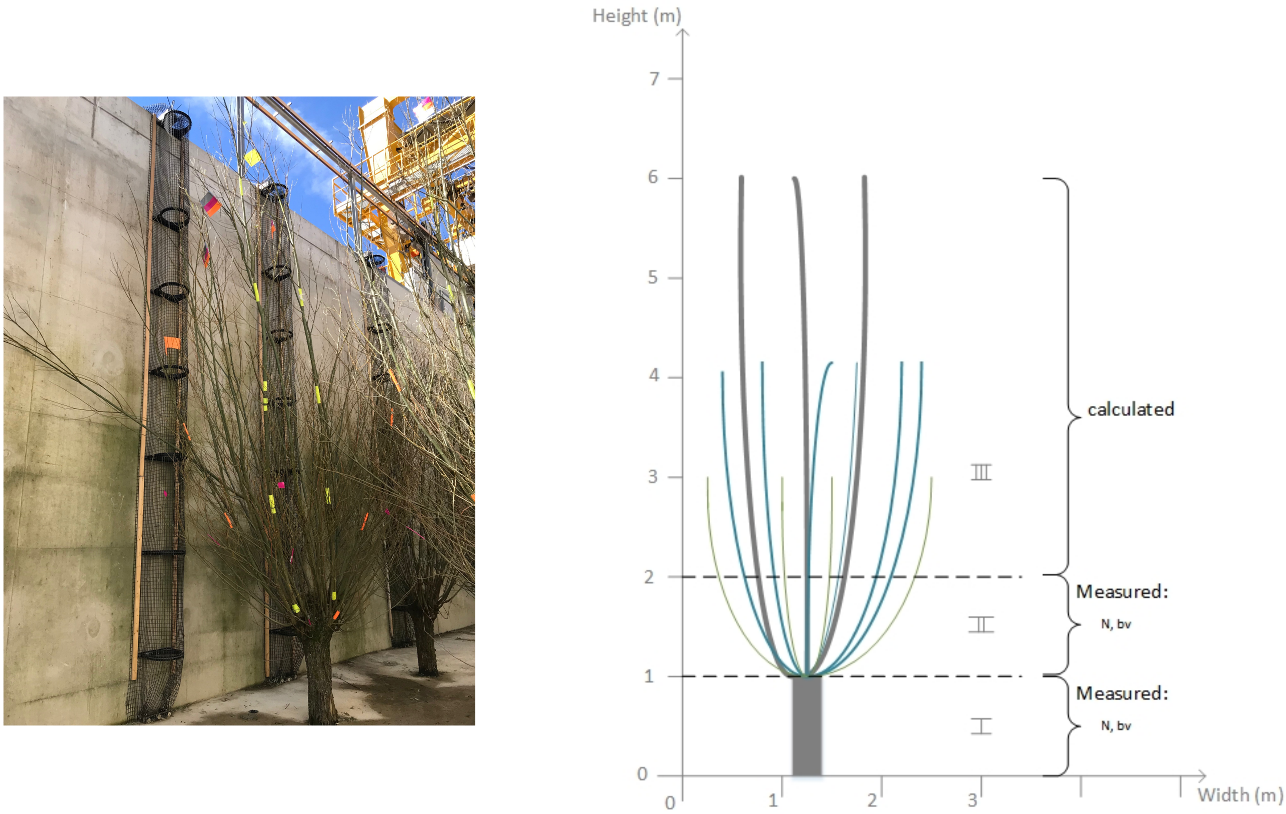

Figure 3.8: Willow tree at the edge of the forest in the flume (Left). The tree model solely based on tree measurements (Right). Regions 1 and 2 are measured, while region 3 is estimated by making calculations

Branching tree models

Looking at figure 3.8, one can see as the tree height can be split in 3 regions. In order to come to more realistic estimations in region 3 (illustrated in figure 3.8), the branching method described in section 3.2.2, is used. The branching method results in a total frontal area per tree. An assumption of this method in previous literature is a linear distribution of the frontal area over the vertical, which is not the case for the used willows. To get an indication on the distribution for willows, one extra set of measurements was done on one willow tree on the 27th of february 2019. This tree located at the West Maas en Waal, where the willows used during the experiments originate. This willow is also of the species Salix Alba and contains branches of the same age. The assumption is that the diameter and density distribution over the vertical for this willow, also holds for the willows used during the experiments. The measured willow tree and the vertical distribution of the frontal area are shown in figure 3.9. The frontal areas out of this model are between 6.5 m^2 and 18 m^2 per tree, where the average tree has a total frontal area of 11 m^2.

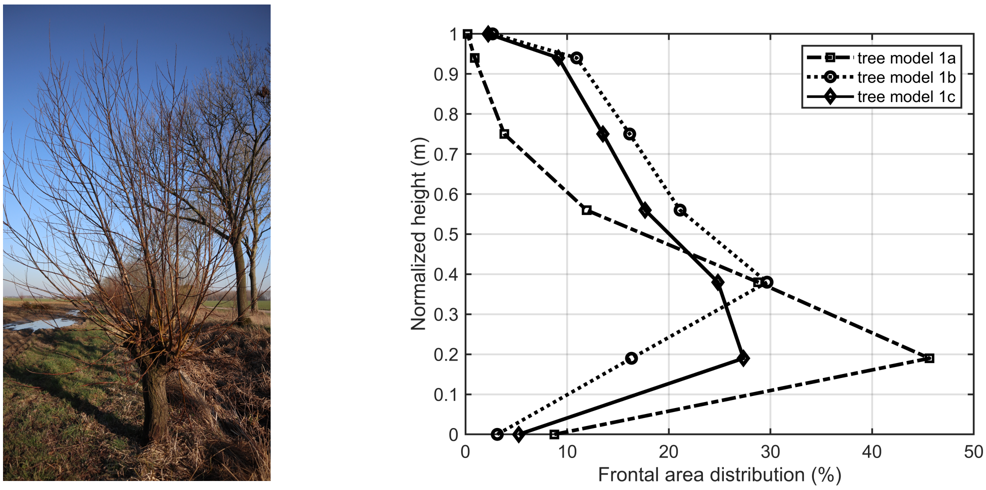

Figure 3.9: Willow tree measured at West Maas en Waal (Left). The frontal area distribution for tree model 1a , 1b and 1c expressed in percentages over the normalized height.(Right).

Including the amount of side branching by means of the branching method increased the total frontal area approximately by 182%. The frontal area distribution over the height is also different between the two models (see figure 3.9). Firstly, there is a larger spread of the frontal area in the height for tree model 1b relative to tree model 1a. The largest amount of area is found slightly under half the length of the tree (≈0.4), while for the primary branch model (tree model 1a) this is reached just above the knot of the tree (≈0.2).

Finally, the adjustment of the branch shape results in an frontal area of approximately half of tree model 1b. Tree model 1c is between the two extremes seen as tree model 1a and tree model 1b (see figure 3.9). Note that figure 3.23 states the frontal area distribution in percentage over the normalized height for the average tree in the flume.

3.3. TLS measurements analysis

3.3.1. Preprocessing

Preprocessed data has been provided in the format of XYZ coordinates. The preprocessing of the raw scans has been done in a program called SCENE. Registration of the point cloud is done during this step, which includes target recognition, clipping etc. Additional processing steps were taken before the actual parameter extractions, which include sub-sampling, segmentation and filtering of the point cloud. The point cloud sizes are around 70 million points, which makes sub-sampling a necessity for the sake of workability (available memory and computation time). This framework is shown in figure 3.10.

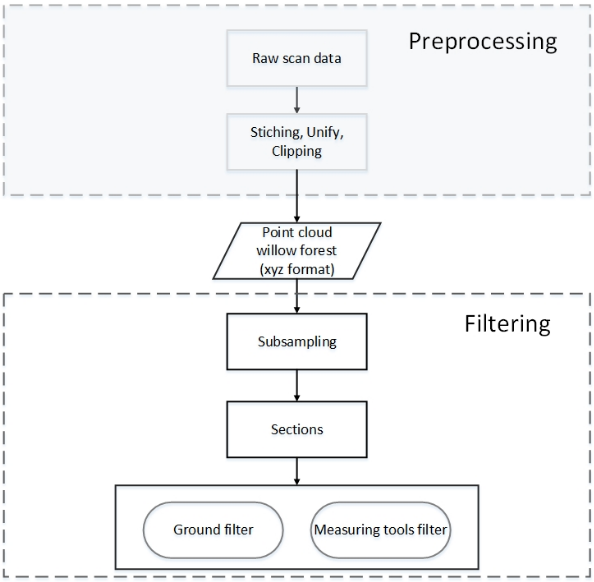

Figure 3.10: Schematic overview of the workflow for TLS data processing

The filtering step and further TLS data analysis is done in CloudCompare, which is a 3D point cloud processing software and in Matlab. The parameters that are taken out of the point cloud are the trunk diameter, tree height, frontal area and the leaf contribution factors. Also the canopy structure is analysed. Two examples of the total point clouds after the preprocessing step are shown in figure 3.11.

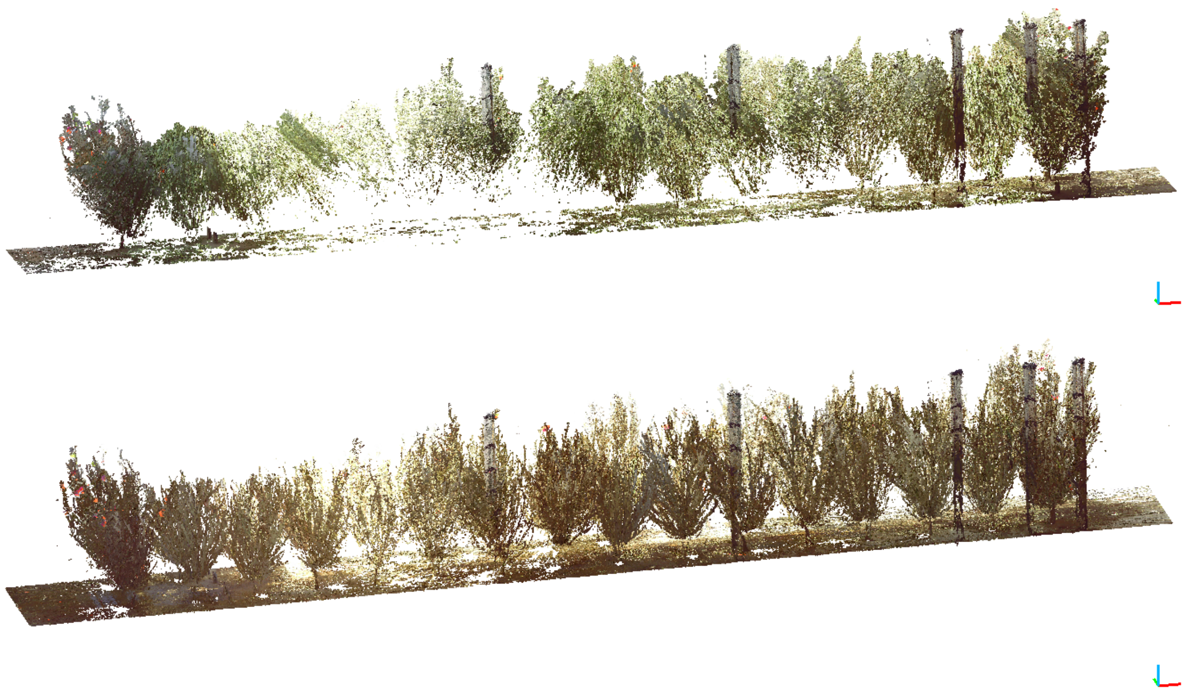

Figure 3.11: Impression of the point cloud with leaves, $scanT001B$ (first panel) and without leaves, $scanT013B$ (second panel). These point clouds show the full forest in the flume. A more complete presentation of the forest can be seen out of the point cloud without leaves (second panel).

3.3.2. Quality of the Point Cloud

Looking at figure 3.11, it can be observed that the point cloud is more dense at the top of the tree and even has missing points in the lower parts of the trees for scan ($T001B$). Overall, the scans performed on the forest without leaves are more accurate in terms of capturing the tree structure than the ones with leaves, which have bigger shadow areas. Therefore the scans without foliage ($T013B$) are used for further analysis.

An impression of the level of detail for the tree structure can be seen in figure 3.12. Even though the scans without foliage are used for analysing the point cloud, there are still missing sections of the trees. In fact, It can be observed from this figure that the point cloud density near the trunk is relatively sparser than in higher elevations in the tree. These trees (A1 and A2) that are well captured relative to other trees in the flume, yet have few missing sections. These are observed at the outer edges of the trunk, just under the knot of the trees. For both trees this area is situated at the facing edges of the flume width. In other cases the trunk is not even captured, described more in subsection 3.3.4.

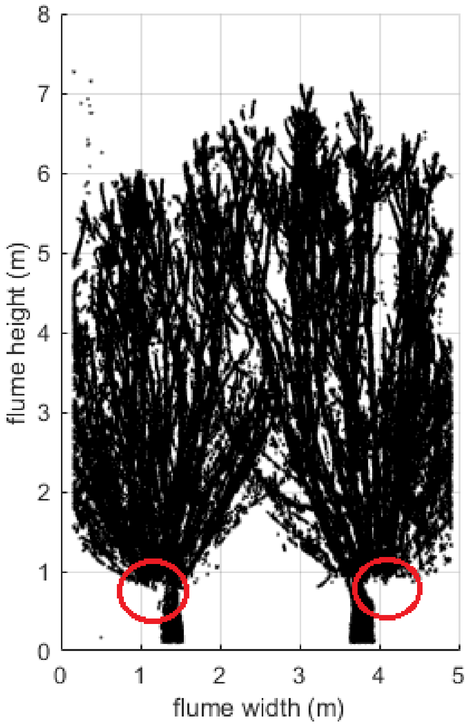

Figure 3.12: Cross-section of the first two trees in the flume from the direction of the wave paddle, namely tree A1 and A2 (Left). The ground points and nets are filtered out. An example of these trees in the foliage state. The flumes bottom had not yet been prepared, also the measuring tools and nets are visible (Right).

Factors that may have influenced the quality of the point cloud are the atmospheric conditions, the properties of the vegetation and the scanning geometry (Soudarissanane, 2016). Properties of vegetation such as the density of the branches, tree height or the shape can influence occlusion. Also, the location of the patches of missing points in the current scans (circled red in figure 3.12) and the positions of the scanner itself (in the center of the width of the flume), show that the configuration and placement of the scanner (distance object-scanner, angle) also play a role in finding this results.
The distribution of the point density inside the canopy and the evolution of the laser beam penetration are also object of analysis in this thesis and they are treated in section 3.3.5 and in section 3.3.8 respectively.

3.3.3. Alphashape area estimate

The frontal area of the point clouds are obtained by using the *alphashape* function in Matlab. The *alphashape* function can be used in 2D and in 3D and it creates a bounding region around the points. This bounding region (or alpha shape) can be created with different levels of detail, controlled with an alpha parameter or alpha radius, which varies from 0 to $+\infty$. The alpha radius is equal to the squared radius of the cyan circles, shown in figure 3.13. If this parameters is large or even infinite, the shape takes the convex hull of the point set. When this parameter is lower, it can lead to non-convex shapes, multiple regions and holes. The appearance of separate points, edges or faces cannot occur because the function in Matlab prevents this by always giving regularized alpha shapes as outcome.

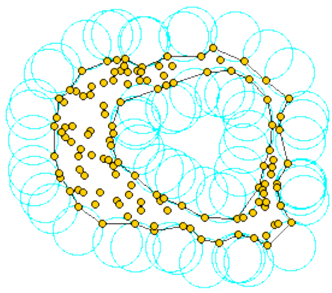

Figure 3.13: Alpha shape function,Source:(Tran Kai Frank Da and Yvinec, 2019)

Different values for the alpha radius are tested to reach to a good representation of the frontal area of the trees. These graphs are given in figure 3.14 and in appendix B.4. The analysis of these graphs showed incomplete branch structures by the point cloud, therefore an overestimation of frontal area of approximately 13 % is seen as acceptable. This coincides with a value of the alpha parameter of 0.01, which is chosen as constant for the further analysis.

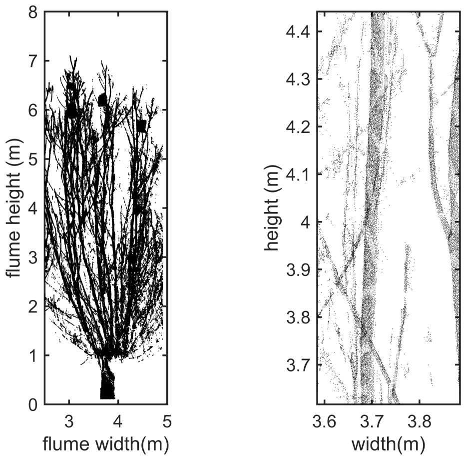

(a) point cloud of tree A1

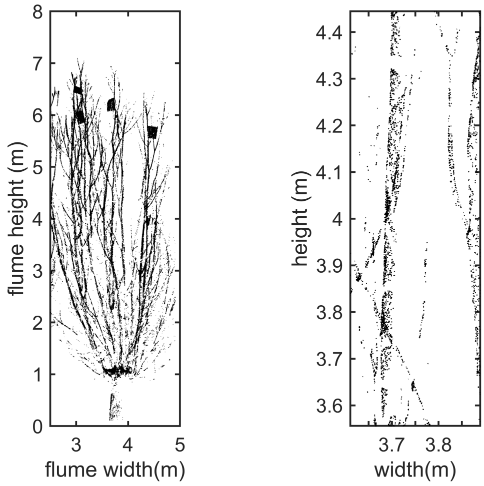

(b) alpha shape radius of 0.001.

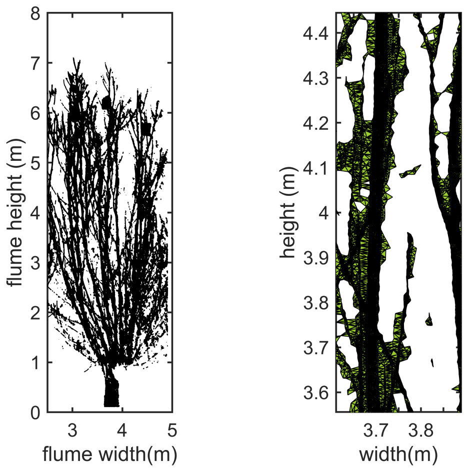

(c) alpha shape radius of 0.01.

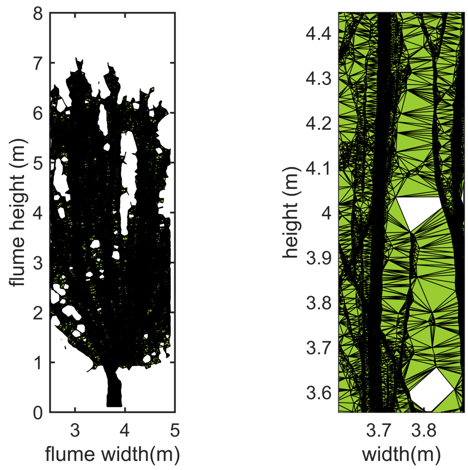

(d) alpha shape radius of 0.05.

Figure 3.14: Different values for the alpha radius and the corresponding area reconstruction.

3.3.4. Trunk dimensions

The trunk dimensions are relevant for obtaining wave attenuation especially for lower water levels. However, the laser scanner (with the used geometry and settings) is not able to capture the trunks very well in terms of frontal area (see figures 3.16 and 3.12). Therefore an analysis is done for each point cloud, including the calibration scan T031B, to obtain the trunk dimension. Even though there were no trees present during the calibration tests, still approximately 20 cm of each trunk was present.

The analysis of the trunks is done by using an circle fitting method, as the trunk diameters are not captured as complete circles by the TLS. The circle fitting method is able to predict the course of a circle without needing a full representation of the trunk out of the point cloud. The applied circle fitting method is done with a Matlab function by Nikolai Chernov, which is based on V. Pratt least-square method. This script is adjusted in order to exclude unreliable outcome. This includes overestimation of the trunk dimensions due to a lack of points or due to insufficient distribution of points around the circumference of the trunk, respectively shown in figure 3.15. The additional parameters to the function involve a minimum amount of points and a minimum angle θ (see figure 3.15). These parameters were set constant to 62 points and 50 degrees for each point cloud.

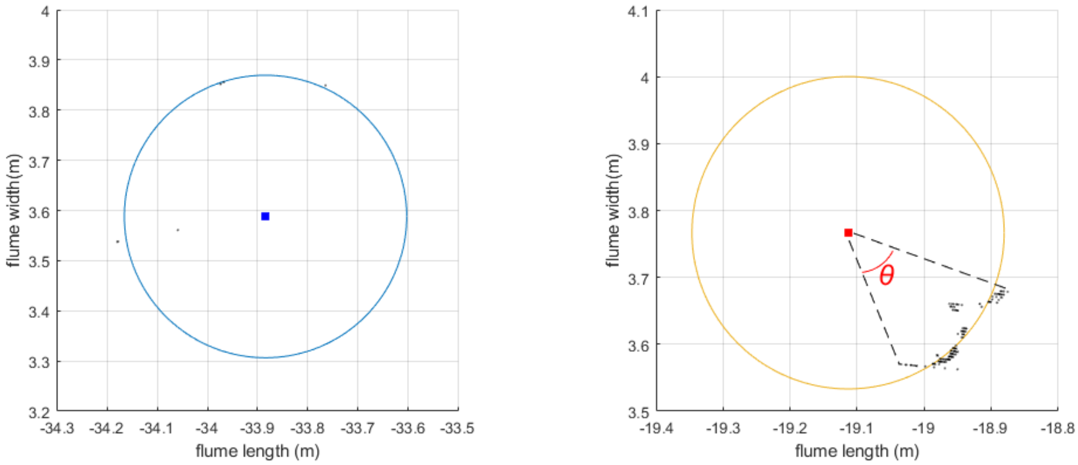

Figure 3.15: *Left*: Gives an example of a lack a points which lead to overestimation of the trunk diameter, *Right*: Gives an example of insufficient distribution of the points around the trunk (small angle θ), which lead to an overestimation of the trunk dimension.

For each scan a strip in the z-direction is used to conduct the circle fitting. The relative error and the absolute error are listed in table 3.9. Only the calibration scan obtains 100 % detection (32 trunks), while the remaining scans detect less than 94 %. It is observed that the detection decreases with the increasing occurrence of vegetation biomass above the trunk region. The trunk detection decreased till 25 % for foliage state of the trees, although if the trunk is captured, then the average error reaches 28 %.

Table 3.9: Lists the trunk detection (%) and the regarding errors (%) for each scan.

Scan	Tree detection (%)	Relative error (%)	Absolute error (%)
T031B	100	-9	11
T023B	94	-14	17
T013B	81	-11	19
T001B	25	-28	28

However, a situation as the calibration scan is not possible for a real willow forest, thus it is not a practical way to retrieve trunk dimensions. Usually the presence of vegetation leads to sparser point density, thus points that follow complete circles are not common in practical scans. The remaining scans namely T023B, T013B and T001B, are therefore a better representation of the practicality of the FARO scans during different vegetation states (50% density, without-and with foliage).

3.3.5. Tree height and canopy shape

The tree height, especially the canopy height and structure are relevant parameters for wave attenuation. The tree height is obtained for each tree in the flume, and is compared to the measured values of the tree height. The tree height extraction from the point cloud is done by first dividing the flume into areas of approximately 2.5 x 2.5 m, which contain one tree. Afterwards, the volume above the trunk is selected for each tree and in which the highest value of the z-coordinates is selected. The requirement of having a position above the trunk for the height estimation is to avoid occlusion of the neighboring tree, which generally leads to an height overestimation if not taken into consideration. An example of occlusion between neighboring trees is given in figure 3.16. The height comparison between TLS found values and the measured values are given in appendix B.5.

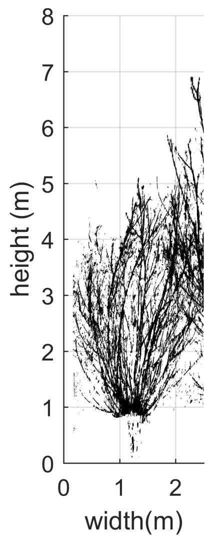

Figure 3.16: Shows an example of occlusion on the right side of a tree in the flume

Besides the tree height, the canopy shape is of importance for the wave dissipation as the parts of the trees where most of the biomass is situated, coincides with increasing values of wave dissipation. The analysis of the canopies is done by looking at different trees in the flume. An overview of the tree numbers and the positions of the laser scanner is given in figure 3.17. The canopy structure is analysed by plotting the point density per unit volume against the Z-axis, shown in figure 3.18. Large amount of the biomass is situated in the centre line of the trees,and decrease with larger distance from the centre line. Figure 3.19 instead is used to analyse the point cloud densities as function of the distance from the bottom of the flume. It can be seen that the densities are larger near the knot and decrease with increasing height for a relatively good point cloud, while for a poor point cloud (tree L1) this evolution is not present. Also a steep peak can be observed from figure3.19, which is the location of knot of the wilows. Furthermore, the blockage of the laser beams by the dense leaves can be seen from figure 3.20.

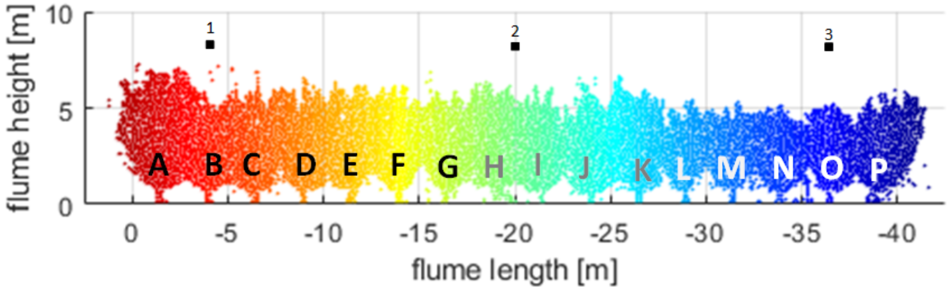

Figure 3.17: Overview of the tree numbers and the scanner positions

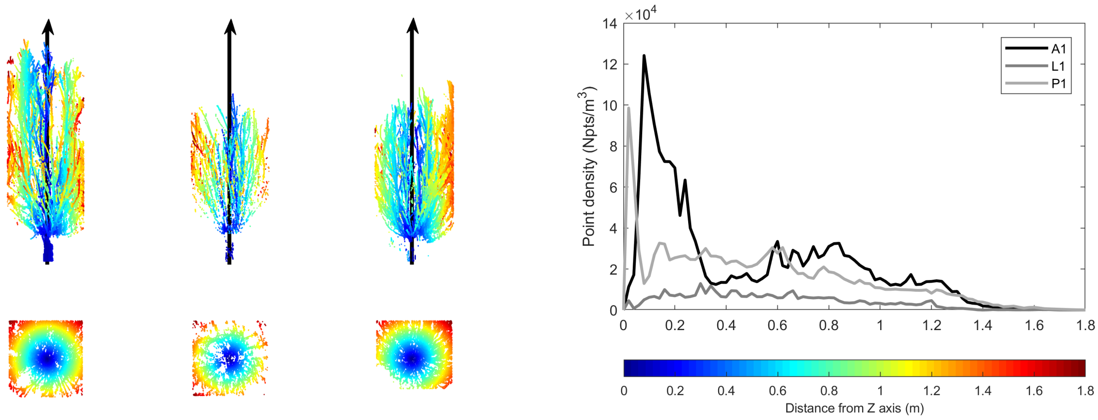

Figure 3.18: Tree (*a*) A1, (*b*) L1 and (*c*) P1 are presented. The graph presents the point density against the distance from the Z-axis given with the black arrow. .

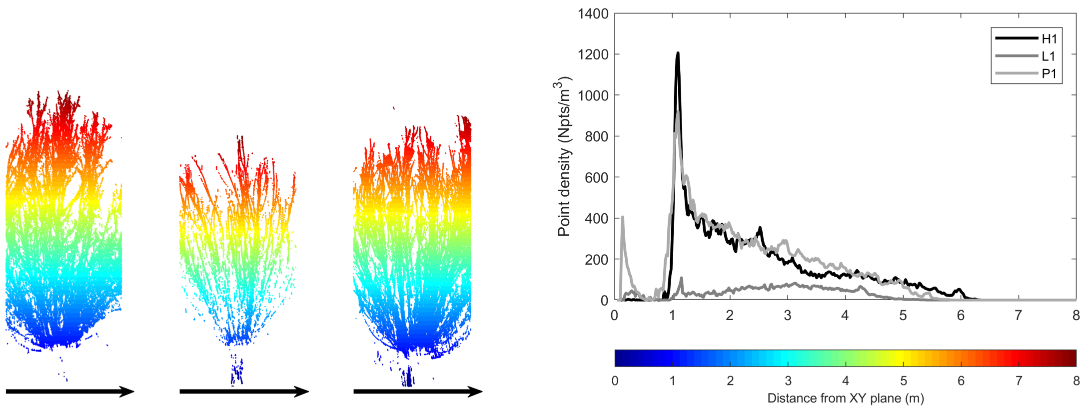

Figure 3.19: Tree H1 (*a*), (*b*) L1 and (*c*) P1 are presented. The graph presents the point density against the distance from the XY-plane presented with the black arrow.

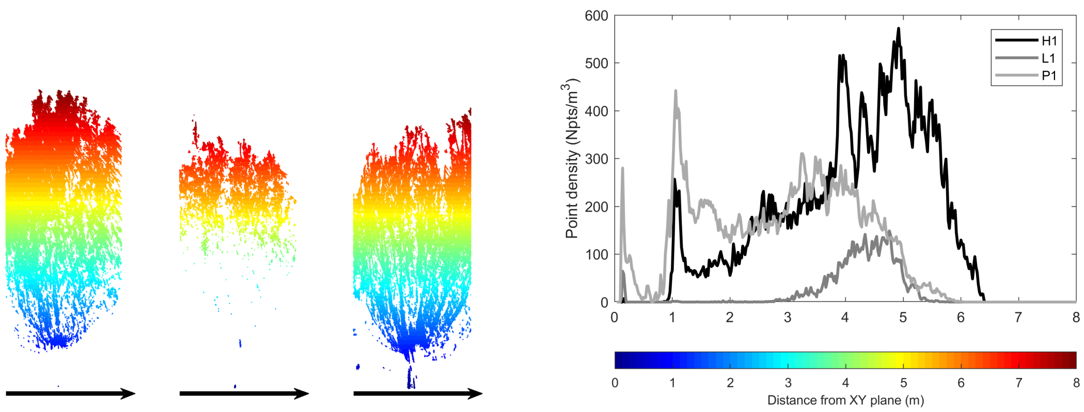

Figure 3.20: Tree H1 (*a*), (*b*) L1 and (*c*) P1 are presented. The graph presents the point density against the distance from the XY-plane presented with the black arrow

3.3.6. Frontal area

The frontal area is estimated in Matlab using the *alphashape* tool with a alpha radius of 0.01. This is done for each single tree, where layers of 1 meter height are made. For each layer the frontal area is calculated and summed up over the height to obtain the total frontal area of the tree. The procedure is shown in figure 3.21, where an example of a single tree is given in the first panel, the area estimation by the *alphashape* function is presented in the second panel, and the estimated frontal area over the height is illustrated on the right panel of the figure. The frontal area is based on the 2D representation of the point cloud facing the wave paddle. This method assumes that the amount of branches behind each other over an width of 2.5 m is negligible. The total frontal area and the comparison with the calculated frontal area for each single tree is included in appendix B.6.

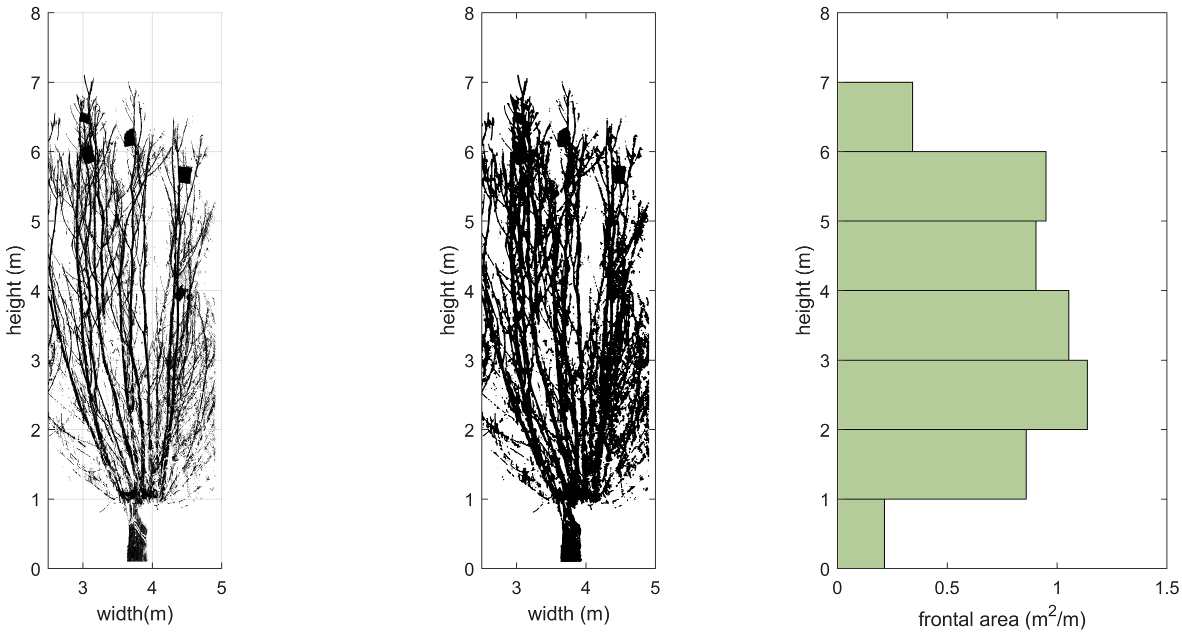

Figure 3.21: Left: Gives a segment of the area containing one tree out of the point cloud ($T013B$, tree A1 without leaves). Middle: Gives the area reconstruction out of the point cloud using a alpha radius of 0.01. Right: Gives the estimate of the frontal area over the height for tree A1.

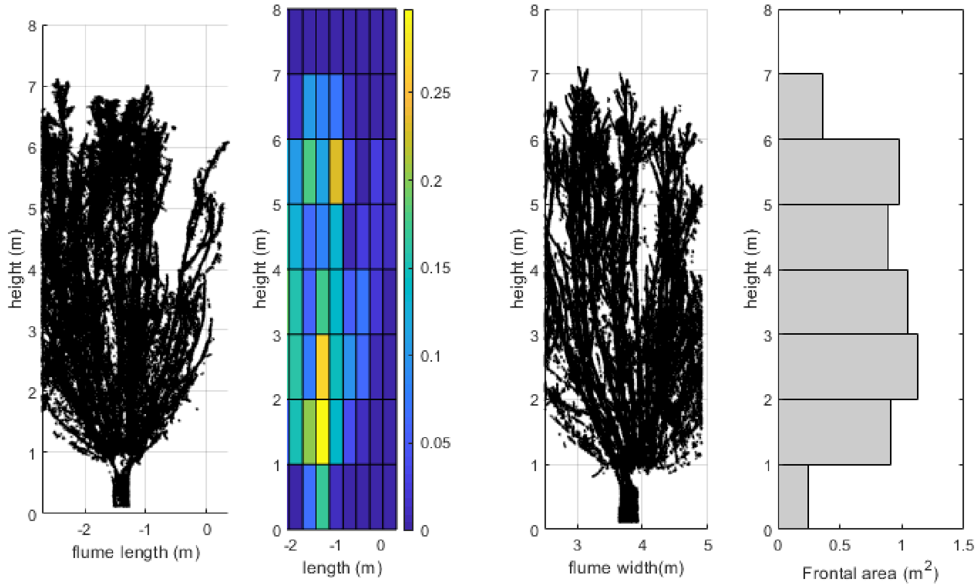

Figure 3.22: The point cloud of tree A1 is given in the length of the flume (first panel) and in along the width of the flume (third panel). A 2D overview of the bins is given as function of the vertical with the corresponding frontal area per bin in the height(second panel). The individual frontal areas are summed up per layer (fourth panel).

3.3.7. Leaf contribution

Deciduous trees mainly go through two extreme states during the year, namely the foliage state and the leafless state. The contribution of the leaves can have a considerable effect on the wave dissipation and is therefore a relevant parameter to obtain from the TLS.

The leaf contribution is defined as a factor that indicates the difference in frontal area between the two cases (case with leaves and leafless case) relative to the leafless case. This factor is referred as the leaf factor (LF). For tree A1, the ratio is determined by the difference between the third panel of figure 3.23 and the third panel of figure 3.21 normalized by the third panel of figure 3.21.

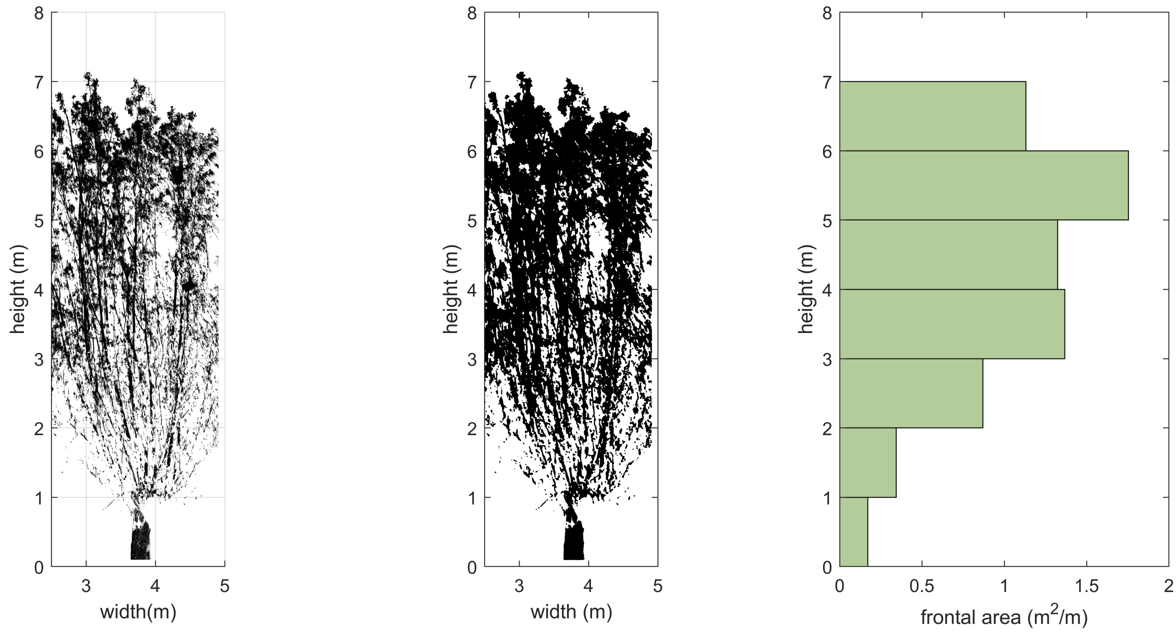

Figure 3.23: Left: Gives a segment of the area containing one tree out of the point cloud ($T001B$, tree A1 with leaves). Middle: Gives the area reconstruction out of the point cloud using a alpha radius of 0.01. Right: Gives the estimate of the frontal area over the height.

Due to the dense foliage layer, the laser pulse penetration is relatively less through the $T001B$ scan (full canopy with leaves) than for $T013B$ scan (full canopy without leaves). This leads to negative values for the leaf factor for heights lower than 3 m and are set to a value of 1. The estimated leaf factor (LF) is averaged over the number of trees for every layer. The result is plotted in figure 3.24.
The total frontal area for a tree with foliage can therefore be determined as:

$$FA_{tree} = \sum_{i=0}^{n} (FA_i * (LF_i))$$

In the case of no leaves LF is equal to 1.

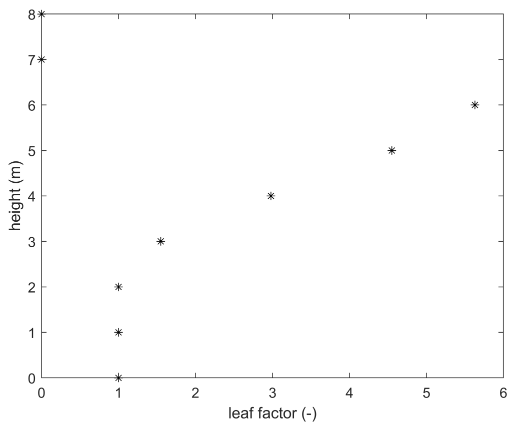

Figure 3.24: The leaf factor against the height for the average tree for tree A1.

3.3.8. Laser beam penetration

In addition to figure 3.12, which shows patches of missing points near the trunk area, an analysis is performed on the laser beam penetration and the corresponding frontal areas. This is an attempt to gain insight on the

errors in the frontal area estimates as function of the beam penetration distance and thereby to find a correction factor to account for these errors.
For trees scanned from more than one position, the effect of the beam penetration error is more complex and cannot be analysed following a simple approach. Therefore, this analysis is performed on tree P1, which is positioned at the outer edge of the forest (see figure 3.17). Hereby the assumption could be made that the tree is solely scanned from one scanning position, neglecting the pulses from the other two scanner positions (as shown in figure 3.2). An overview of the frontal area for tree P1 is given in figure **??**. This figure shows the comparison of the frontal area over the vertical from the TLS and tree model 1c (branching model). This comparison is based on tree model 1c, because it includes the side branches as well accounts for the tapering form of the branches.

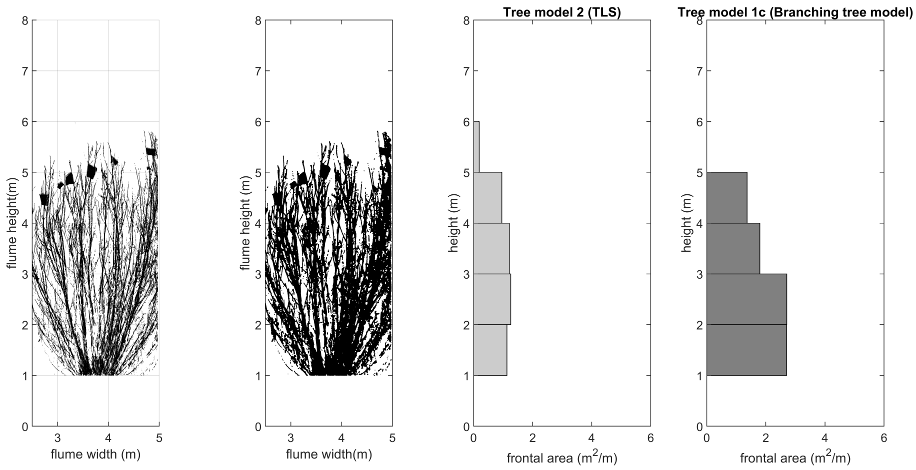

Figure 3.25: The point cloud of tree P1 (first panel) and the area construction by alpha shape out of this point cloud (second panel) give the frontal area estimates for each layer by the laser scanner (third panel) for tree P1. The frontal area used as reference gives larger values and is based on the branching method (tree model 1c) (fourth panel).

The difference in frontal area between these two measuring methods is assigned to a number of points per layer, assuming a uniform distribution of the frontal area over the canopy width and layer height. By translating the Cartesian coordinates (x, z) of these points to polar coordinates (r,θ) (see figure 3.26) with the assigned frontal area per point, bins in the beam distance can easily be selected from the r-coordinates. For each bin in r, the points (containing the assigned error) are summed up. This results in figure 3.27, which plots the distance along the laser beams against the relative error. It can be seen that the error increases with the penetration of the laser beam, as expected. Although this evolution can be strongly dependent on the area distribution over the height by tree model 1c. Thus, changing the distribution will effect the comparison with the TLS and the evolution of the error in space.

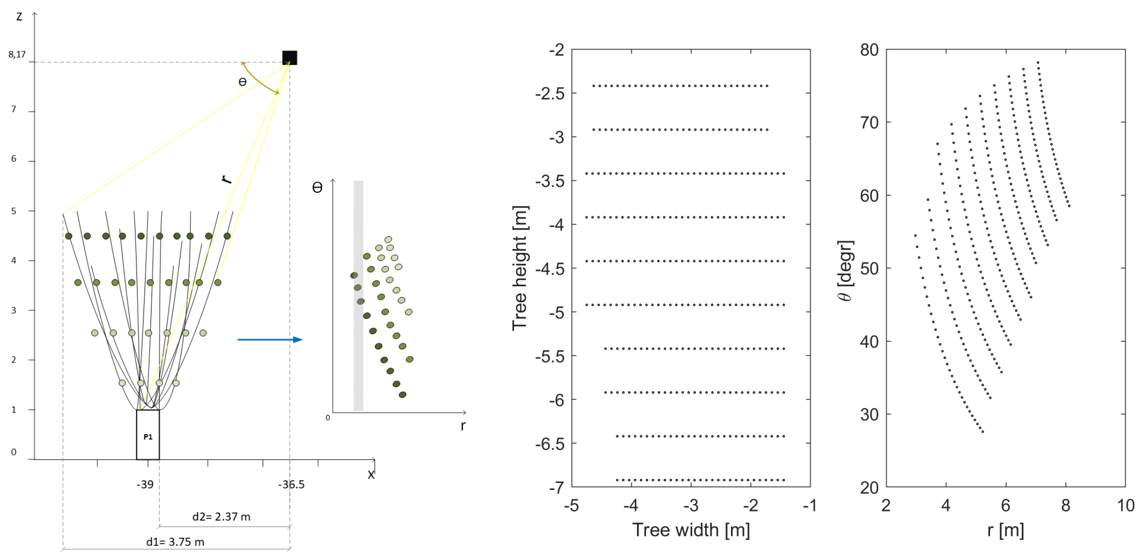

Figure 3.26: Shows tree P1, with laser position, theta as the angle with the horizon and the distance of the laser penetration, r. The y-direction is neglected. The points centered around the scanner position in Cartesian coordinates (x,z) and polar coordinates, (r,θ)

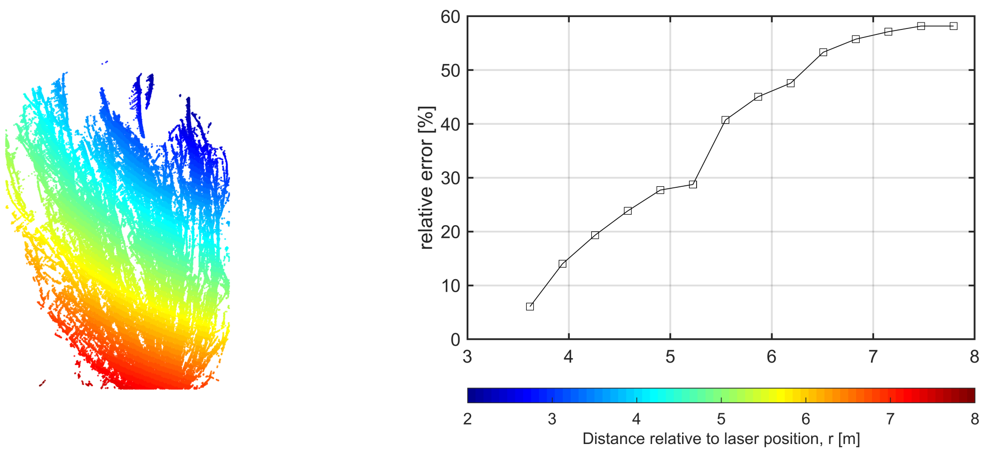

Figure 3.27: Tree P1 (a) with corresponding graph containing the relative error of the laser scanner as function of the penetration distance of the beam, r. The colors and the horizontal axis indicate the distance from the laser scanner.

If the error can be assumed to be mainly due to occlusion, it seems that a prediction can be made for the frontal area that accounts for this error by means of a correction factor.

The base assumption is that the amount of occlusion resulting from one fixed laser position is a function of the amount of blockage encountered by the laser beams. This amount of blockage is dependent on the amount of biomass density between laser position and area of interest (section of the tree).
Therefore if the top part of the tree has a high biomass density, the amount of blockage will be high. As a consequence, many points pulsed by the laser will be concentrated on the top part of the tree and less on the lower part (low beam penetration). In order to find a correction factor therefore is logical to assume that the amount of blockage is proportional to the point density. In this way, the error can be accounted for by a correction factor computed based on the point density of a specific region of the canopy.
An attempt is made to quantify a correction factor on the frontal area computed of the TLS data for tree P1.

$$FA_n = FA_{TLS,n} * f_{correction} \text{ , where} \tag{3.2}$$

$$f_{correction} = \frac{N_t}{N_t - \sum_{i=n+1}^{i=m} N} \tag{3.3}$$

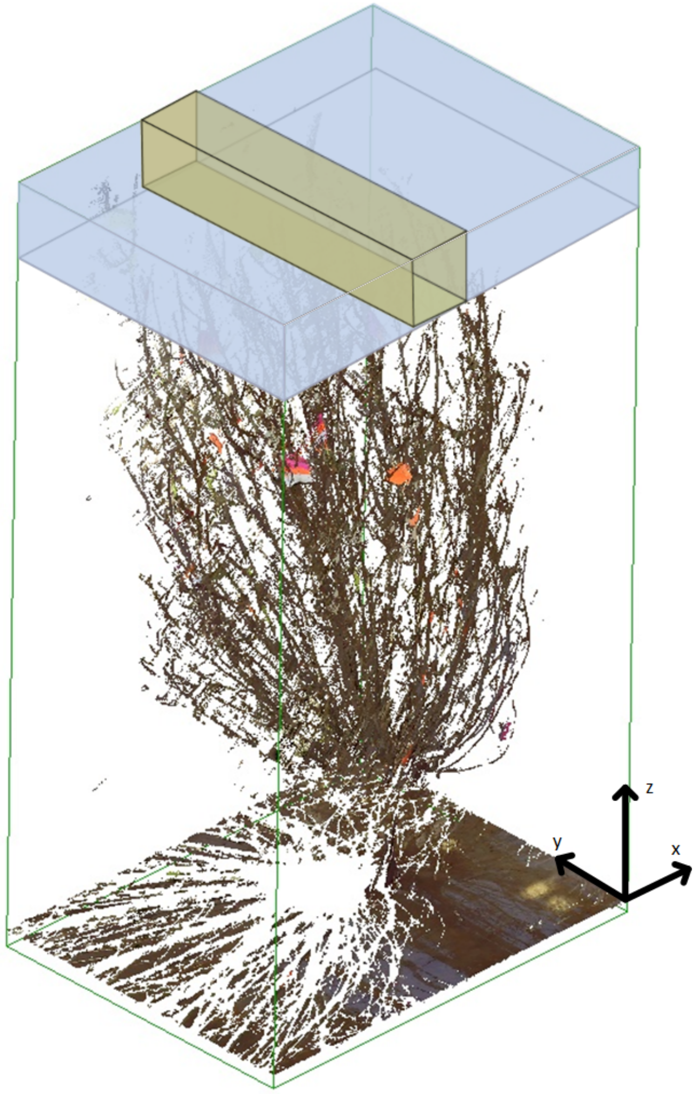

Figure 3.28: Point cloud of tree P1. The variation in the y-direction is neglected.

Where N is the number of points in the layers above the current layer, N_t is the total number of points in the point cloud (including the ground points), in this case the total number of points of tree P1 (see figure 3.28. According to the proposed definition $f_{correction}$ is 1 in the first layer. This implies, the closest to the laser, the estimate of the TLS corresponds to reality, which a fairly safe assumption given that the beam has not encountered other biomass that could cause blockage. This factor then increases for the next layers. The corrected total frontal area for P1 is approximately 7.2 m^2, this is an increase of frontal area of 2.45 m^2. The corresponding distribution over the height is given in figure 3.29.

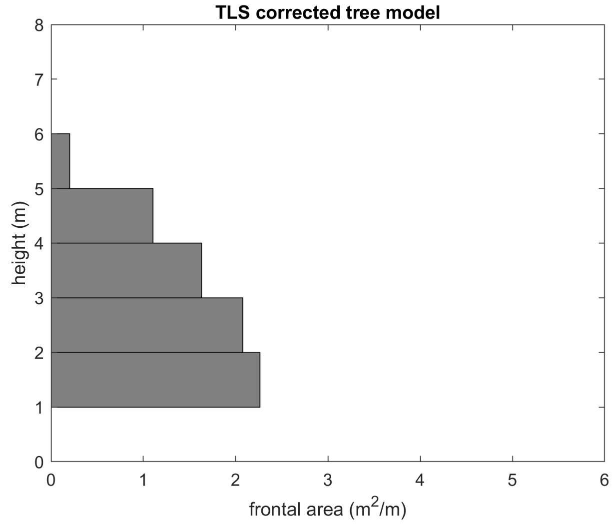

Figure 3.29: Corrected values for the frontal area of tree P1

This correction is only applicable for tree P1, as the other trees are also scanned from the other scanning positions and also influenced by the branches from the neighboring trees. Therefore the correction could not be applied to the other trees.

3.3.9. Tree model 2

Using an alpha shape radius of 0.01, the resulting frontal area out of the point cloud is between 0.5 m^2 and 5.5 m^2, which is approximately 30 % lower than the primary branch model (tree model 1a). This is the average resulting error of the whole forest, thus also including the relatively poor represented trees. The reason for this is that the TLS data seems to be more reliable on the top layers than the lower layers due to the laser pulse penetration. The upper layers still give a better estimation of the frontal area than the lower layers. This can be seen by the comparison of the average TLS values with the measured values in figure 3.30.

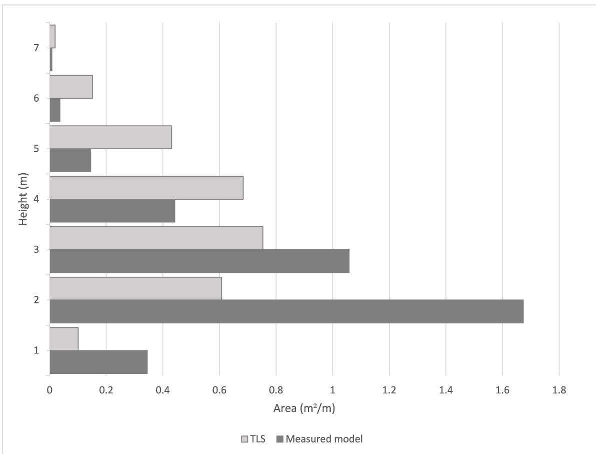

Figure 3.30: Comparison frontal area out of the TLS with the frontal area out of primary branch method (tree model 1a)

3.4. Comparison between tree models

An overview of the computed frontal areas over the height for the tree models is given in figure 3.31. From this figure it can be seen that the TLS (tree model 2) underestimates the frontal area over the vertical, but gives slight overestimation near for higher elevations in comparison to tree model 1a. The tree models from the measurements (1a,1b and 1c) result in similar frontal areas till breast height, as these areas are measured during the physical experiments.

The foliage contribution is taken into account through a leaf factor (LF) for each tree model. The total amount of leaves of 18 m^2, described in section 3.2.1, is assumed to be uniformly distributed over the height. An increasing ratio is therefore required in order to obtain a uniform distribution of the leaf area. This ratio is assumed for heights from 1 meter above the trunk till the height of the canopy, as the density of the leaves is sparse near the trunk. This estimation of the leaf contribution is only for the tree models 1a,1b and 1c.

Even though the terrestrial laser scanner shows lower values than the primary branch model (tree model 1a), it is still used as input in SWAN. This tree model tends to have relatively more uniform distribution of the frontal area and uses the Leaf factor obtained by the difference between the leaf-on scans and leaf-off scans (as described in section3.3.7). The amount of frontal area added by the Leaf factor from the TLS scans is approximately 1.7 m^2 for the average tree.

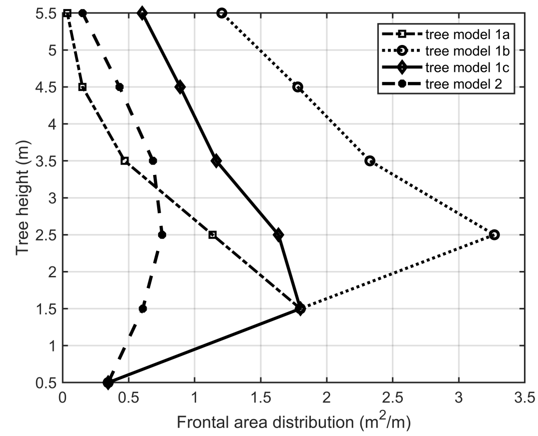

Figure 3.31: Shows the comparison between the tree models (without leaves).

4

Numerical model

The SWAN model, which includes the drag force model of (Mendez and Losada, 2004) implemented by (Suzuki et al., 2011b) is used to account for vegetation. The tree models obtained in the previous chapters are used as vegetation input to reproduce the physical modelling results. First, the numerical model set-up and model calibration are explained in section 4.1. The analysis of the model outcome is presented in section 4.2. Finally an overview is given of the relevant findings from this chapter in section 4.3.

4.1. Numerical model set-up

4.1.1. General model description

SWAN (Simulating WAves Nearshore) is a practical tool for computing waves in coastal areas (Booij et al., 1999). This phase-averaged model uses the action balance equation instead of the energy balance equation, due to the presence of currents nearshore. This balance is equal to source terms, which redistribute, dissipate or add energy to the equation (Delft). SWAN is able to account for physical processes such as wave energy dissipation due to white capping, bottom friction, depth-induced breaking, wave energy generation by wind, and shifting due to wave-wave interactions like quadruplets (in deep and intermediate waters) and triads (more apparent in shallow water). Furthermore, depending on the application, the user can decide to include wave dissipation due to mud, turbulence or vegetation. The vegetation module is a source term in SWAN using the Mendez and Losada formula (see equation (Suzuki et al., 2011a).

4.1.2. Model set-up and calibration

The model is used in its 1D stationary, third generation mode in Cartesian coordinates. A regular computational grid is set to extend pass the dike and reaches up to 260 meters. The bottom profile is equal to the flume setup during the experiment, excluding dike behind the forest, and the grid size is 1 m. The frequency space is discretized in 180 bins between a lower frequency of 1/35 Hz and the highest frequency of 2 Hz. The relevant wave parameters are outputted at the locations of the WHMs and Radacs used during the experiments. Mainly the positions relative to WHM06 and Radac02 are of interest in this study, which are respectively locations in front and behind the forest. An overview of the 1D model setup for the flume experiments is shown in figure 4.1.

Bottom friction, wave breaking, and wave dissipation due to vegetation are physical processes which were relevant during the experiments and therefore they are included in the model. Other phenomena like white capping, wind growth and turbulence dissipation are not included.

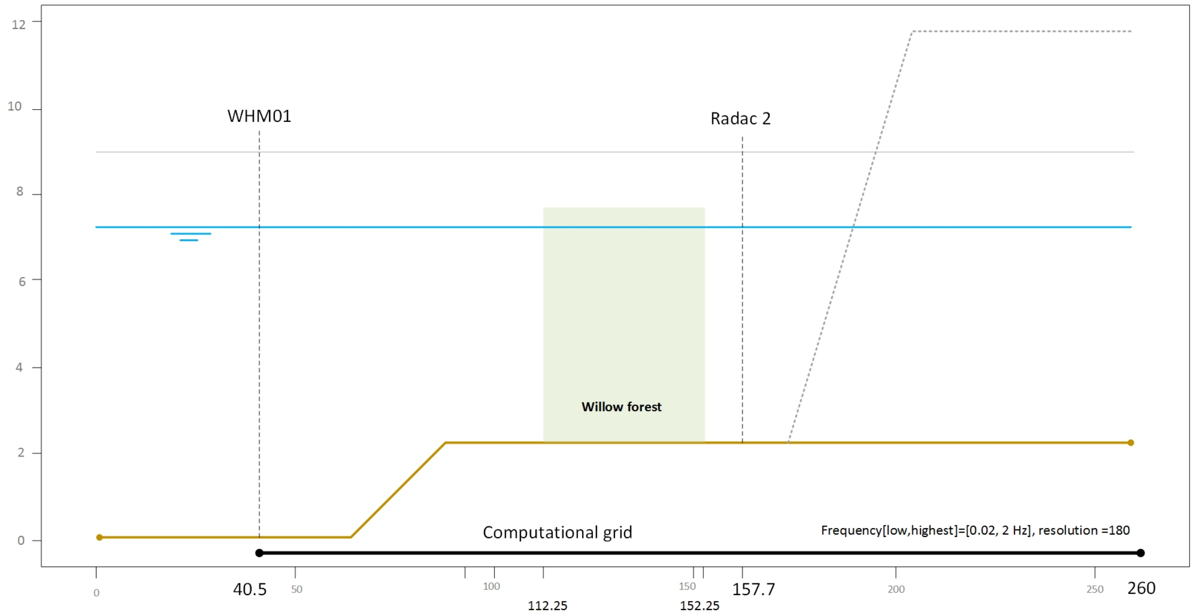

Figure 4.1: The 1D SWAN set-up for the physical experiments.

The wave boundary condition is taken out of the incident spectrum at the location of WHM01, as these measurements are not affected by the forest. Shoaling and depth-induced breaking due to the plateau in front of the forest are calculated by the model. The water level condition is set to be constant in space. Behind the forest there is an open boundary such that no energy is reflected back into the computational grid. No reflection is taken into account.

Calibration

The outcome and setup of the calibration test runs (Test series 5) were used to calibrate the model in terms of the setup and the roughness coefficient for the bottom friction. Out of the calibration test the errors in the significant wave heights were in the order of 5 cm, which are similar to the uncertainty in the physical measurements. These results could be due to errors of the measurements (during the extraction the reflected energy from the measured spectra). The bottom friction is eventually calibrated at a JONSWAP roughness coefficient of 0.07 m^2/s^{-3} (Padilla-Hernandez and Monbaliu, 2001) which is in line with what found by Bouws and Komen (2002).

Vegetation set-up

The tree models described in the previous chapter are used as vegetation input. The trees are averaged over the forest length, thus no horizontal variety is taken into account. The vertical structure of the canopy is included in SWAN by using vertical layers with a thickness of approximately 1 m. This leads to six layers for the average tree height of 5.325 meter. The averaged vegetation area over the height is translated in $N * b_v$ as input for SWAN. The vegetation input for each tree model is given in tables 4.2, 4.3, 4.4 and 4.5 with corresponding graph that illustrates the layers over the height.
The last column of the table reports the value of factor n which accounts for the canopy density relative to a specific test series. The vegetation parameters during TS 3, in fact, contain 100% of the canopy density, while for TS 4 this has been reduced to approximately 60 % of the original canopy density. This change in density is accounted for by multiplications of the number of stands per area by factor $n = 0.6$. The overview of the test series is given in table 4.1.2. In the case of n equal to 1 there is no change to the number of branches, while for TS 4 only 0.6 of the total amount of branches is considered. For the calibration test there was no vegetation, so n is equal to 0.

Table 4.1: The density coefficient that accounts for the change of canopy density for each test series

Test series	Vegetation configuration	n (-)
TS1	leaves	1
TS2	leaves	1
TS3	without leaves	1
TS4	40 % density removed	0.6
TS5	calibration	0

Table 4.2: Vegetation input parameters for tree model 1a.

layer thickness (m)	$b_v(m)$	N (m^{-2})
1.023	0.338	0.16
1	0.021	14.24
1	0.011	17.92
1	0.01	8
0.866	0.009	2.88
0.463	0.007	0.8

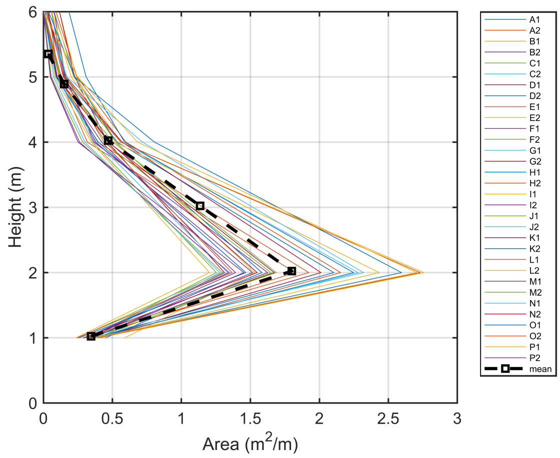

Figure 4.2: Tree model 1a.

Table 4.3: Vegetation input parameters for tree model 1b.

layer thickness (m)	$b_v(m)$	N (m^{-2})
1.023	0.338	0.16
1	0.021	14.24
1	0.011	51.52
1	0.01	41.44
0.866	0.009	36.32
0.463	0.007	29.12

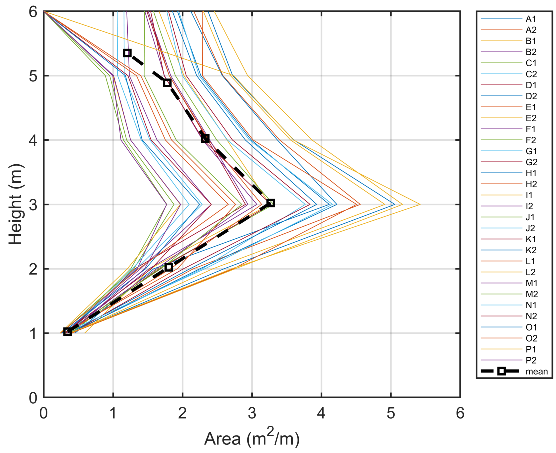

Figure 4.3: Tree model 1b.

Table 4.4: Vegetation input parameters for tree model 1c.

layer thickness (m)	$b_v(m)$	N (m^{-2})
1.023	0.338	0.16
1	0.021	14.24
1	0.011	25.76
1	0.01	20.8
0.866	0.009	18.08
0.463	0.007	14.56

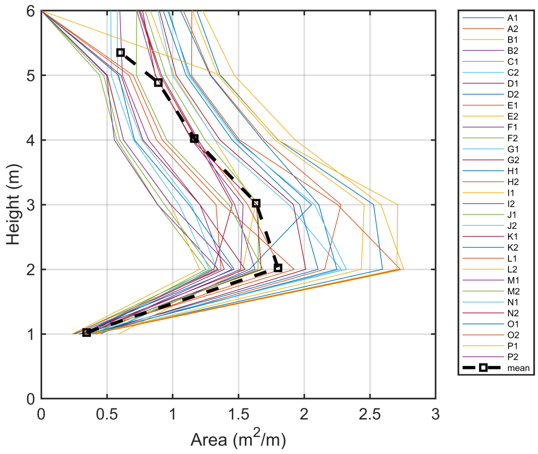

Figure 4.4: Tree model 1c.

Table 4.5: Vegetation input parameters for tree model 2.

layer thickness (m)	$b_v(m)$	N (m^{-2})
1.023	0.338	0.16
1	0.021	14.24
1	0.011	11.84
1	0.01	12
0.866	0.009	8.48
0.463	0.007	3.36

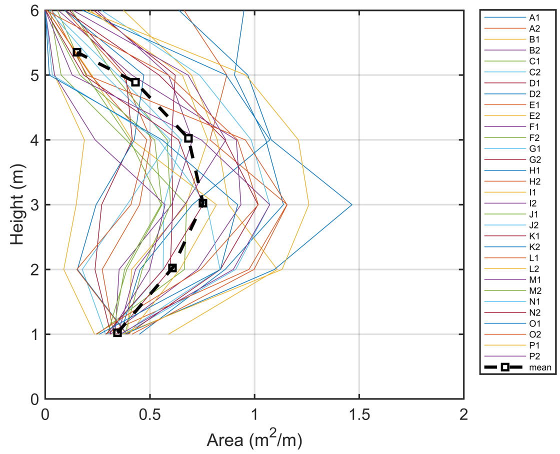

Figure 4.5: Tree model 2.

4.2. Numerical model outcome

This section presents the analysis of the modelled results from the different vegetation input (tree model 1a, 1b, 1c and 2). First, the wave dissipation of each tree model is determined by setting the drag coefficient to a constant value of 1. These outcome are compared to the measured wave reduction. Finally, an overview is given of the optimal drag coefficients for each tree model and the relations with dimensionless flow parameters, such as KC and Re, are analysed for one selected tree model.

4.2.1. Tree models

A value for the drag coefficient is often assumed to be in the order of 1 for simple rigid vegetation (De Oude, 2010). However, other findings showed that this value for the bulk drag coefficient can change depending on the vegetation density and the flow conditions (Ozeren et al., 2014; Suzuki, 2011). For the sake of comparison between the tree models regarding their effect on wave reduction, the C_D is initially set to 1 disregarding the flow conditions per test. In a later stage, the drag coefficient is calibrated for each test with corresponding tree models (see section 4.2.2).
The analysis begins with the comparison between modelled and measured wave heights behind the forest for each tree model. The results from tree model 1a, 1b, 1c and tree model 2 are plotted respectively in figures 4.6, 4.7, 4.8 and 4.9. These figures show the outcome of each test series, except test series 5, as defined in table 4.1.2. The relative effect on wave attenuation by different vegetation configurations, such as the effect of thinned canopy density and leaf area input, can hereby be observed from these plots.

The wave height predictions obtained by these tree models is analysed by looking at the bias and the 'root-mean-square-error' (RMSE) . The bias gives an indication whether the model mainly under predicts or over predicts the measured values and the RMSE states the accuracy of the predictions (Sutherland et al., 2004).

Results from tree model 1a and tree model 2 show foremost underestimations of the wave attenuation, as most data points are situated above the reference line containing a bias of respectively 0.01 and 0.06 m. This holds for all the data points from tree model 2, however tree model 1a shows an overestimation of the wave dissipation for Test series 2 (figure 4.9). This is due to the difference in amount of area input of the leaves between the two tree models. Tree model 2 is based on the frontal area of the leaves from the TLS data (see section 3.3.7), while tree model 1a uses the frontal area estimate from biomass measurements of the gathered leaves (described in subsection 3.2.1). This means that the computed frontal area by the TLS is too low, as already expected by the comparison with tree model 1a in terms of frontal area (see section 3.4). The frontal area estimate for the leaves are therefore also underestimated, as the leaf factor is multiplied by the frontal area of the branches. A low branch area, will therefore lead to a low frontal area of the leaves.
The results of tree model 1b show an relatively large overestimation of the wave damping, where most of the points lie beneath the reference line with a corresponding bias of -0.04 m. This model includes the side branches as cylinders and therefore has high frontal area and more wave dissipation. Tree model 1c, which also includes the side branches, shows slight overestimation of wave damping containing a bias of -0.01 m. This overestimation is less than for tree model 1b due to the lower area by considering the tapering form of the branches. Approximately similar dissipation values are observed for TS 2 between tree model 1a, 1b and 1c. Furthermore, the prediction of amount of wave dissipation increases with higher wave heights for tree models 1a, 1b and 1c. This trend can be related to the inundation level of the trees and the flexibility of the branches that are subject to the higher wave forces due to higher orbital velocities. These effects are not taken into account in the model, thus leading to higher predictions of wave attenuation. This effect is generally taken into account by lowering the bulk drag coefficient (Jalonen and Järvelä, 2014).

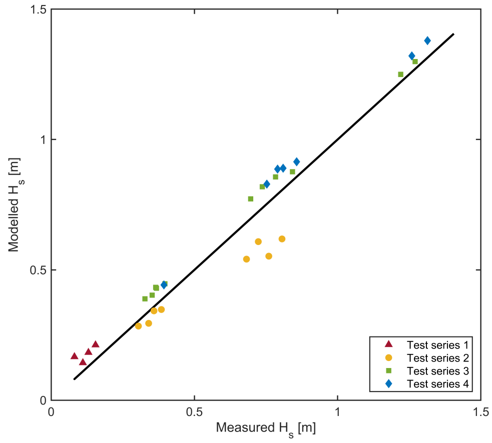

Figure 4.6: The measured significant wave height is plotted against the modelled significant wave height at the location of RADAC02 (behind the forest) for tree model 1a (primary branch model).

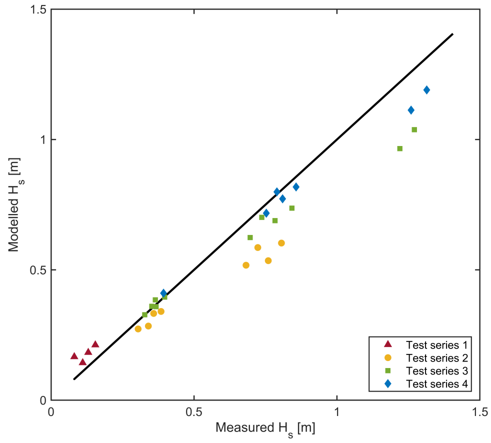

Figure 4.7: The measured significant wave height is plotted against the modelled significant wave height at the location of RADAC02 (behind the forest) for tree model 1b (branching model 1).

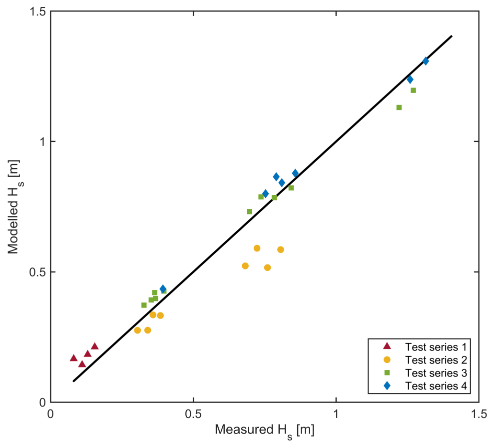

Figure 4.8: The measured significant wave height is plotted against the modelled significant wave height at the location of RADAC02 (behind the forest) for tree model 1c (branching model 2).

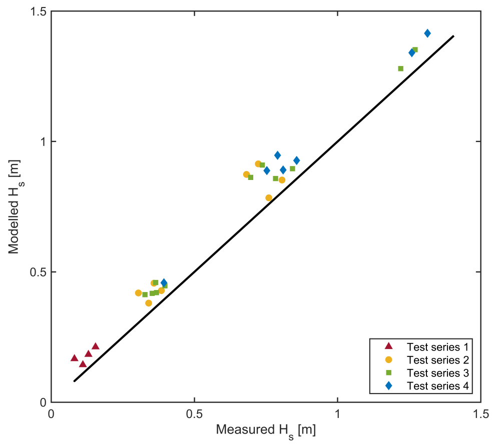

Figure 4.9: The measured significant wave height is plotted against the modelled significant wave height at the location of RADAC02 (behind the forest) for tree model 2 (TLS).

In order to assess the validity of the tree models the analysis is narrowed down to test series 3 only (full canopy density and no leaves). In this way, the uncertainties in amount of canopy density removal and leaf areas can be avoided. This analysis is done by comparing the measured wave reduction, R with the modelled wave reduction. The wave attenuation is expressed with the ratio, R where :

$$R = \frac{H_{s,0} - H_{s,2}}{H_{s,0}} \tag{4.1}$$

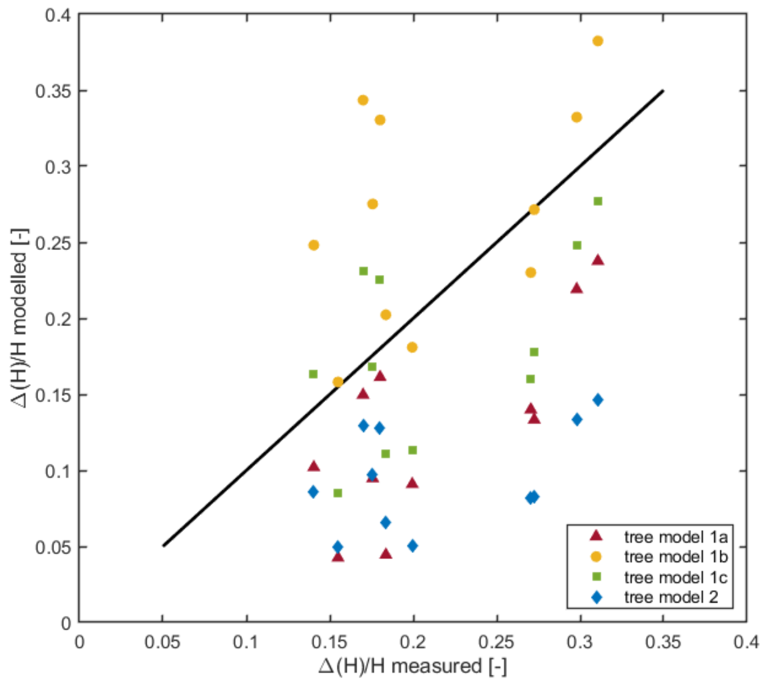

Figure 4.10: Wave attenuation computed as $\frac{\Delta(H)}{H}$ for Test series 3.

The comparison between the measured wave reduction (R) and the modelled wave reduction is shown in figure 4.10. This shows a scatter for each tree model and the reference line that presents the fit with the measured wave reduction. The measured wave reduction is 0.21, for H_s between 0.45 and 1.55 m and water depths between 3 and 4.5 meters at the foreshore. The RMSE and the bias for each tree model during Test series 3 are listed in table 4.2.1.

Table 4.6: RMSE and bias of R (wave reduction) for Test series 3

$\Delta(H)/H$	Tree model 1a	Tree model 1b	Tree model 1c	Tree model 2
RMSE	0.096	0.087	0.067	0.13
Bias	-0.085	0.054	-0.036	-0.119

From figure 4.10 and table 4.2.1, it appears that the reduction of the wave height by the measurements shows a better agreement with tree model 1c than with the other tree models which need tuning of the bulk drag coefficient to fit the measured values. This may be due to an overestimation or underestimation of the frontal area depending on the tree model, but also the physical processes such as flexibility and wave non-linearity which can be accounted for in this parameter. Furthermore, the flow conditions, thus hydraulic parameters influence the amount of drag exerted on a object. Therefore in the following section the drag coefficient for each test is obtained with the corresponding hydraulic parameters such as KC and Re.

4.2.2. Drag coefficient and hydraulic parameters

The hydraulic parameters used to define the flow conditions are the Reynolds number (Re) and the Keulegan-Carpenter number (KC). The Reynolds number is determined by the following formula:

$$Re = \frac{DU_{0,max}}{\nu} \tag{4.2}$$

Where D is the average diameter of the vegetation branches over the water level, and $U_{0,max}$ is the maximum horizontal orbital velocity in front of the forest. The Reynolds number defines the ratio between advection and viscous effects, therefore a low Reynolds number relates to laminar flowS and a high Reynolds number to turbulent flows.

The Keulegan-Carpenter number is instead determined by the following formula:

$$KC = \frac{U_{0,max} T}{D} \tag{4.3}$$

Where T is the average wave period equal T_{m02}, $U_{0,max}$ is the maximum horizontal velocity and D is the average diameter of the stems over the water level. Both non-dimensional parameters use the horizontal orbital velocity computed based on linear wave theory. The mean period used is T_{m02} determined as the square root of the ratio between the zeroth and second order spectral moments. The hydraulic parameters for each test are listed in table 4.7.

Table 4.7: KC and Re range for each test series.

	KC	Re. 10^3
TS 1	2.1- 3.8	98.69-118.00
TS 2	79- 253	6.92- 17.97
TS 3	80- 500	6.91- 18.58
TS 4	80- 500	8.56- 18.92

The drag coefficient of the trunk is set equal to 1, while the canopy drag coefficient is varied to match the results of the physical experiments. A range of C_D values from 0.1 until 2.0 with a resolution of 0.01 are simulated in SWAN. After increasing the drag coefficient for the canopy, the modelled wave heights behind the forest obtained with tree model 1a showed a better agreement with the measured wave heights for tree model 1a. On the contrary, decreasing the canopy drag coefficient led to to a better match with the measured wave heights for tree model 1b and 1c. The canopy drag coefficients averaged per test series are listed in table 4.8. A more detailed list, which contains the canopy drag coefficient for each test per tree model is given in appendix B.8.

Table 4.8: Optimal drag coefficients averaged for each test series

Test series	h_v [m]	H_s [m]	C_D			
			Tree model 1a	Tree model 1b	Tree model 1c	Tree model 2
TS 1 (Trunks)	0.6- 0.7	0.17- 0.26	6.92	6.92	6.92	6.92
TS 2 (Canopy with leaves)	3- 4.5	0.46- 1.05	0.53	0.39	0.47	1.67
TS 3 (Canopy without leaves)	3- 4.5	0.45- 1.55	1.55	0.65	1.15	1.78
TS 4 (Reduced canopy density)	3- 4.5	0.45- 1.55	1.63	0.69	1.19	1.88

Table 4.9: Optimal drag coefficients for each tree model for test series 3

TS 3 (Canopy without leaves)	h_v [m]	H_s [m]	C_D			
			Tree model 1a	Tree model 1b	Tree model 1c	Tree model 2
T13	3	0.45	1.56	0.9	1.57	1.75
T14	3	1.01	1.69	0.61	1.17	1.75
T15	3	0.5	1.56	1.12	0.27	1.75
T16	3	1.05	1.32	0.7	1.17	1.75
T17	4.5	0.45	1.56	0.76	1.47	1.56
T18	4.5	0.95	1.56	0.45	0.87	1.56
T19	4.5	0.47	1.56	0.85	0.27	1.56
T20	4.5	0.98	1.21	0.4	0.77	1.55
T21	4.5	1.47	0.88	0.27	0.56	1.06
T22	4.5	1.55	1.03	0.36	0.77	1.41

The drag coefficients found for Test series 1 (trunk) are similar for all the tree models, as the same trunk dimensions are used. These values are relatively higher than the drag coefficients found in the other test series and this can be related to the difference in flow conditions (see table 4.7).
Test series 2 shows low canopy drag coefficients for each tree model, as this vegetation configuration includes leaves. The presence of leaves during TS2 increases the frontal area of the trees, but is not effective in dissipating wave energy as the effective frontal area of leaves decreases under hydraulic loads.
During the physical experiments of test runs of Test series 3 (100 % canopy density without leaves) and Test series 4 (60 % canopy density without leaves) a considerable amount of swaying of the upper branches was observed. Flexibility in the used analytical model is not accounted for, thus this phenomena is taken into account by decreasing the drag coefficient relative to the drag coefficients obtained from Test series 1 and 2.

The obtained canopy drag coefficients from tree model 1a give a lower limit to the total area of the willow trees, as no side branches are taken into account. The highest canopy drag coefficients are found for tree model 2, which is expected due to the underestimation of the frontal area per tree of 30% relative to tree model 1a (only primary branches). Furthermore, relatively low drag coefficient correspond to tree model 1b, as the side branches most likely lead to an overestimation of the frontal area. Based on the obtained optimal drag coefficients, previous analysis with a C_D equal to 1 and findings from literature, tree model 1c (based on branching method 2) is chosen for further analysis on the relation with hydraulic parameters.

The relations with dimensionless parameters such as KC and Re are shown in figure 4.11 4.12. A clearer relation is observed between KC and the obtained canopy drag coefficients (see figure 4.11) than with Reynolds number. An overall decay is observed for the canopy drag coefficients with higher KC numbers. This decay is also present for test series with leaves, but this trend is shifted under the drag coefficients of test series 3 an test series 4. A slightly higher C_D is needed for test series 4 relative to test series 3 for equal KC numbers.

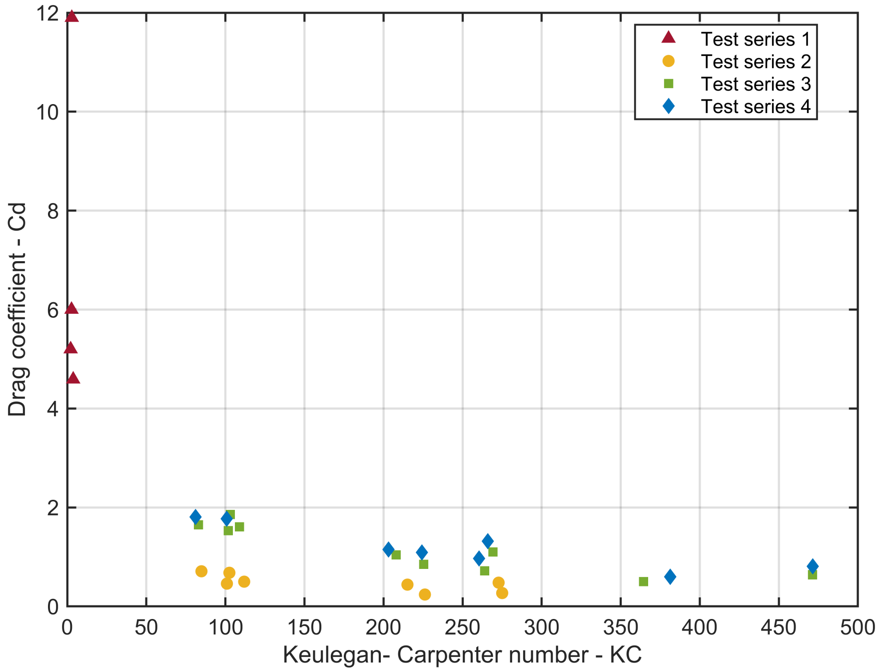

Figure 4.11: Optimal C_D values relative to tree model 1c plotted over KC.

Just considering the different configurations of vegetation (leaves, no leaves and thinned canopy) does not show a clear relation between C_D and the Reynolds number (see figure 4.12). A slight decay of drag coefficient is observed for test series 3 (without leaves) and test series 4 (thinned canopy density), but this trend is not seen for test series 2 (with leaves). It is observed that for high Reynolds number in Test series 1 the C_D coefficients assumes considerably higher values.

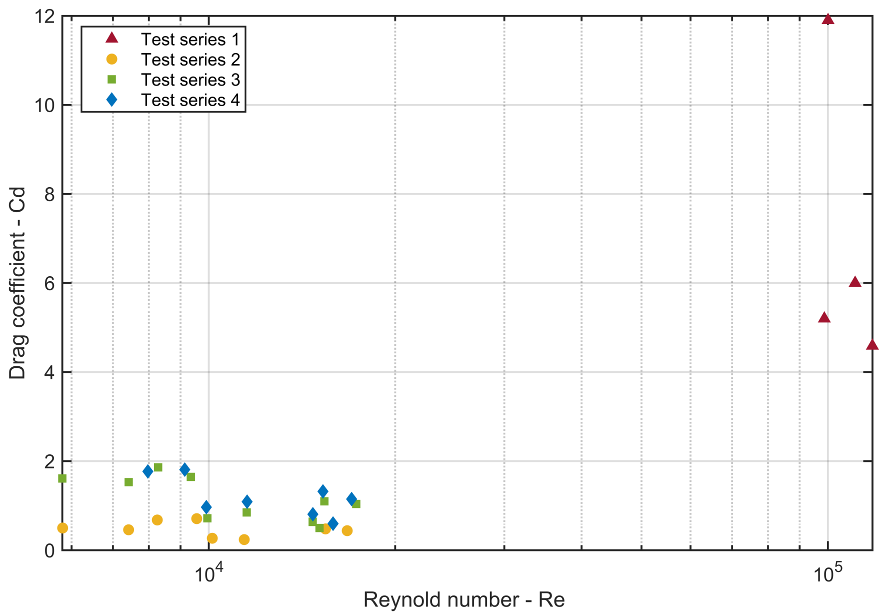

Figure 4.12: Optimal C_D values relative to tree model 1c plotted over Re.

4.3. Summary

A comparison between tree models is made by considering the outcome of the SWAN simulations. The first analysis focuses on an complete comparison between the test series and different tree models. At this stage, the drag coefficient is set to a value of 1 for all the test cases. In the next analysis the optimal drag coefficient is found for the canopy, as the frontal area of the canopy differs for each tree model. These optimal drag coefficients give an indication of how well the tree model is performing in predicting the measured wave attenuation.

The relevant observations are listed below:

- Tree model 1a is seen as a lower limit of the frontal area as only the main branches (excluding side branches) are considered. The underestimation of the wave dissipation is a consequence of underestimated frontal area input in SWAN, observed from the first analysis (using $C_D = 1$). This tree model underestimates the wave attenuation due to the lack of area of the side branches. The optimal drag coefficients found for this tree model is therefore in the range of 0.88 and 1.69 for test series 3, which is higher than in the other tree models (excluding tree model 2).
- Tree models 1a, 1b and 1c included the same amount of frontal area of the leaves. The leaf area input for tree models 1a, 1b and 1c results in an average canopy drag coefficient of respectively 0.53, 0.39 and 0.47. These differences are due to the variety in the frontal area of the branches between tree models.
- The TLS underestimates the frontal area of the trees and therefore underestimates the wave damping. This is observed with a $C_D = 1$, where tree model 2 leads to an RMSE of 0.13 for measured reduction levels of 0.21 (Hs=0.45-1.55 m). The leaf factor of this model is dependent on the frontal area without leaves (as given in section 3.3.7, thus also leading to an underestimation of the frontal area and less contribution to the amount of wave damping.
- Tree model 1c is used to find relations with Re and KC. A better correlation is found between the obtained canopy drag coefficients C_D and KC, than with Re.

5

Discussion and recommendations

This chapter presents discussions regarding relevant vegetation characteristics, the obtained tree models and the corresponding SWAN outcome. Furthermore, recommendations and future works follow in section 5.4.

5.1. Vegetation characteristics

From the physical experiments the highest amount of wave dissipation occurred during test series 2 (canopy including leaves) at mid water level (3 meter), with 2-4 % difference in wave dissipation with respect to test series 3 (canopy without leaves). This water elevation corresponds with the highest canopy densities, thus this is the location where the largest frontal area of the trees is centered. Furthermore, the effect by the leaves is relatively low, even though leaves have considerably higher frontal area than the branches. Meaning that the effective frontal area of the leaves decreases when objected to wave forces and therefore contribute less to the wave attenuation for willow vegetation. In contrary, leaves are found in literature to have a more significant effect on the wave dissipation from the field observations on mangrove forests (Mazda et al., 2006). This could be due to the difference in leaf characteristics such as the roughness and thickness. According to (Mazda et al., 2006), the intertwining of the leaves causes turbulent eddies and therefore higher wave attenuation and is more notable for thick leaves.

Furthermore in higher elevations and high wave forcing, not only the frontal area is relevant but also the stiffness of the branches is of importance, this is inline with the findings of (Paul et al., 2016). The stiffness is indirectly related to the biomass, as higher biomass lead to stiffer branches (Paul et al., 2016).

It is expected that the wave damping is also effected by the relative vegetation height h_v/h, where h_v is the total height of the vegetation and h is the water depth. Due to the swaying motion observed during the physical experiments, the relative velocities between the plant and the waves decrease and thereby the force by the stems differ over the height. Lower wave damping is expected for larger excursions due to swaying motion. However, this decrease in wave damping can also be the effect of lower canopy frontal areas, as the canopy frontal area decreases over the vertical. This decrease in drag coefficient with increasing water depth is also observed for pneumatophoris of Sonneratia sp. (roots), as they are also characterized by a tapering form (Mazda et al., 2006).

The vertical variation of vegetation parameters makes it more complex and therefore also lead to different hydrodynamic responses and thus wave damping. However simplifications of vegetation have been successful and practical. These assume rigid cylinders over the vertical with different frontal areas expressed as density (N) times average diameter(b_v) and a bulk drag coefficient (C_D) which covers for the unaccounted processes.

5.2. Tree models

Manual methods to obtain frontal area are generally time consuming, especially for tall woody vegetation. The frontal area distribution needs to be collected for the entire height if the woody vegetation has to endure high water levels. In the case of riparian vegetation, these heights can reach tens of meters. Remote sensing techniques are a more efficient way to obtain these data, but also has its limitations. This section discusses the advantages and limitations of each tree model.

5.2.1. Tree models 1a

Manual measurements at breast height are relatively easier to obtain than parameters t higher elevations in the tree. Using allometric relations is a well known method to gain information of tree specie containing measurements of only few parameters, which are easier reachable to measure.

These allometric relations are made for branches of the pollarded willow type Salix Alba. These relations capture the measured diameter at breast height in relation with the total length of the branch. Also the relation between the diameter at breast height and the weight of the branch is made. However, the pollarding practice on these trees may effect the outcome of these allometric relations in comparison to the same species in its natural form.

5.2.2. Tree models 1b

To obtain the information regarding the side branches (these branches were not measured during the experiments), another method is used. This method focuses on ratios between branch parameters (namely the diameter ratio, branching ratio and the length ratio) between subsequent branches. Good agreement is found with literature for the ratios between the lowest orders of branches. In the work by Järvelä on White Willow branches, the obtained values were namely R_b=4.22, R_d=1.86 and R_L=1.51. The highest order branch diameter was 0.0086 m with a height of 0.7 m (Järvelä, 2004). These values are comparable with the factors between the lower order branches for example between the branch tip ($m = 1$) and the subsequent branch ($m = 2$), which were R_b=4.2, R_d=1.7 and R_L=1.4.

However, the ratios between the highest order branches (branches that sprout directly out of the knot, $m = m_{high}$) and its following branch ($m = m_{high} - 1$) were relatively high (R_b=10.6, R_d=6.3 and R_L=4.5). These ratios were obtained from measurements on branches after the experiments, which may include damaged branches and the sample size was relatively low. Above this, it is likely that the difference between a natural willow and a managed willow influences to the growing pattern of the tree (Saifuddin et al., 2010), and thus these branching factors.

The branching factors in literature ((Antonarakis et al., 2009),(Järvelä, 2004),(McMahon and Kronauer, 1976)) are constant between branch orders. Nonetheless, in this work, in order to account for the large differences between the factors within a pollard willow, the ratios were not averaged for a tree but applied separately on the corresponding orders. Lastly, the results of the branching method do not take into account the decay of the branch diameter over the height. This leads to an overestimation of the frontal area, thus providing a upper limit of the frontal area per tree.

5.2.3. Tree model 1c

This tree model is based on the branching method, but only accounts for decay in the diameter over the height. This decay is based on diameter measurements over the height and is accounted for by applying a factor 0.5 on the obtained frontal areas by the branching method. This tree model is just as tree model 1b, dependent on the type of tree and does not provide information of the frontal area distribution over the height.

5.2.4. Tree model 2

The terrestrial laser scanner has proven to be a faster method relative to the hand measurements for gathering tree information. Although this information is in the form of a point cloud and requires processing steps. These steps can be intensive due to the size of the point clouds and memory restrictions. Also relatively detailed information is required from these scans to obtain reliable values of the frontal area for wave dissipation.

This level of detail could not be obtained by executing 3 single scans for the whole 40 meters of forest. The positions of these scans were solely taken from above the trees, changing the x-direction along the flume (see 3.1.1). These chosen positions for the lasers were resulting in an relatively good representation of the upper layers in the trees, but the mismatch with tree model 1b seems to increase with increasing penetration distance in the canopy. Furthermore the scan resolutions were set on (Quality of 2x and Resolution of 176.9 MPts) which can be increased for better results, but the occlusion due to the biomass density seemed to be the source of the discrepancies in frontal area estimates. The viewpoint locations of the scanner are also important to avoid errors due to the maximum range and incident angles. Having multiple scans of one object will reduce these error. However, having more scanning positions decreases the practicality of this method (due to time of the scans and processing). Therefore a method for including a correction factor to the area scanned from one laser position could be beneficial. The attempt is made in finding a correction factor for a selected tree in the flume, as described in the subsection 3.3.8.

5.3. SWAN observations

Methods for quantifying the frontal area of woody vegetation are analysed by looking at the effect of different tree models on computed wave dissipation in SWAN. Comparison with previous literature and the limitation of SWAN are discussed in this section.

Past studies on live kelps found bulk drag coefficients of aprroximately 0.2 with evident relation to the KC number (Mendez and Losada, 2004). For mangroves, (Hendriks, 2014) found C_d values between 2 and 4, which is an order of magnitude larger than the drag coefficients found for kelps from (Mendez and Losada, 2004). An comparison between the found relation with KC and from literature is given in figure 5.1. This figure shows that the test series with leaves are situated below the line for salt marshes taken from (Jadhav et al., 2013), while the test series without leaves are above this line. All of the found drag coefficients lie below the line taken from (Ozeren et al., 2014), as these experiments are done for rigid mimics of flexible vegetation. The range of KC number during the tests of (Ozeren et al., 2014) were between 5 and 40. A good agreement is seen between the drag coefficients for Test series 1 and the drag coefficients for the low KC numbers of (Ozeren et al., 2014) (see figure 5.2). These high drag coefficients for low KC numbers can be explained by the relative importance of inertia for low KC numbers (KC<10). This comparison shows that drag coefficients for woody vegetation without leaves are situated in between rigid vegetation and more flexible salt marshes found from literature.

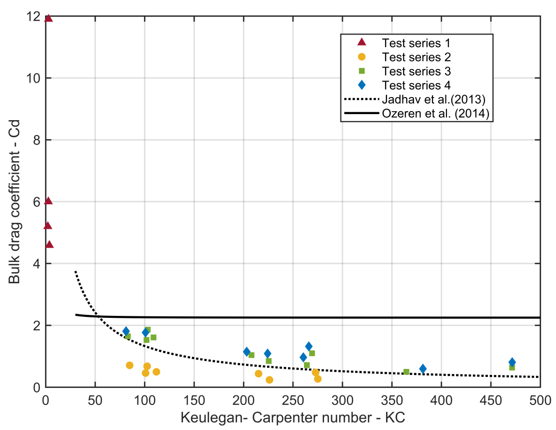

Figure 5.1: Comparison with literature C_D relation with KC

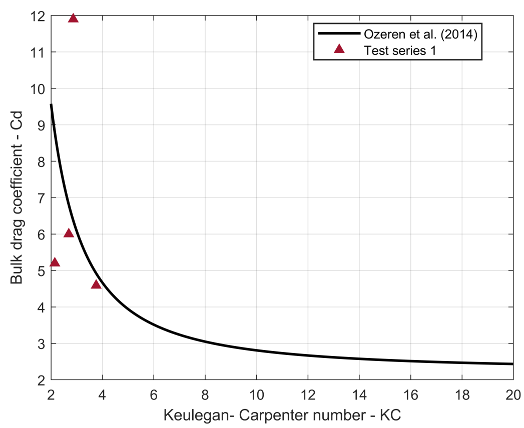

Figure 5.2: Comparison for low KC values

The drag coefficient not only depends on the type of vegetation, but also on the age and density. As the density is often shown in past research to influence the amount of wave damping. A study on plant mimics for regular and irregular waves, which found that the close enough stems lead to higher drag forces due to interactions with neighboring stems under oscillatory flow (Paul et al., 2016). In the contrary, the drag coefficients for Test series 4 are slightly higher than for test series 3, even though test series 4 has less canopy density (see figure 5.1. The latter observation is in line with the study of (Parsons, 1999) for steady flow. In study high densities lead to wake interaction and sheltering effect, which can lead to lower bulk drag coefficient. This has also been observed from a study with multiple cylinders under oscillatory flow (Suzuki, 2011). Also field observations showed that the drag coefficient decreases with increasing density caused by sheltering effects (Hendriks, 2014).

Furthermore, most of the physical experiments we conducted using vegetation set-up that could be characterized by single diameter values in space, while the setup of woody vegetation is more complex. This can develop different flow along the elements under the same flow conditions, and thus lead to difference in the amount of dissipation.

Even though SWAN is used as a check for the amount of wave attenuation due to different tree models, it has its own limitations of reproducing the measured wave dissipation of the experiments. First of all, the analytical formula in SWAN does not account for possible changes in wave celerity through the forest. Which can lead to an overestimation of wave attenuation by the model. Secondly, the vegetation stiffness is not taken into account in this formula, which can also lead to an overestimation of the wave damping by the model, as stiff branches dissipate more than flexible branches. Furthermore, possible measurement errors during the physical experiments and thereby errors in the wave boundary conditions in the swan model may also have influenced the results of SWAN.

5.4. Recommendations

Although this study found allometric relations for the willows used during the physical experiments, the quality of these findings can be increased. Further studies are therefore recommended to:

- To gain more reliable values for the branching ratios (R_b, R_d and R_L) it is recommended to take a larger number of branch samples. A number of 22 primary branches was used in a previous study (Antonarakis et al., 2009). This work is based on detailed sketches of nine primary branches after the experiments. Also doing these measurements on undamaged and fresh branches is more accurate, because dry branches become more fragile and difficult to handle.

Additionally, this study found that the frontal area reconstruction of the TLS data resulted in underestimations of the frontal area of the vegetation, although from the collected data it was not possible to fully analyse the potential of the TLS, therefore further studies are required. The following recommendations are given to contribute to this research:

- In literature successful scans were executed by taking two or three different scanning positions per tree to gain insight on the branch structures of individual trees (Antonarakis et al., 2009). In one paper two scans from opposite sides of a sample tree were sufficient for good representation (Saarinen et al., 2017). The scans during the physical experiments were made from above the flume, which resulted in missing points underneath the dense layer of foliage. Practical scans in the winter are recommended for willow trees, as leaves block the laser beams and contribute relatively little to the amount of wave dissipation.
- In the case that scans of woody vegetation with foliage are needed, it is recommended to do the scan from ground level instead from above the tree. This will avoid missing points underneath the dense layer of foliage. This geometry of the position of the laser scanner will also capture the trunk area better where most of the biomass area is concentrated.
- In this work, the comparison of the TLS is done with a branching method, which is also assumed to be an estimation of the true frontal area. The difference plots between the TLS and highly reliable frontal area estimates can be made by measuring the tree in its whole and having a better estimation of the distribution of this measured area over the vertical. The location of the branches must be known to find a correct relation between vegetation width and scanning error. Measuring the whole tree in detailed as possible can be achieved by conducting scans of an individual trees (more than one scanning position) and making a comparison with the scan data from one laser position. Furthermore, the relation between vegetation density and the scanning error can be investigated.
- By executing TLS scans on less flexible vegetation, the factor of flexibility that also can influence the amount of wave damping can be left out. In this was the effect by the frontal area input due to hand measurements compared to the frontal area by the TLS can result in more reliable outcome from a numerical model that does not directly account for the flexibility.

Finally, to gain more insight on the vegetation modelling for willow vegetation the following recommendations are made:

- The drag coefficient can be determined for each layer in the vertical, in order to find a relation with the flexibility of the branch.
- Also relations with hydraulic parameters such as KC can be analyzed further to obtain parameterization of the drag coefficient.

6 Conclusions

This chapter concludes the findings of this study. First, the sub-questions (described in section 1.2.1) are tackled. This chapter concludes with the answer to the main research question. The aim of this study was to gain insight on an effective way for obtaining vegetation parameters relevant for wave attenuation. In order to achieve this objective, the following sub-questions are answered:

What are the relevant vegetation parameters for wave attenuation?

From the literature study followed that the amount of wave attenuation due to vegetation depends on the hydraulic conditions and on the vegetation parameters. These vegetation characteristics include vegetation density, geometry, buoyancy, stiffness, foliage abundance, relative vegetation height and degrees of freedom of motion of the plant. Depending on the vegetation type, few of these characteristics can be neglected, such as the stiffness for relatively rigid vegetation. In the case of rigid vegetation, a commonly used approach is the cylinder approach, where the frontal area is the main vegetation parameter for wave attenuation. This frontal area is generally expressed in terms of vegetation density (Number of branches per m^2) multiplied with the plant area per unit height (m).

Which link can be found between the vegetation characteristics and the amount of wave damping out of the physical experiments?

The physical experiments showed most wave reduction for water depths of 3 meter, which corresponds to the elevation of the willows where most of the canopy density is situated.
The canopy density (units/m^2) and average diameters of the stems were measured at breast height during the physical experiments. The measurements and additional allometric relations, resulted in three tree models, where a tree model is the representation of the willow trees in terms of frontal area over the vertical.
The first tree model (tree model 1a) presents the frontal area of only the primary branches (excluding the side branches), while the other tree model (tree model 1b) presents the frontal area of the total amount of branches (primary branches including the side branches). The decay of the average diameter over the vertical has been taken into account in tree model 1a by using allometric relations. While tree model 1b does not include the decay of the diameters as it assumes the branches to be cylindrical objects. An adjustment in the assumption of the shape of the branch in the branching method leads to tree model 1c. These tree models are used in the numerical model SWAN in order to estimate corresponding wave attenuation and to compare these results with the measured wave attenuation. The value of the drag coefficients are set to 1 to gain a better understanding of the effect by the tree models.

A comparison of the results with expected drag coefficients from literature, showed that solely considering the primary branches (tree model 1a) of willow trees does not give sufficient frontal area to reproduce the measured wave attenuation. It can be said that the side branches cannot be left out of the frontal area even though they are relatively flexible to the main branches. While leaves show to have a minor effect on the amount of wave attenuation, as very low drag coefficients correspond to the tests done with leaves. Furthermore, results showed that relatively low drag coefficients were sufficient in reproducing the measured wave reduction for high water levels and high waves. This can be strongly related to the flexibility of willow branches which lead to relatively lower wave dissipation during the experiments, thus a lower drag coefficient in SWAN.

Which effective measure can be obtained out of the TLS data to characterize the trees regarding the wave attenuation?

By executing multi scans of the 40 meter willow forest from three positions above the flume, point cloud data of the vegetation was achieved during the physical experiments. The frontal area of the vegetation was obtained out of the point cloud by area reconstruction using alpha shape built-in function in Matlab. The resulting area reconstruction for the average tree is compared with the results from the measured tree models. Results showed an underestimation of 30 % with primary branch model (excluding side branches) and an underestimation of 55 % with adjusted branching model (including side branches) and. Two key attributes to this, are the density of the canopy and the geometry of the scanners. The vegetation density affects the amount of occlusion in the case of the willow vegetation and therefore the resulting frontal areas.

How does the TLS input affect the SWAN output?

In this study, SWAN is used to compare the effect of different calculated areas (referred as tree model input) on wave attenuation. Tree model 2 (from TLS data) results in underestimations of the frontal area for the average tree and therefore a canopy drag coefficient of 1.78 for the leafless willow with full density. This is a too high drag coefficient for willow trees, as the canopy drag found for tree model 1a gives a drag coefficient of 1.55 and tree model 1c results in a canopy drag coefficient of 1.15.

The main question of this report:
How to determine relevant vegetation parameters for wave damping?

Woody riparian vegetation is seen as relatively rigid vegetation, but considerable amount of swaying has been observed during the physical experiments, especially under extreme wave conditions. Only measuring the base diameters at the knot and using allometric relations to determine the frontal area of the primary branches does not provide sufficient frontal area and thereby leads to underestimation of the wave dissipation. Furthermore the disadvantage is that the allometric relation is tree specific.

A branching method based on the branch structure of willows is a relatively easy way to obtain the total frontal area of these willow trees if these factors are known for this specific type of vegetation. However, this method does not provide information on the distribution of the frontal area over the vertical and it assumes the branches as cylinders. This leads to an overestimation of the frontal area.

This overestimation of the frontal area by assuming cylindrical objects can be corrected by applying a factor to the computed frontal area of the cylinders. This factor is based on tapering form of branches over the vertical. This method resulted in the most accurate estimates of the frontal area of the willow trees, but it also tree specific and is time consuming.

In this study, the frontal area estimates obtained from the TLS are considerably lower than the previous estimates. By analysing the beam penetration through the canopy, it was possible to observe that the branches progressively blocked a considerable part of the laser beams, therefore larger distances from the laser positions resulted in larger discrepancies in the frontal area. This led to point clouds which were not sufficiently accurate to come to reliable frontal area estimates. Results of the analysis of the beam penetration show that it is most likely that this error can be corrected for in the frontal area. Hereby a better and more economical way for obtaining tree parameters can be achieved.

Bibliography

Deltares, 2018 (accessed November 12, 2018). URL `https://www.deltares.nl/en/news/willow-woods-as-breakwaters-to-improve-flood-protection`.

J. Aerts. Project A09 Financial arrangements for disaster losses under climate change: Adaptation cost in the Netherlands:Climate Change and flood risk manamgement. 1953:7, 2009. URL `http://www.climatechangesspatialplanning.nl/media/default.aspx/emma/org/10354094/34-44+Adaptation+cost+in+the+Netherlands+-+Climate+Change+and+flood+risk+management.pdf`.

A. S. Antonarakis, K. S. Richards, J. Brasington, and M. Bithell. Leafless roughness of complex tree morphology using terrestrial lidar. *Water Resources Research*, 45(10):1–14, 2009. ISSN 00431397. doi: 10.1029/2008WR007666.

A. S. Antonarakis, K. S. Richards, J. Brasington, and E. Muller. Determining leaf area index and leafy tree roughness using terrestrial laser scanning. *Water Resources Research*, 46(6):1–12, 2010. ISSN 00431397. doi: 10.1029/2009WR008318.

A. Armanini, M. Righetti, and P. Grisenti. Direct measurement of vegetation resistance in prototype scale. *Journal of Hydraulic Research*, 43(5):481–487, 2005. ISSN 00221686. doi: 10.1080/00221680509500146.

T. Q. Bao. Effect of mangrove forest structures on wave attenuation in coastal Vietnam. *Oceanologia*, 53(3): 807–818, 2011. ISSN 00783234. doi: 10.5697/oc.53-3.807.

N. Booij, R. C. Ris, and L. H. Holthuijsen. A third-generation wave model for coastal regions: 1. Model description and validation. *Journal of Geophysical Research*, 104(C4):7649–7666, 1999. ISSN 0148-0227. doi: 10.1029/98JC02622. URL `http://doi.wiley.com/10.1029/98JC02622`.

E. Bouws and G. J. Komen. On the Balance Between Growth and Dissipation in an Extreme Depth-Limited Wind-Sea in the Southern North Sea, 2002. ISSN 0022-3670.

K. Bradley and C. Houser. Relative velocity of seagrass blades: Implications for wave attenuation in low-energy environments. *Journal of Geophysical Research: Earth Surface*, 114(1):1–13, 2009. ISSN 21699011. doi: 10.1029/2007JF000951.

R. A. Dalrymple, J. T. Kirby, and P. A. Hwang. Wave diffraction due to areas of energy-dissipation. *Journal of Waterway Port Coastal and Ocean Engineering-Asce*, 110(1):67–79, 1984.

R. De Oude. Modelling wave attenuation by vegetation with SWAN-VEG: Model evaluation and application to the Noordwaard polder. (January):116, 2010.

T. S. t. T. Delft. SWAN scientific and technical documentation. SWAN Cycle.

F. Ferrini. Pollarding and its effects on tree physiology : a look to mature and senescent tree management in Italy. *1er colloque européen sur les trognes, Vendôme, 26, 27 et 28 octobre 2006*, (January):1–8, 2006.

A. Gijón Mancheño. Interaction between wave hydrodynamics and flexible vegetation. 2016. doi: uuid:bbaaf195-27e2-46ec-969c-603d6dd8f8c0.

V. Heller. Scale effects in physical hydraulic engineering models. *Journal of Hydraulic Research*, 49(3):293–306, 2011. ISSN 00221686. doi: 10.1080/00221686.2011.578914.

J. M. Hendriks. Wave Dissipation in Mangroves (M.Sc Thesis). (February):1–101, 2014.

E. M. Horstman, C. M. Dohmen-Janssen, P. M. Narra, N. J. van den Berg, M. Siemerink, and S. J. Hulscher. Wave attenuation in mangroves: A quantitative approach to field observations. *Coastal Engineering*, 2014. ISSN 03783839. doi: 10.1016/j.coastaleng.2014.08.005.

T. Houston Durrant, D. de Rigo, and G. Caudullo. Salix alba in Europe: distribution, habitat, usage and threats T. *San-Miguel- Ayanz, J., de Rigo, D., Caudullo, G., Houston Durrant, T., Mauri, A. (Eds.), European Atlas of Forest Tree Species. Publ. Off. EU,*, page 2016, 2016.

Z. Hu, T. Suzuki, T. Zitman, W. Uittewaal, and M. Stive. Laboratory study on wave dissipation by vegetation in combined current-wave flow. *Coastal Engineering*, 2014. ISSN 03783839. doi: 10.1016/j.coastaleng.2014.02.009.

H. W. Iversen and R. Balent. A correlating modulus for fluid resistance in accelerated motion. *Journal of Applied Physics*, 22(3):324–328, 1951. ISSN 00218979. doi: 10.1063/1.1699949.

R. S. Jadhav, Q. Chen, and J. M. Smith. Spectral distribution of wave energy dissipation by salt marsh vegetation. *Coastal Engineering*, 77:99–107, 2013. ISSN 03783839. doi: 10.1016/j.coastaleng.2013.02.013. URL `http://dx.doi.org/10.1016/j.coastaleng.2013.02.013`.

J. Jalonen and J. Järvelä. Estimation of drag forces caused by natural woody vegetation of different scales. *Journal of Hydrodynamics*, 26(4):608–623, 2014. ISSN 18780342. doi: 10.1016/S1001-6058(14)60068-8.

J. Järvelä. Determination of flow resistance caused by non-submerged woody vegetation. *International Journal of River Basin Management*, 2(1):61–70, 2004. ISSN 18142060. doi: 10.1080/15715124.2004.9635222.

J. M. J. Journée and W. W. Massie. Wave forces on slender cylinders. *Offshore Hydromechanics*, (January), 2001.

G. Keulegan and L. Carpenter. Forces on cylinders and plates in an oscillating fluid. *Journal of Research of the National Bureau of Standards*, 60(5):423, 1958. ISSN 0091-0635. doi: 10.6028/jres.060.043. URL `http://nvlpubs.nist.gov/nistpubs/jres/60/jresv60n5p423_A1b.pdf`.

L. Lenssinck. Del077-woody:full scale hydraulic and ecological optimisation of a dike-forest combination @ONLINE, Dec. 2018. URL `https://publicwiki.deltares.nl/display/TKIP/`.

W. Lin, Y. Meng, Z. Qiu, S. Zhang, and J. Wu. Measurement and calculation of crown projection area and crown volume of individual trees based on 3D laser-scanned point-cloud data. *International Journal of Remote Sensing*, 38(4):1083–1100, 2017. ISSN 13665901. doi: 10.1080/01431161.2016.1265690. URL `http://dx.doi.org/10.1080/01431161.2016.1265690`.

I. J. Losada, M. Maza, and J. L. Lara. A new formulation for vegetation-induced damping under combined waves and currents. *Coastal Engineering*, 2016. ISSN 03783839. doi: 10.1016/j.coastaleng.2015.09.011.

M. Luhar and H. M. Nepf. Flow-induced reconfiguration of buoyant and flexible aquatic vegetation. *Limnology and Oceanography*, 56(6):2003–2017, 2011. ISSN 00243590. doi: 10.4319/lo.2011.56.6.2003.

M. Luhar and H. M. Nepf. Wave-induced dynamics of flexible blades. *Journal of Fluids and Structures*, 61:20–41, 2015. ISSN 10958622. doi: 10.1016/j.jfluidstructs.2015.11.007.

W. Luo and J. Monbaliu. energy balance for gravity waves in shallow water Wave Project (JONSWAP) expression viscosity friction model The empirical Sbf Coc =. 99, 1994.

S. R. Massel and R. M. Brinkman. On the determination of directional wave spectra for practical applications. *Applied Ocean Research*, 20(6):357–374, 1998. ISSN 01411187. doi: 10.1016/S0141-1187(98)00026-1.

Y. Mazda. Mazdaetal_1997.pdf, 1997.

Y. Mazda, M. Magi, Y. Ikeda, T. Kurokawa, and T. Asano. Wave reduction in a mangrove forest dominated by Sonneratia sp. *Wetlands Ecology and Management*, 14(4):365–378, 2006. ISSN 09234861. doi: 10.1007/s11273-005-5388-0.

A. Mcivor, I. Möller, T. Spencer, and M. Spalding. Reduction of Wind and Swell Waves by Mangroves. *Natural Coastal Protection Series*, pages 1–27, 2012. ISSN ISSN 2050-7941. doi: ISSN2050-7941. URL `http://www.naturalcoastalprotection.org/documents/reduction-of-wind-and-swell-waves-by-mangroves`.

T. A. McMahon and R. E. Kronauer. Tree structures: Deducing the principle of mechanical design. *Journal of Theoretical Biology*, 59(2):443–466, 1976. ISSN 10958541. doi: 10.1016/0022-5193(76)90182-X.

F. J. Mendez and I. J. Losada. An empirical model to estimate the propagation of random breaking and non-breaking waves over vegetation fields. *Coastal Engineering*, 51(2):103–118, 2004. ISSN 03783839. doi: 10.1016/j.coastaleng.2003.11.003.

J. Morison, J. Johnson, and S. Schaaf. The Force Exerted by Surface Waves on Piles. *Journal of Petroleum Technology*, 2(05):149–154, 1950. ISSN 0149-2136. doi: 10.2118/950149-G. URL `http://www.onepetro.org/doi/10.2118/950149-G`.

N.-e. Nordh and T. Verwijst. Above-ground biomass assessments and ÿrst cutting cycle production in willow (Salix sp .) coppice — a comparison between destructive and non-destructive methods. 27:1–8, 2004. doi: 10.1016/j.biombioe.2003.10.007.

Y. Ozeren, D. G. Wren, and W. Wu. Experimental Investigation of Wave Attenuation through Model and Live Vegetation. *Journal of Waterway, Port, Coastal, and Ocean Engineering*, 2014. ISSN 0733-950X. doi: 10.1061/(ASCE)WW.1943-5460.0000251.

R. Padilla-Hernandez and J. Monbaliu. Energy balance of wind waves as a function o f the bottom friction formulation. *Coastal Engineering*, 43:131–148, 2001.

R. M. Parsons. Drag, Turbulence, and Diffusion in Flow Through EmergentVegetation. *Water Resources Research*, 35(2):479–489, 1999.

M. Paul, F. Rupprecht, I. Möller, T. J. Bouma, T. Spencer, M. Kudella, G. Wolters, B. K. van Wesenbeeck, K. Jensen, M. Miranda-Lange, and S. Schimmels. Plant stiffness and biomass as drivers for drag forces under extreme wave loading: A flume study on mimics. *Coastal Engineering*, 2016. ISSN 03783839. doi: 10.1016/j.coastaleng.2016.07.004.

V. L. H. Phuoc and S. R. Massel. Experiments on wave motion and suspended sediment concentration at Nang Hai, Can Gio mangrove forest, Southern Vietnam. *Oceanologia*, 48(1):23–40, 2006. ISSN 00783234.

S. Quartel, A. Kroon, P. G. Augustinus, P. Van Santen, and N. H. Tri. Wave attenuation in coastal mangroves in the Red River Delta, Vietnam. *Journal of Asian Earth Sciences*, 29(4):576–584, 2007. ISSN 13679120. doi: 10.1016/j.jseaes.2006.05.008.

M. Report. WOODY - Large scale physical model tests of wave attenuation by willow trees.

N. Saarinen, V. Kankare, M. Vastaranta, V. Luoma, J. Pyörälä, and T. Tanhuanpää. ISPRS Journal of Photogrammetry and Remote Sensing Feasibility of Terrestrial laser scanning for collecting stem volume information from single trees. *ISPRS Journal of Photogrammetry and Remote Sensing*, 123:140–158, 2017. ISSN 0924-2716. doi: 10.1016/j.isprsjprs.2016.11.012. URL `http://dx.doi.org/10.1016/j.isprsjprs.2016.11.012`.

M. Saifuddin, A. B. Hossain, N. Osman, M. A. Sattar, K. M. Moneruzzaman, and M. I. Jahirul. Pruning impacts on rot-shoot growth, biochemical and physiological changes of Bougainvillea glabra. *Australian Journal of Crop Science*, 4(7):530–537, 2010. ISSN 18352693.

G. Songy. Wave Attenuation by Global Coastal Salt Marsh Habitats. *Tudelft repository*, (June), 2016. URL `uuid:f00e7416-f330-4d99-90fe-bf54367da78b`.

S. Soudarissanane. *The geometry of terrestrial laser scanning*. 2016. ISBN 9789462332034.

S. Srinivasan, S. C. Popescu, M. Eriksson, R. D. Sheridan, and N. W. Ku. Terrestrial laser scanning as an effective tool to retrieve tree level height, crown width, and stem diameter. *Remote Sensing*, 2015. ISSN 20724292. doi: 10.3390/rs70201877.

M. M. Stam. *Reliability of willows for wave load reduction on river dikes*. PhD thesis, TU Delft, Delft, 2018.

J. Sutherland, A. H. Peet, and R. L. Soulsby. Evaluating the performance of morphological models. *Coastal Engineering*, 51(8-9):917–939, 2004. ISSN 03783839. doi: 10.1016/j.coastaleng.2004.07.015.

T. Suzuki. *Wave dissipation over vegetation fields*, volume PhD thesis. 2011. ISBN 9789491211447.

T. Suzuki and T. Arikawa. Numerical analysis of bulk drag coefficient in dense vegetation by immersed boundary method. *Coastal Engineering*, 2010.

T. Suzuki, M. Zijlema, B. Burger, M. C. Meijer, and S. Narayan. Wave dissipation by vegetation with layer schematization in SWAN. *Coastal Engineering*, 2011a. ISSN 03783839. doi: 10.1016/j.coastaleng.2011.07.006.

T. Suzuki, M. Zijlema, B. Burger, M. C. Meijer, and S. Narayan. Wave dissipation by vegetation with layer schematization in SWAN. *Coastal Engineering*, 2011b. ISSN 03783839. doi: 10.1016/j.coastaleng.2011.07.006.

E. Tabacchi, D. L. Correll, R. Hauer, G. Pinay, A. M. Planty-Tabacchi, and R. C. Wissmar. Development, maintenance and role of riparian vegetation in the river landscape. *Freshwater Biology*, 40(3):497–516, 1998. ISSN 00465070. doi: 10.1046/j.1365-2427.1998.00381.x.

H. L. Tolman. An evaluation of expressions for wave energy dissipation due to bottom friction in the presence of currents. *Coastal Engineering*, 16(2):165–179, 1992. ISSN 03783839. doi: 10.1016/0378-3839(92)90035-S.

S. L. Tran Kai Frank Da and M. Yvinec. CGAL 4.14 3d alpha shapes, 2019. URL `https://doc.cgal.org/latest/Alpha_shapes_3/index.html#title3`.

K. Van Looy, T. Tormos, M. Ferréol, B. Villeneuve, L. Valette, A. Chandesris, N. Bougon, F. Oraison, and Y. Souchon. Benefits of riparian forest for the aquatic ecosystem assessed at a large geographic scale. *Knowledge and Management of Aquatic Ecosystems*, (408):06, 2013. doi: 10.1051/kmae/2013041.

A. van Rooijen, J. van Thiel de Vries, R. McCall, A. van Dongeren, J. Roelvink, and A. Reniers. Modeling of wave attenuation by vegetation with XBeach. *E-proceedings of the 36th IAHR World Congress, The Hague, the Netherlands*, pages 1–7, 2015. ISSN 01496395. doi: 10.1081/SS-100102084.

K. Västilä and J. Järvelä. Modeling the flow resistance of woody vegetation using physically based properties of the foliage and stem. *Water Resources Research*, 50(1):229–245, 2014. ISSN 00431397. doi: 10.1002/2013WR013819.

K. Västilä, J. Järvelä, and J. Aberle. Characteristic reference areas for estimating flow resistance of natural foliated vegetation. *Journal of Hydrology*, 492:49–60, 2013a. ISSN 00221694. doi: 10.1016/j.jhydrol.2013.04.015.

K. Västilä, J. Järvelä, and J. Aberle. Characteristic reference areas for estimating flow resistance of natural foliated vegetation. *Journal of Hydrology*, 492:49–60, 2013b. ISSN 00221694. doi: 10.1016/j.jhydrol.2013.04.015.

P. Vo-Luong and S. Massel. Energy dissipation in non-uniform mangrove forests of arbitrary depth. *Journal of Marine Systems*, 74(1-2):603–622, 2008. ISSN 09247963. doi: 10.1016/j.jmarsys.2008.05.004. URL `http://dx.doi.org/10.1016/j.jmarsys.2008.05.004`.

V. Vuik, S. N. Jonkman, B. W. Borsje, and T. Suzuki. Nature-based flood protection: The efficiency of vegetated foreshores for reducing wave loads on coastal dikes. *Coastal Engineering*, 116:42–56, 2016. ISSN 03783839. doi: 10.1016/j.coastaleng.2016.06.001. URL `http://dx.doi.org/10.1016/j.coastaleng.2016.06.001`.

V. Vuik, S. van Vuren, B. W. Borsje, B. K. van Wesenbeeck, and S. N. Jonkman. Assessing safety of nature-based flood defenses: Dealing with extremes and uncertainties. *Coastal Engineering*, 139(December 2017):47–64, 2018. ISSN 03783839. doi: 10.1016/j.coastaleng.2018.05.002. URL `https://doi.org/10.1016/j.coastaleng.2018.05.002`.

C. Wilson, P. Xavier, T. Schoneboom, J. Aberle, H. P. Rauch, W. Lammeranner, C. Weissteiner, and H. Thomas. The Hydrodynamic Drag of Full Scale Trees. *River Flow 2010*, 2010.

S. Wunder, B. Lehmann, and F. Nestmann. Determination of the drag coefficients of emergent and just submerged willows. *International Journal of River Basin Management*, 9(3-4):231–236, 2011. ISSN 18142060. doi: 10.1080/15715124.2011.637499.

K. Wuyts, T. Wuytack, F. Kardel, S. Adriaenssens, R. Samson, and K. Verheyen. The potential of biomonitoring of air quality using leaf characteristics of white willow (Salix alba L.). *Environmental Monitoring and Assessment*, 171(1-4):197–204, 2009. ISSN 0167-6369. doi: 10.1007/s10661-009-1271-4.

A

Delta flume tests

A.1. Willow trees

The willow trees are placed over approximately 40 m with about 2.5 m between them in the x-direction. The relatively higher trees are placed in the outer left of the forest, in this case towards the wave maker. An map of flume can be seen in figure A.1. Also some impressions of the willows in the flume are given in figure A.2 and figure A.3.

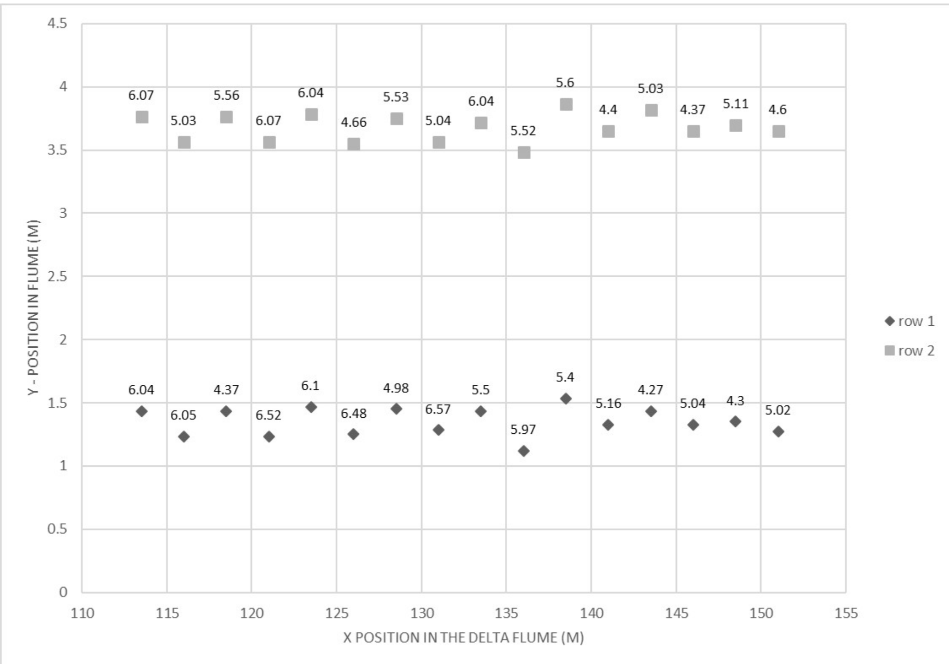

Figure A.1: Staggered position of the willows in the flume with their corresponding height. The x-position is measured from the wave paddle and the y-position is taken from the opposite side of the measurement cabin.

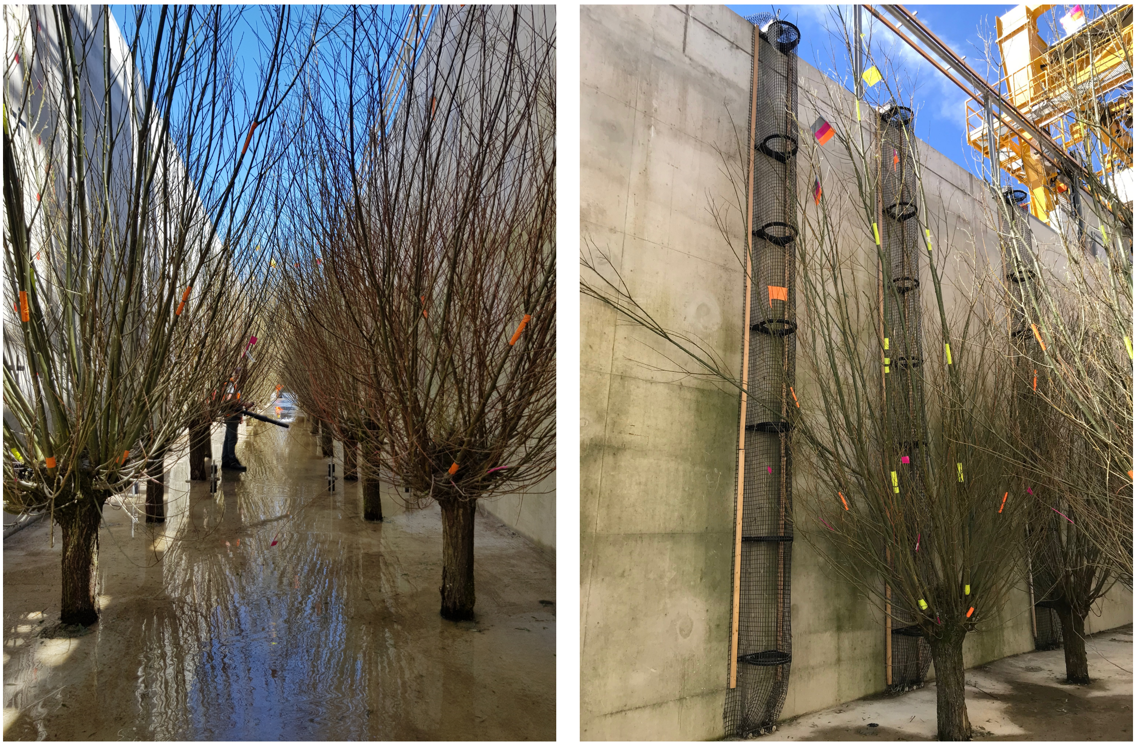

Figure A.2: Left: De-leaved willows in the flume, Right: One de-leaved willow in the second row around x = 113 m

Figure A.3: Left: Just emerged willows in the flume, for test T005 (see table **??** of appendix A.2), Right: Thinned out willows in the flume for test series 4 (see table **??** of appendix A.2).

A.2. Test program

Test program							
Test	h (m)	H_{m0} (m)	T_p (s)	s(-)	Vegetation state	Dissipation through:	Test series
T001	2.93	0.2	1.79	0.04	leaves	stems	TS 1
T002	2.93	0.2	2.53	0.02	leaves	stems	TS 1
T003	3.03	0.25	2.00	0.04	leaves	stems	TS 1
T004	3.03	0.25	2.83	0.02	leaves	stems	TS 1
T005	5.33	0.50	2.83	0.04	leaves	canopy	TS 2
T006	5.33	1.06	4.00	0.04	leaves	canopy	TS 2
T007	5.33	0.50	4.00	0.02	leaves	canopy	TS 2
T008	5.33	1.01	5.66	0.02	leaves	canopy	TS 2
T009	6.83	0.50	2.83	0.04	leaves	canopy	TS 2
T010	6.83	1.03	4.00	0.04	leaves	canopy	TS 2
T011	6.83	0.50	4.00	0.02	leaves	canopy	TS 2
T012	6.83	1.00	5.66	0.02	leaves	canopy	TS 2
T013	5.33	0.50	2.83	0.04	no leaves	canopy	TS 3
T014	5.33	1.17	3.58	0.05	no leaves	canopy	TS 3
T015	5.33	0.50	4.00	0.02	no leaves	canopy	TS 3
T016	5.33	1.0	5.66	0.02	no leaves	canopy	TS 3
T017	6.83	0.5	2.83	0.04	no leaves	canopy	TS 3
T018	6.83	1.0	4.00	0.04	no leaves	canopy	TS 3
T019	6.83	0.50	4.00	0.02	no leaves	canopy	TS 3
T020	6.83	1.0	5.66	0.02	no leaves	canopy	TS 3
T021	6.83	1.61	4.90	0.04	no leaves	canopy	TS 3
T022	6.83	1.52	6.93	0.02	no leaves	canopy	TS 3
T027	6.83	1.0	4.00	0.04	no leaves	canopy	TS 3
T028	6.83	1.0	5.66	0.02	no leaves	canopy	TS 3
T023	5.33	0.5	2.83	0.04	50 % density	canopy	TS 4
T024	5.33	1.0	3.58	0.05	50 % density	canopy	TS 4
T025	5.33	0.5	4.00	0.02	50 % density	canopy	TS 4
T026	5.33	1.0	5.66	0.02	50 % density	canopy	TS 4
T029	6.83	1.5	4.90	0.04	50 % density	canopy	TS 4
T030	6.83	1.5	6.93	0.02	50 % density	canopy	TS 4
T031	2.93	0.2	1.79	0.04	nothing	-	Calibr.
T032	2.93	0.2	2.53	0.02	nothing	-	Calibr.
T033	5.33	0.5	2.83	0.04	nothing	-	Calibr.
T034	5.33	1.0	3.85	0.05	nothing	-	Calibr.
T035	5.33	0.5	4.00	0.02	nothing	-	Calibr.
T036	5.33	1.0	5.66	0.02	nothing	-	Calibr.
T037	6.83	1.61	4.90	0.04	nothing	-	Calibr.
T038	6.83	1.52	6.93	0.02	nothing	-	Calibr.
T039	3.03	0.25	2.00	0.04	nothing	-	Calibr.
T040	3.03	0.25	2.83	0.02	nothing	-	Calibr.
T041	6.83	1.5	4.90	0.04	nothing	-	Calibr.
T042	6.83	1.5	6.93	0.02	nothing	-	Calibr.

B

Manually gathered

B.1. Relations tree parameters

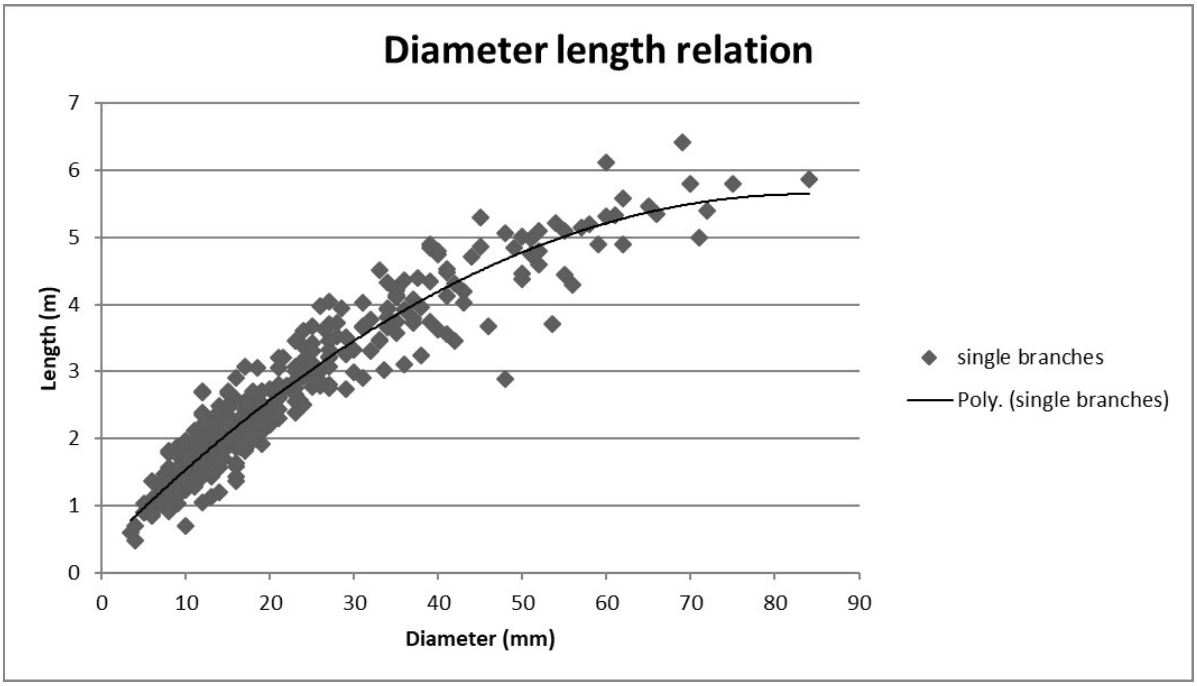

Figure B.1: diameter-length relation for willow branches.

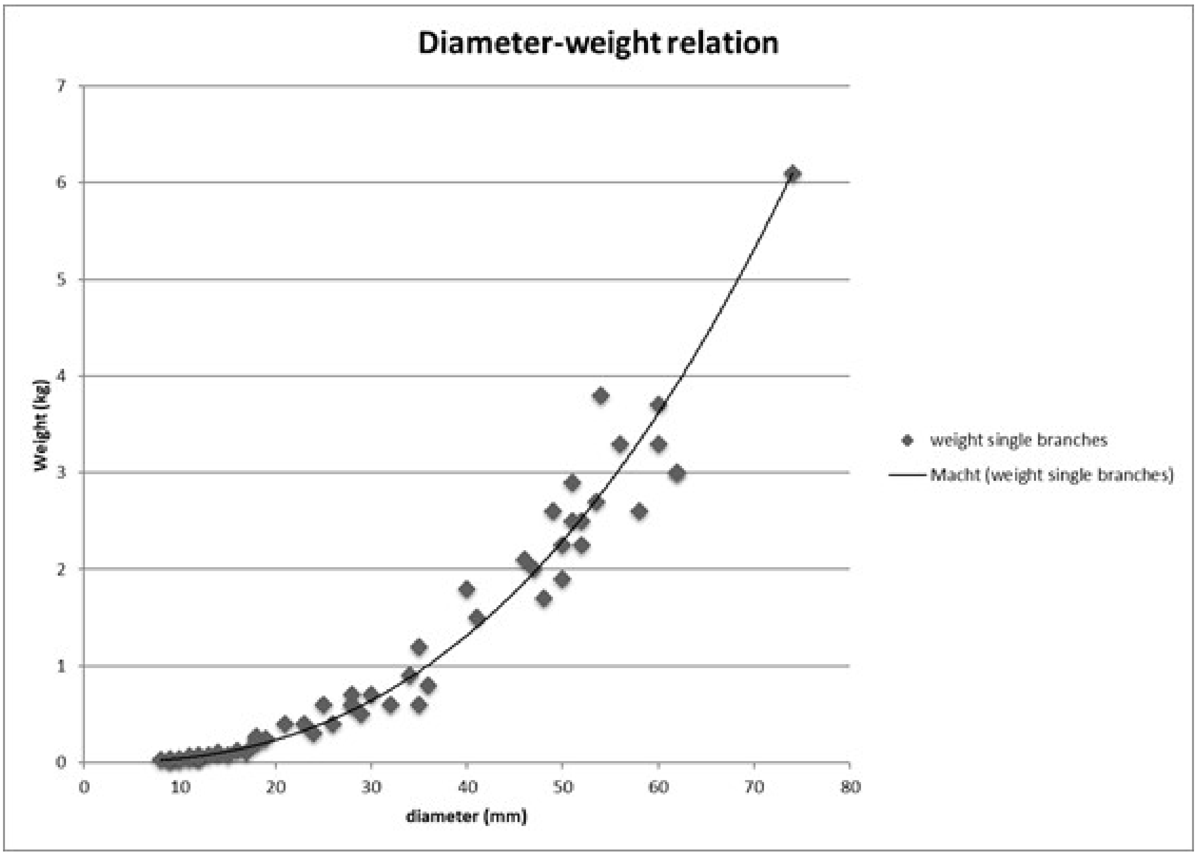

Figure B.2: diameter-weight relation for willow branches.

B.2. Gathered biomass

Figure B.3: Left: Biomass after test series 1, right: Biomass after test series 2

Figure B.4: Left: Biomass after test series 4, right: Impression of the amount of biomass after a test series and the method for capturing it

B.3. Detailed branch graphs

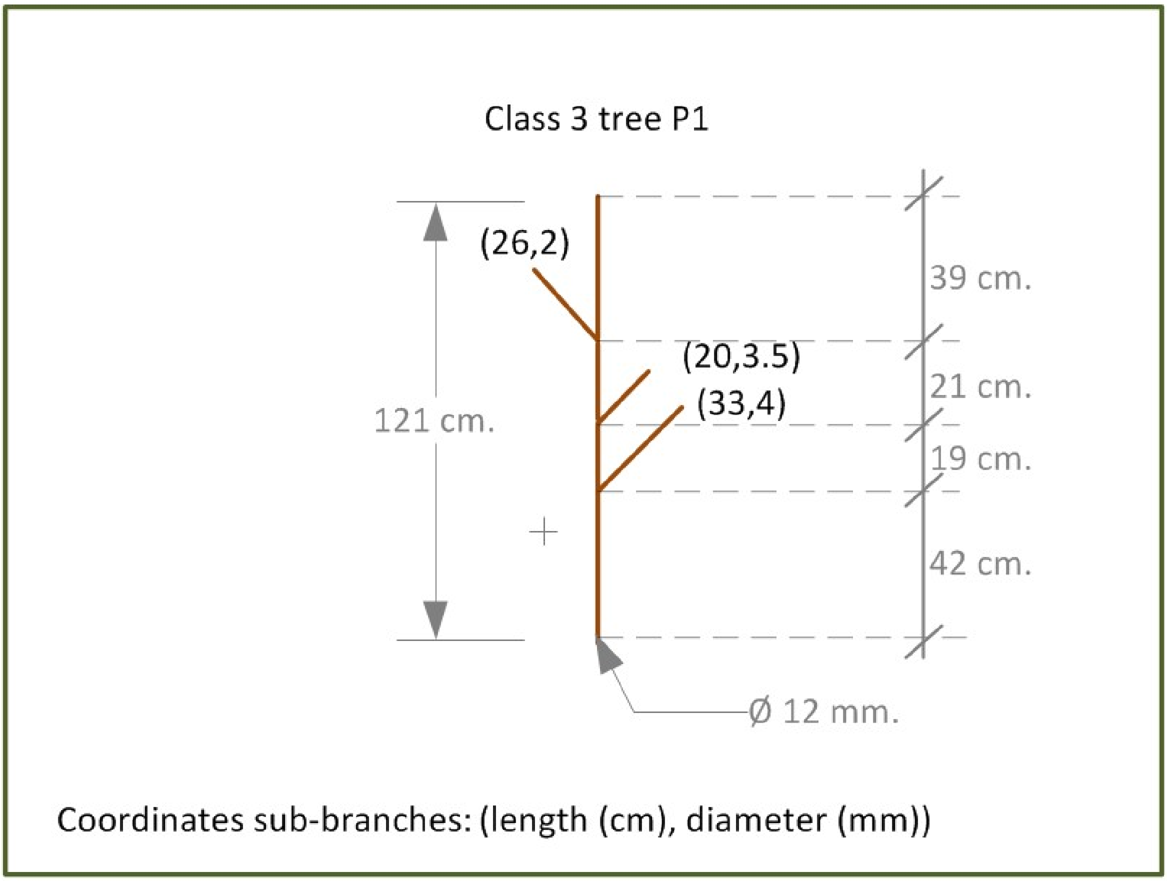

Figure B.5: Fully detailed graph for a class 3 branch

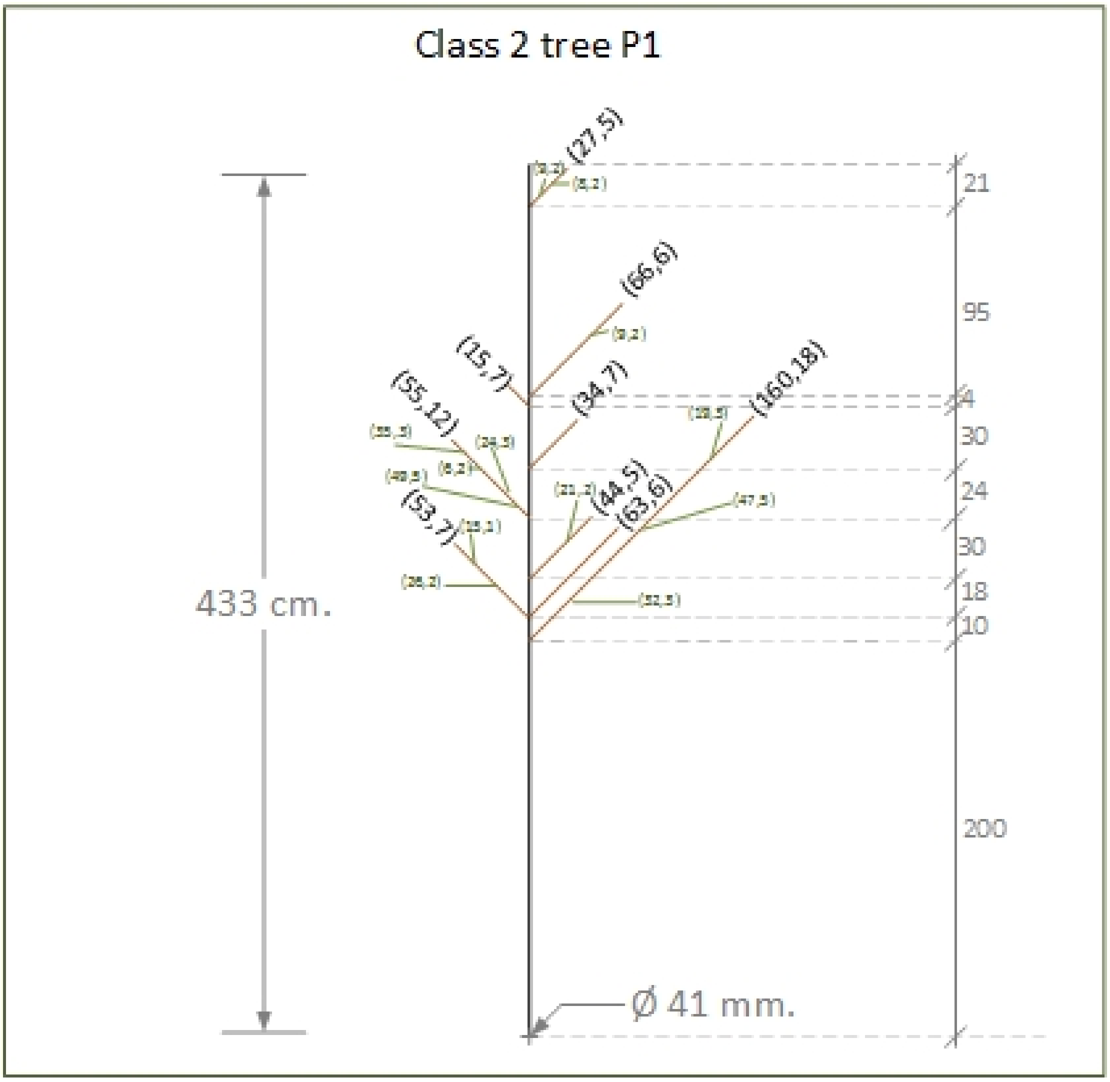

Figure B.6: Fully detailed graph for a class 2 branch

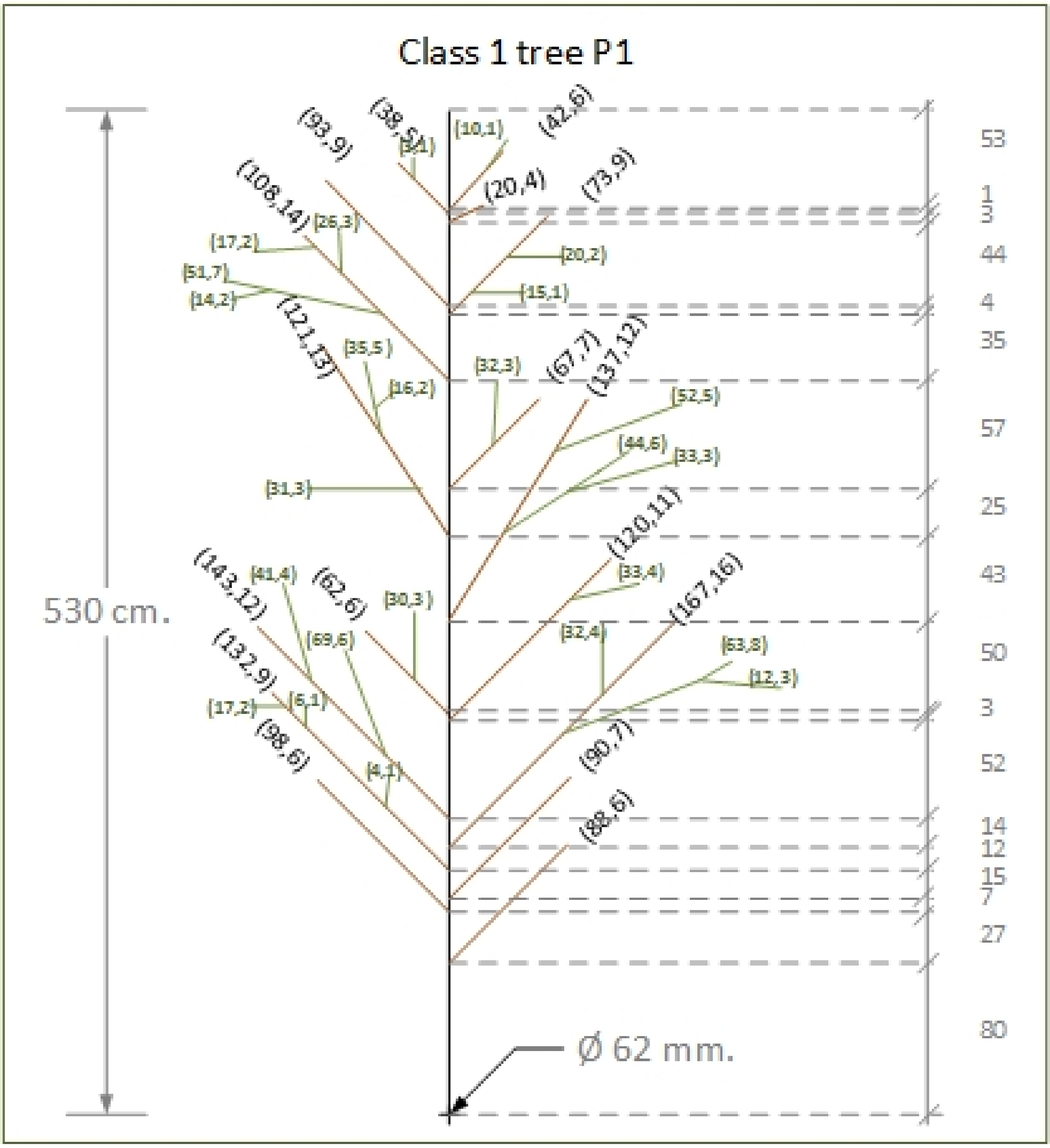

Figure B.7: Fully detailed graph for a class 1 branch

B.4. Alpha shape 2D analysis

The alpha radius value is a parameter of the alpha shape function in Matlab. This parameter determines how well the point cloud is represented, thus how reliable the area estimation is. The alpha radius used for further computations in this report is determined by varying the alpha radius and looking at the resulting area occupation. This analysis is done on a detailed zoom of a point cloud. The detailed zoom is done for one front tree (A1), given in figure B.8

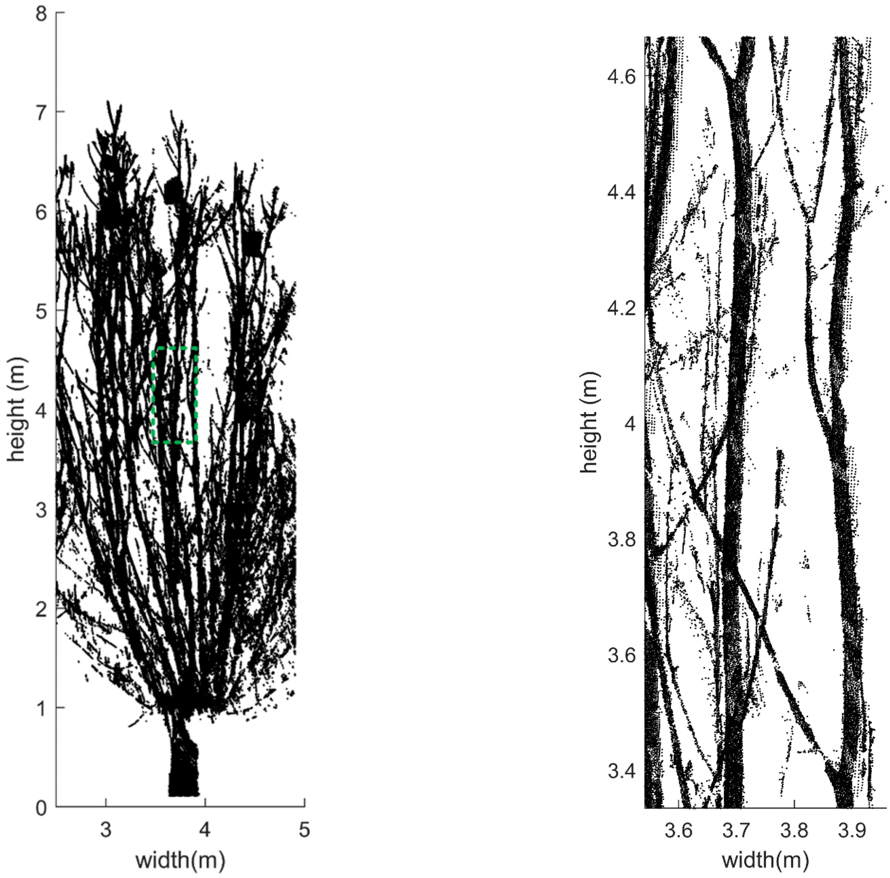

Figure B.8: Point cloud of tree A1 with the location of the detailed graph given within the green box (Left) and the respecting detailed zoom (right).

The total area contribution by the alpha shape is compared to the area covered by the point cloud itself. This is done for alpha values ranging from 0.008 to 0.025. The comparison between the point cloud, alpha values of respectively 0.025, 0.01 and 0.008 are shown in figure for the detailed graph B.9.

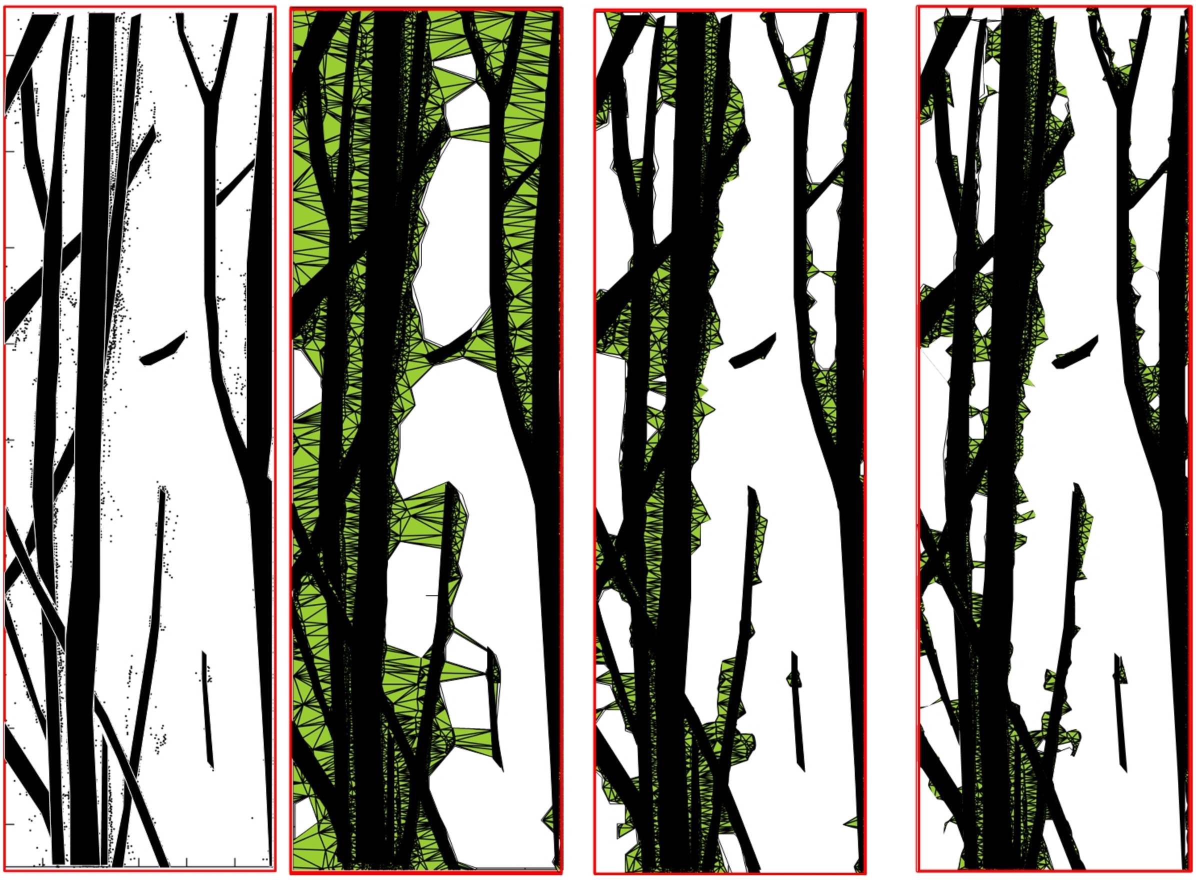

Figure B.9: Covered areas due to the point cloud (First Panel), the alpha shape function with alpha values of 0.025 (second panel), 0.01 (third panel) and 0.008 (fourth panel). The areas by the point cloud are given in black and alpha shape estimation of the areas are illustrated in green.

In this case the overestimation by the alpha shape varied between 8 % to 35 %, which is strongly dependent on the quality of the point cloud. It can be observed out of the detailed zoom shown in figure B.9, that the point cloud contains noncontinuous branches. This non-realistic phenomena out of the point cloud, motivated to use a alpha value radius with a slight overestimation of the area. Using a alpha value of 0.01 resulted in an overestimation of approximately 13 %.

B.5. Tree height comparison

Tree	TLS height (m)	Measured height (m)	relative error (%)	absolute error (%)
A1	6.62	6.04	10%	10%
A2	6.01	6.07	-1%	1%
B1	6.62	6.05	9%	9%
B2	5.09	5.03	1%	1%
C1	4.73	4.37	8%	8%
C2	5.76	5.56	4%	4%
D1	6.53	6.52	0%	0%
D2	5.82	6.07	-4%	4%
E1	5.76	6.1	-6%	6%
E2	6.22	6.04	3%	3%
F1	5.53	6.48	-15%	15%
F2	4.47	4.66	-4%	4%
G1	5.59	4.98	12%	12%
G2	5.85	5.53	6%	6%
H1	6.32	6.57	-4%	4%
H2	4.75	5.04	-6%	6%
I1	5.26	5.5	-4%	4%
I2	6.14	6.04	2%	2%
J1	6.31	5.97	6%	6%
J2	4.97	5.52	-10%	10%
K1	6.65	5.4	23%	23%
K2	5.45	5.6	-3%	3%
L1	5.38	5.16	4%	4%
L2	4.9	4.4	11%	11%
M1	4.98	4.27	17%	17%
M2	4.79	5.03	-5%	5%
N1	4.37	5.04	-13%	13%
N2	5.04	4.37	15%	15%
O1	4.36	4.3	1%	1%
O2	5.16	5.11	1%	1%
P1	5.61	5.02	12%	12%
P2	4.58	4.6	0%	0%
Average			2%	7%

B.6. Frontal area comparison

Tree number	Tree model 1a frontal area(m^2)	TLS frontal area (m^2)	relative error (%)	absolute error (%)
A1	3.91	5.46	40%	40%
A2	4.88	4.75	-3%	3%
B1	4.23	4.10	-3%	3%
B2	3.15	3.21	2%	2%
C1	2.68	2.02	-25%	25%
C2	4.79	4.08	-15%	15%
D1	3.40	2.88	-15%	15%
D2	4.51	3.36	-26%	26%
E1	3.69	1.76	-52%	52%
E2	5.67	2.83	-50%	50%
F1	3.59	2.58	-28%	28%
F2	2.86	1.72	-40%	40%
G1	2.98	2.34	-22%	22%
G2	4.46	3.43	-23%	23%
H1	5.24	5.31	1%	1%
H2	3.88	3.43	-12%	12%
I1	5.10	2.19	-57%	57%
I2	3.40	2.78	-18%	18%
J1	3.73	2.23	-40%	40%
J2	5.03	1.52	-70%	70%
K1	3.71	1.51	-59%	59%
K2	5.75	1.45	-75%	75%
L1	5.50	1.28	-77%	77%
L2	2.65	0.51	-81%	81%
M1	2.77	1.39	-50%	50%
M2	3.71	1.71	-54%	54%
N1	2.81	2.24	-21%	21%
N2	3.43	2.30	-33%	33%
O1	3.15	2.51	-20%	20%
O2	3.10	3.29	6%	6%
P1	5.70	4.87	-14%	14%
P2	2.96	2.92	-2%	2%
Average			-29%	32%

B.7. SWAN file

```
PROJ 'willow' '013'
SET LEVEL 5.311 RHO 1000.00 cartesian
MODE stationary oneDIMENSIONAL
COORDINATES cartesian
CGRID regular 40.50 0.00 0.00 219.500 0.000 220 0 SECTOR -120.00
120.00 240 0.02857143 2.00000000 180
INPGRID BOTTOM regular 0.00 0.00 0.00 260 0 1.000 0.000
READINP BOTTOM -1 'df_willow_013.bot' 3 FREE
INPGRID NPLANTS regular -0.25 0.00 0.00 105 0 2.500 0.000
READINP NPLANTS 1 'df_willow_013.veg' 3 FREE
vegetation 1.023 0.338 1 1.000 &
1.000 0.021 89 1.000 &
1.000 0.011 112 1.000 &
1.000 0.010 50 1.000 &
0.866 0.009 18 1.000 &
0.463 0.007 5 1.000
BOUNDSPEC SIDE WEST CLOCKWISE CONSTANT FILE 'df_willow_i013.sp1'
1
GEN3
off windgrowth
off quadrupl
off wcapping
off refrac
friction jonswap constant 0.07
NUMERIC STOPC 0.005 0.010 0.005 99.999 STATIONARY 50  0.000
0.001
POINTS 'WHM' FILE 'df_willow_whm_013.out'
POINTS 'RADAC' FILE 'df_willow_rac_013.out'
TABLE 'WHM' INDEXED 'df_willow_whm_par_013.tab' HSIGN RTP TPS
TMM10 TM01 TM02 WATLEV BOTLEV VEL DIR NPLANTS DISSIP DISVEG
DISBOT
TABLE 'RADAC' INDEXED 'df_willow_rac_par_013.tab' HSIGN RTP TPS
TMM10 TM01 TM02 WATLEV BOTLEV VEL DIR NPLANTS DISSIP DISVEG
DISBOT
SPECOUT 'WHM' SPEC1D  ABSOLUTE 'df_willow_whm_sp1_013.nc'
SPECOUT 'RADAC' SPEC1D  ABSOLUTE 'df_willow_rac_sp1_013.nc'
$TEST 1,0
COMPUTE STAT
STOP
```

Figure B.10: Example of SWN file

It must be noted that the Number of branches is per tree in the Vegetation command line, but is multiplied by (2.5 *2.5) which is the area covered by one tree. In this matter N is in $units/m^2$.

B.8. Optimal drag coefficients

Table B.3: The optimal bulk drag coefficients per test for each tree model and corresponding water levels.

		Hs [m]	hv [m]	Cd			
				Tree model 1a	Tree model 1b	Tree model 1c	Tree model 2
TS1	T001	0.17	0.6	5.2	5.2	5.2	5.2
	T002	0.2	0.6	11.9	11.9	11.9	11.9
	T003	0.21	0.7	6	6	6	6
	T004	0.26	0.7	4.59	4.59	4.59	4.59
TS2	T005	0.46	3	0.77	0.56	0.71	2
	T006	1.02	3	0.48	0.36	0.44	2
	T007	0.5	3	0.74	0.55	0.68	2
	T008	1.05	3	0.51	0.39	0.48	2
	T009	0.45	4.5	0.55	0.4	0.46	1.49
	T010	0.94	4.5	0.28	0.2	0.24	0.92
	T011	0.47	4.5	0.58	0.42	0.5	1.86
	T012	0.99	4.5	0.31	0.23	0.27	1.12
TS3	T013	0.45	3	2	0.91	1.65	2
	T014	1.01	3	1.31	0.62	1.04	2
	T015	0.5	3	2	1.12	1.86	2
	T016	1.05	3	1.32	0.71	1.1	2
	T017	0.45	4.5	2	0.77	1.53	2
	T018	0.95	4.5	1.72	0.46	0.85	1.75
	T019	0.47	4.5	2	0.86	1.61	2
	T020	0.98	4.5	1.21	0.41	0.72	1.55
	T021	1.47	4.5	0.88	0.27	0.5	1.06
	T022	1.55	4.5	1.03	0.37	0.64	1.41
TS4	T023	0.44	3	2	1	1.81	2
	T024	0.99	3	1.44	0.68	1.15	2
	T025	0.48	3	2	1.07	1.77	2
	T026	1.05	3	1.58	0.84	1.32	2
	T027	0.95	4.5	2	0.59	1.09	2
	T028	0.98	4.5	1.64	0.55	0.97	2
	T029	1.47	4.5	1.07	0.34	0.6	1.28
	T030	1.55	4.5	1.3	0.47	0.81	1.78